Effect of welding parameters on bead geometry and metallurgy in SAW process using CCD

Submitted by:

ARJYAJYOTI GOSWAMI

(Roll No. : **02/PRD/2010**)

Mechanical Engineering Department

In partial fulfillment of the requirement of the degree of

MASTERS OF TECHNOLOGY in

Production Engineering

Under the guidance of:

Dr. Reeta Wattal

Associate Professor

Department of Mechanical Engineering

Department of Mechanical Engineering

DELHI TECHNOLOGICAL UNIVERSITY

(Formerly Delhi College of Engineering)

Bawana Road, New Delhi

June 2012

CERTIFICATE

This is to certify that the report entitled **"Effect of welding parameters on bead geometry and metallurgy in SAW process using CCD"** submitted by **Arjyajyoti Goswami** (Roll No.:02/PRD/2010) in partial fulfillment for the award of Masters of Technology in Production Engineering from Delhi Technological University, is a record of bonafide project work carried out by him under my supervision and guidance.

Dr. Reeta Wattal
Associate Professor
Department of Mechanical Engineering
Delhi Technological University, Delhi

ACKNOWLEDGEMENT

I wish to express my deep and sincere gratitude to my project guide, Dr. Reeta Wattal, Associate Professor, Department of Mechanical Engineering, for her invaluable guidance, encouragement and patient review during this project. Her continuous inspiration has enabled me to complete this project successfully.

I am grateful to Prof. B.D Pathak, HOD (Mechanical and Production Engineering) and all faculty members of the department for providing necessary help and support.

I would also like to thank my parents for their blessings and unconditional support during this project.

Arjyajyoti Goswami

(02/PRD/2010)

M.Tech (Production Engineering)

Delhi Technological University

ABSTRACT

Submerged Arc Welding is the most extensively used permanent joining process for joining of thick sections. The most important features of this process are high deposition rate, ability to weld thick sections with ease and longer weld runs. Effect of process parameters: Arc voltage, Welding current, Travel speed and Nozzle-to-plate-distance, on the weld process is determined by co relating the process parameters with bead geometry features such as, bead reinforcement height, bead width and bead penetration.

The design matrix was prepared on the basis of 4 factors, 5 levels, rotatable Central Composite Design. Response Surface Methodology was used to develop the mathematical models co relating the process parameters with the bead geometry features. The models once developed were checked for adequacy using ANOVA technique. From the adequate models the significant terms were selected using p test. The finally proposed models contains only the significant terms. Main and interaction effects of the process variables on weld bead geometry are presented in graphical form. The developed models can be used for prediction of important weld bead dimensions and control of the weld bead quality by selecting appropriate process parameter values.

Use of artificial neural networks for modelling of the Submerged Arc Welding process was done. Artificial Neural Network architecture, using back propagation algorithm was developed which provided satisfactory outputs. Comparison of the performance of the RSM models and the ANN model was also done and it was concluded that the when number of factors are less, RSM yields more satisfactory results.

iv

Metallurgical investigations determining the variation of micro hardness across the weld metal zone, heat affected zone and the base metal were carried out. Effect of parameters on the variation of the Knoop's micro hardness is determined. Also the microstructure of the resultant welded metal was co-related with the process variables.

This thesis is divided in 8 chapters. The first chapter discusses the objective and motivation of the project, followed by the statement of problem and lastly the plan of investigation, which was undertaken to achieve the objectives. The next chapter gives an insight regarding the research work which has been carried out in related fields such as ANN modeling, RSM application to welding problems, metallurgical investigations etc. Chapter 3 gives a brief introduction to the concepts of SAW, ANN, RSM and weld metallurgy, followed by the experimental procedures undertaken to carry out the project work. Chapter 4 discusses the development of mathematical models. It is followed by Chapter 5 where in discussions of the effects of process variables on bead geometry parameters are done. Chapter 6 is dedicated to use of ANN for modeling of the SAW process. A comparison of the 2 modeling approaches is also done. Chapter 7 discusses the metallurgical investigations in micro hardness and micro structure. Chapter 8 states the results and conclusions drawn from this study.

Keywords: Submerged Arc Welding, Central composite design, Response Surface Methodology, Artificial neural Network, Weld Metallurgy, Micro Hardness,

TABLE OF CONTENTS

LIST OF FIGURES

LIST OF TABLES

LIST OF SYMBOLS

Symbol	Represents	units
P	Bead Penetration	(mm)
W	Bead Width	(mm)
H	Bead Height	(mm)
V	Voltage	(Volts)
A	Current	(Ampere)
S	Travel Speed	(mm/min)
N	Nozzle-to-plate-distance	(mm)

ABBREVIATIONS

CCD	Central Composite Design
RSM	Response Surface Methodology
ANN	Artificial Neural Network
HAZ	Heat Affected Zone

Chapter 1

INTRODUCTION

1.1 Introduction

Submerged Arc Welding is a commonly used metal joining process in the industry, especially suited for joining of thick and heavy sections. The quality of any weld process is characterised by the weld distortion, mechanical properties and weld bead geometry. Out of these factors, the weld bead geometry is the easiest to measure and control. Thus by controlling the weld bead geometry we can successfully control the weld quality. But the relationship between the process variables and the weld bead geometry is very complex and necessitates a robust mathematical approach to quantify the relationship between them.

Design of experiment using CCD and modelling using RSM may be used to develop mathematical models establishing mathematical relationships between the input process variables and the output parameters. ANN provides another approach of modelling the SAW process, wherein a Feed Forward Back Propagation Neural Network is capable of producing the outputs to a given set of inputs after sufficient amount of training. This network is used to make predictions about the bead geometry features.

Apart from influencing the bead geometry, the input process variables also affect the metallurgical aspects of the metal being joined. The micro hardness, the different

phases constituting the micro structure, the percentage of different phases, grain size etc. are largely influenced by the input process variables and ultimately they affect the performance of the welded metal in different applications.

1.2 Motivation and Objective

The motivation of this project was to study the SAW process in its totality and to explore the potential of controlling the process so as to get desired outputs by simply manipulating the input process variables. To be able to successfully use a process in industry it is imperative that we have a robust way of controlling the outputs as per our needs.

The main objective of this project was to understand the influence of process variables such as Arc Voltage, Current, Travel Speed and Nozzle-to-plate-distance on the bead geometry features and to quantify the relationships through development of mathematical models co-relating the two. Further prediction of the bead geometry features was done through ANN by developing neural network architecture. The effect of welding parameters on metallurgy was also studied.

1.3 Statement of the Problem

"**Effect of welding parameters on bead geometry and metallurgy in SAW process using CCD**"

The research work describes the development of mathematical models through experimental observations made on a mild steel plate through bead-on-plate technique using RSM and development of neural network architecture for modelling the SAW process to predict the bead geometry features for a given set of inputs. The

metallurgical aspects of the welded metal were also studied and an attempt was made to co-relate the observed values with the input process variables.

1.4 Plan of Investigation

The research work was planned to be carried out in following steps:

1. Identification of important process control variables

2. Deciding the working range of the process control variables, viz. Arc Voltage (V), Current (A), Travel Speed (S) and Nozzle-to-plate-distance (N)

3. Developing the design matrix

4. Conducting the experiments as per the design matrix

5. Recording the responses viz. bead height (H), bead width (W) and bead penetration (P)

6. Developing the mathematical models

7. Checking the adequacy of the models

8. Finding the significance of co-efficient

9. Developing the final proposed models

10. Plotting of graphs and drawing conclusions

11. Development of an ANN architecture to model and to predict the bead geometry

12. Comparison of performances of RSM models and ANN models

13. Metallurgical analysis to co-relate the micro hardness and the micro structure of the welded material with the process variables

14. Discussion of the results

Chapter 2

LITERATURE REVIEW

2.1 Introduction

Welding is a fabrication process that joins two metals or non-metals by producing coalescence between them. This is generally achieved by heating the specimen up to their melting temperature with or without the addition of filler materials, to form a pool of molten metal that cool and solidifies to become a strong joint. While often an industrial process, welding can be done in many different environments, including open air, under water and in outer space.

With the advent of newer materials, stringent performance and quality requirements in the industry, engineers became increasingly aware of the weld quality. The major factors which decide the quality of a joint are mechanical properties of the welded joint, distortion of the welded structure and the bead geometry features. The studies of the effects of various welding process parameters on the formation of bead and bead geometry have attracted the attention of many researchers to carry out further investigations. Design of experiment (DOE) combined with Response surface methodology (RSM) is a powerful statistical tool to determine and represent the cause and effect relationship between responses and input control variables influencing the responses as a two or three dimensional hyper surface. Recent developments in the evolution of artificial neural networks have been found to be useful in solving many engineering problems. In different fields of engineering, back

propagation neural network has proved to be one of the best algorithms for predictive type of work.

The mechanical performance and application of any welded joint is affected by the metallurgical properties of the welded joints. Over the years researchers have carried out investigations to understand the metallurgical changes taking place during the welding and to co-relate these changes with the welding process variables.

The present literature review has been carried out in the areas concerning the influence of input process variables in the bead geometry, application of RSM to develop mathematical models to model the relationships between the inputs and the outputs of a process, application of ANN for modelling of a process and prediction of outputs and influence of process variables on the metallurgical changes taking place during welding.

2.2 Influence of Input Process Variables on the Bead Geometry

R.S. Chandel [1] presented theoretical predictions of the effect of current, electrode polarity, electrode diameter and electrode extension on the melting rate, bead height, bead width and weld penetration, in submerged-arc welding. They studied that the melting rate of SAW can be increased by four methods: (i) using higher current; (ii) using straight polarity; (iii) using a smaller diameter electrode; and (iv) using a longer electrode extension. The percentage difference in melting rate, bead height, bead width, and bead penetration is affected by the current level and polarity. When a smaller diameter electrode is used, the increase in the current level does not make much difference to the percentage change in bead height, bead width, and weld penetration.

Erdal Karadeniz et al [2] in their study, the effects of various welding parameters on welding penetration in Erdemir 6842 steel having 2.5 mm thickness welded by robotic gas metal arc welding were investigated. The welding current, arc voltage and welding speed were chosen as variable parameters. The depths of penetration were measured for each specimen after the welding operations and the effects of these parameters on penetration were researched. The welding currents were chosen as 95, 105, 115 A, arc voltages were chosen as 22, 24, and 26 V and the welding speeds were chosen as 40, 60 and 80 cm/min for all experiments. As a result of this study, it was found that increasing welding current increased the depth of penetration. In addition, arc voltage is another parameter in incrimination of penetration. However, its effect is not as much as current's. The highest penetration was observed in 60 cm/min welding current.

Gunaraj and Murugan [3] have highlighted the use of RSM to develop mathematical models and plot contour graphs relating important input parameters namely the open-circuit voltage, wire feed-rate, welding speed and nozzle- to-plate distance to some responses namely, the penetration, reinforcement, width and percentage dilution of the weld bead in SAW of pipes. They demonstrated that all responses decrease with increasing welding speed. Also, when the nozzle-to-plate distance increases all responses decrease, but reinforcement increases. Moreover, an increase in the wire feed-rate results in an increase in all responses but the width remains unchanged.

In 1999, **Gunaraj and Murugan [4]** also studied the effect of SAW parameters on the heat input and the area of HAZ for low-carbon steel with two joint types, bead-on-plate and bead-on-joint, using mathematical models developed by RSM. They found that for the same heat input, the area of the HAZ is greater for the bead-on-plate

6

than that for bead-on-joint. They found that the effect of SAW parameters on the area of HAZ in both cases follows the same trend.

Yang et al [5] have used linear-regression equations for computing the weld features (melting rates, total fusion area, penetration, deposit area, bead height and bead width) from SAW process variables (electrode extensions range, welding voltage, welding current, welding speed and electrode diameter) using both positive and negative electrode polarity. The base material was a 19 mm thick ASTM A36 steel plate. They managed to develop regression equations for each weld feature in both polarity conditions. Their results indicated that the linear-regression equations were equally useful for computing the various features of the SAW process.

Bipin Kr, Srivastav et al [6] reviewed the effects of arc welding parameters on mechanical properties of ferrous metals/alloys.Their study of the various works, review that, the selection of the suitable process parameters are the primary means by which acceptable heat affected zone properties, optimized bead geometry and minimum residual stresses are created. Some researchers realized that the mechanical properties of weld are influenced by the composition of the base metal and to a large extent by the weld bead geometry and shape relationship as well. Some of the researchers observed that with increase in electrode stick out, hardness of the weldment increases, yield strength and impact value decreases, ultimate tensile strength of the joint initially decreases but thereafter increases provided welding current and voltage are kept at constant levels.

From the discussion on the above-mentioned literature it is observed that in different welding processes the weld bead parameters such as penetration, bead width, reinforcement height etc. are largely influenced by various welding parameters such

as arc current, voltage, and travelling speed. In SAW the main factors affecting the bead geometry are arc voltage, current, travel speed, and nozzle plate distance.

2.3 Application of CCD matrix and regression analysis for designing the experiments and developing the mathematical model

It consists of the following steps:

➢ Designing of a set of experiment for adequate and reliable measurement of the true mean response of interest.

➢ Determination of mathematical model with best fits

➢ Representing the direct and interactive effects of process variables on the best parameters through two dimensional and three dimensional graphs.

Benyounis et al [7] have proposed models using RSM to investigate the effect of welding parameters in SAW (welding current, arc voltage and welding speed) on the impact strength at two testing temperatures of 50 ^{0}C and 27 ^{0}C. The aim was to predict and optimize the impact strength of the spiral-welded joints with respect to the process parameters. It was observed that the welding current was the most significant factor associated with the impact strength, then the welding speed, whereas the welding voltage has no significant effect within the factors domain investigated. They listed the optimal welding conditions that would lead to acceptable impact strength with improving the process productivity.

Murugan and Gunaraj [8] used 5 level 4 factor central composite rotatable design matrix for Prediction and control of weld bead geometry and shape relationships in submerged arc welding of pipes. Arc voltage, wire feed rate; welding speed and nozzle-to-plate distance were considered as the main factors affecting the bead

geometry. Mathematical models have been developed for SAW of pipes using five level factorial techniques to predict three critical dimensions of the weld bead geometry and shape relationships. The models developed have been checked for their adequacy and significance by using the *F*-test and the *t*-test, respectively. Out of the four process variables considered, wire feed rate had a significant positive effect but welding speed had an appreciable negative effect on most of the important bead parameters. Penetration increased by about 1.3mm as wire feed rate was increased from −2 to +2 limit whereas penetration decreased by about 1mm as welding speed was increased from −2 to +2 limit. Arc voltage had a less significant negative effect on penetration and reinforcement but had a positive effect on bead width, penetration size factor and reinforcement form factor. As wire feed rate had a positive effect but welding speed had a negative effect on most of the bead parameters, the interaction effects of wire feed and travel speed were similar for most of the parameters. Penetration, width, penetration size factor and reinforcement form factor all increased with the increase in wire feed rate for all values of welding speed but this increasing rate of the bead parameters with the increase in wire feed rate is gradually decreased with the increase in travel speed.

Koleva [9] has carried out another work by applying RSM to establish the relationship between performance characteristics (weld-depth, weld-width and thermal efficiency) and its influencing factors (beam power, welding velocity, focus position, focusing current of the beam and the distance to the sample surface) for EBW of austenitic stainless steel. Optimal welding regimes were found through the thermal efficiency optimization. New statistical approaches were proposed to choose the focus position at a condition of maximum thermal efficiency and welding depth.

Benyounis et al [10] have applied RSM to investigate the effect of laser welding parameters (laser power, welding speed and focal point position) based on four responses (heat input, penetration, bead width and width of HAZ) in CO2 laser butt-welding of medium carbon steel plates of 5 mm thick. They found that the heat input plays an imported rule in the weld-bead parameters; welding speed has a negative effect while laser power has a positive effect on all the responses.

Heiderzadeh et al [11] applied RSM for his investigations of the tensile behaviour of friction stir welded AA 6061-T4 aluminium alloy joints. In this investigation response surface methodology based on a central composite rotatable design with three parameters, five levels and 20 runs, was used to develop a mathematical model predicting the tensile properties of friction stir welded AA 6061-T4 aluminium alloy joints at 95% confidence level. The three welding parameters considered were tool rotational speed, welding speed and axial force. Analysis of variance was applied to validate the predicted model. Microstructural characterization and fractography of joints were examined using optical and scanning electron microscopes. Also, the effects of the welding parameters on tensile properties of friction stir welded joints were analyzed in detail. The results showed that the optimum parameters to get a maximum of tensile strength were 920 rev/min, 78 mm/min and 7.2 kN, where the maximum of tensile elongation was obtained at 1300 rev/min, 60 mm/min and 8 kN.

The literature review has brought about an understanding of the use of regression analysis to determine and represent the cause and effect relationship between true mean response and input control variables influencing the response as a two or three dimensional hyper surface.

2.4 Application of Artificial Neural Network (ANN) for modeling of process

The main attractive feature of ANN is their ability to to derive meaning from a given set of data and to understand the relationship between the input and output sets, that are too complex to understand by humans or other computer techniques. Their ability to learn by example makes them conducive for experimental investigations. The parallel architecture of the neural network makes them well suited for real time systems because of their fast response and computational times. The following literature survey has been made to study the application of ANN in welding and other engineering problems.

Anderson et al [12] in 1990 pioneered the use of artificial neural networks for the modelling of an arc welding process. In their paper Artificial neural networks were studied to determine their applicability to modelling and control of physical processes. Some basic concepts relating to neural networks and how they can be used to model weld-bead geometry in terms of the equipment parameters selected to produce the weld were explained. Approaches to utilizing neural networks in process control are discussed. The need for modelling transient as well as static characteristics of physical systems for closed-loop control is pointed out, and an approach to achieve this is presented. The performance of neural networks for modelling is evaluated using actual welding data. It was concluded that the accuracy of neural network modelling is fully comparable with the accuracy achieved by more traditional modelling schemes.

George E. Cook et al. [13] evaluated artificial neural networks for monitoring and control of the Variable Polarity Plasma Arc Welding process. Three areas of welding

application were investigated: weld process modeling, weld process control, and weld bead profile analysis for quality control.

D.S. Nagesh, G.L. Datta [14] in their work used artificial neural networks to model the shielded metal-arc welding process. Back-propagation neural networks are used to associate the welding process variables with the features of the bead geometry and penetration. These networks have achieved good agreement with the training data and have yielded satisfactory generalization. A neural network could be effectively implemented for estimating the weld bead and penetration geometric parameters. The results of these experiments show a small error percentage difference between the estimated and experimental values.

Sukhomay pal et al [15] used ANN for modelling of weld joint strength prediction of pulsed MIG using arcs signals. Their paper addressed the weld joint strength monitoring in pulsed metal inert gas welding (PMIGW) process. Response surface methodology was applied to perform welding experiments. A series of experiments were carried out by applying response surface method.. A multilayer neural network model was developed to predict the ultimate tensile stress (UTS) of welded plates. Six process parameters, namely pulse voltage, back-ground voltage, pulse duration, pulse frequency, wire feed rate and the welding speed, and the two measurements, namely root mean square (RMS) values of welding current and voltage, were used as input variables of the model and the UTS of the welded plate is considered as the output variable. The obtained experimental data was used to train and test ANN model of various architectures; and 8-13-18-1 architecture with learning rate and momentum coefficient of 0.9 and 0.35, respectively, was found as the best one for the current purpose. A multiple regression model was also developed and its performance was compared with the performance of the ANN model. It was found

that the error in prediction of weld strength from the neural network model is less than that from the regression model.

The study of **Abdulkadir C`evik et al [16]** presented use of neural network (NN) for the prediction of ultimate capacity of arc spot welding. The proposed NN model is based on experimental results. The ultimate capacity of arc spot welding is modelled in terms of weld strength, average welding thickness and diameter. The results of the proposed NN model are later compared with results of existing codes and are found to more accurate. Parametric studies are also carried out to analyze the effect of each variable.

2.5 Influence of process variables on the metallurgy of the welded specimen

The metallurgy of the base metal plays a major role in deciding the mechanical properties and application of the base metal. Research work has been carried out to co-relate the metallurgical changes with the input process variables and thus, to control the metallurgy of the welded specimen.

M. Eroglu et al [17] carried out investigations to study the effect of coarse initial grain size on microstructure and mechanical properties of weld metal and HAZ of low carbon steel. In this study, the effects of coarse initial grain size with varying heat inputs on microstructure and mechanical properties of weld metal and heat-affected zone (HAZ) were investigated. The original and grain-coarsened specimens were welded using a submerged arc welding machine with heat inputs of 0.5, 1 and 2 kJ/mm. Following the welding, microstructure, hardness and toughness of weld metals and HAZs were investigated. From the results, they tried to establish a relationship between initial grain size, microstructure, hardness and toughness of weld metals and HAZs. Considering the heat input, it was observed that the coarse initial grain size had a great influence on the microstructure, hardness and

toughness of HAZ of low carbon steel. Thus, taking into consideration the plate thickness, a higher heat input should be used with respect to the maximum toughness of the HAZ in the welding of grain-coarsened low carbon steels.

D.V.Kiran et al [18] investigated the influence of process variables on weld bead quality in 2 wire tandem submerged arc welding of HSLA steel. In particular, the quantitative effects of the trailing wire current pulses and negative current pulse duration, leading wire current, and welding speed on the weld bead dimensions and mechanical properties are studied at fifty different sets of welding conditions that are designed following the principle of two-level, five factor central composite rotatable design. The experimental results show that the final weld bead width and reinforcement height are primarily influenced by the trailing wire current while the penetration is influenced by the leading wire current with the other conditions remaining constant. Increase in welding speed tends to reduce weld pool size leading to higher cooling rate that encourages greater volume fraction of acicular ferrite phase and better weld bead mechanical properties. The predictions of weld dimensions and mechanical properties from the empirical relations, which are developed based on the experimental results, are in fair agreement with the corresponding measured values within the ranges of the welding conditions considered in the work.

Gunaraj et al [19] developed mathematical models for prediction and comparison of area of the heat-affected zone for the bead-on-plate and bead-on-joint in submerged arc welding of pipes. The amount of heat input to the weld metal increases as voltage or wire feed rate or both increase. The heat input decreases with increase in travel speed. They found that voltage and wire feed rate had a positive effect on area of HAZ while travel speed and nozzle-to-plate distance had a negative effect.

For the same heat input the area of HAZ is greater on the plate tan on the joint. The direct and indirect effects of process variables on the area of the HAZ on both the bead-on-plate and the bead-on-joint are found to be the same. It is also found that the slopes of the individual plots are generally equal.

Kolhe et al [20] carried out a detailed work in prediction of microstructure and mechanical properties of multi pass SAW. A detailed study on the microstructure, phase analysis and mechanical properties, HAZ width of SA weld metal multipass joint and heat-affected zone of 16mm thick mild steel plate was carried out. The various sub-zones in the microstructure were observed in the HAZ of SA weld are spheroidized, partially transformed, grain refined and grain coarsened. Welding heat input can control the percentage of phases in the welded structures. More variations in bulk hardness of the fractured samples were observed than welded samples. More HAZ width at top region of welded specimen was seen than that of bottom region. For increase in heat input the percentage of graphitic phase was slightly decreased whereas the percentage of ferrite sharply increased and finally the ferritic structures were observed. The proportionate value of micro hardness was observed for low heat input whereas for increased heat input variations in hardness value was observed.

Adnan Celik [21] investigated the effect of cooling rate on microstructure and mechanical properties of AISI 1020, AISI 1040 and AISI 1060 steels. The samples were heated and treated at 1250°K for 4 h and subsequently were cooled by three different methods. For this purpose, the microhardness and microstructure of these steels after heat treatment were examined by optical microscopy and hardness tests, respectively. Experimental results have shown that the microstructure of these steels can be changed and significantly improved by varying the cooling rate. Thus, heat

treatment (heating and cooling) is used to obtain desired properties of steels such as improving the toughness, ductility or removing the residual stresses, etc. The micro hardness increases with the increasing cooling rate and carbon content due to solid solution hardening and formation of the martensite phase. Thus heat treatment (heating and cooling) is used to obtain desired properties of steels such as improving the toughness, ductility or removing the residual stresses.

2.6 Conclusions

From the literature review it is observed that independent work has been done in development of mathematical models for welding process, their modeling through neural network and metallurgical studies have been carried out independently. But an integrated approach of studying the effects of various welding process variables on bead geometric descriptors using 5 level full factorial central composite design, use of regression analysis to develop mathematical models for predicting the weld bead geometry, modeling of the process through Artificial Neural Network and studying the influence of process parameters on the metallurgy of the welded specimen in submerged arc welding of plates is hardly found in any literature. The present research work attempts to address this issue.

Chapter 3

THEORY AND EXPERIMENTATION

3.1 Submerged Arc Welding

3.1.1 Introduction

Submerged arc welding (SAW) is an arc welding process that fuses together the parts to be welded by heating them with one or more electric arcs between one or more bare electrodes and the work piece.
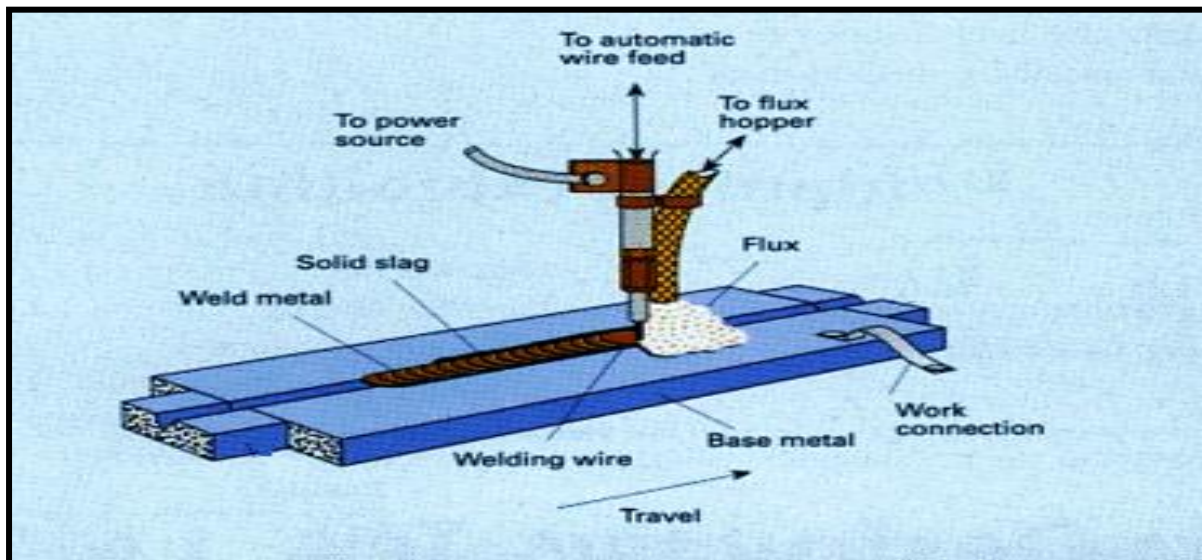
Figure 3.1: Schematic view of the SAW process

It is commonly used to join thick sections in the flat position **[36]**. It requires a continuously fed consumable solid or tubular (metal cored) electrode. The wire is fed continuously to the arc by a feed unit of motor-driven rollers. The flux is fed from a hopper fixed to the welding head and a tube from hopper spreads the flux in a continuous manner in front of the arc. The molten weld and the arc zone are protected from atmospheric contamination by being "submerged" under a blanket of granular fusible flux. Schematic of SAW process is shown in fig 3.1. SAW is usually

operated either as fully mechanized or automatically processed. During SAW process, operator cannot observe the weld pool and not directly interfere with the welding process. The un-melted flux acts as an insulator and is reclaimed for reuse. The slag that forms on the weld bead normally peels off on its own or alternatively can be detached with the help of a chipping hammer. As the arc is completely covered by the flux layer, heat loss is extremely low. This produces a thermal efficiency as high as 60% (compared with 25% for manual metal arc). There is no visible arc light, welding is spatter-free and there is no need for fume extraction. As the automation in the SAW process increases, direct effect of the operator continuously decreases and the precise setting of parameters become much more important than manual welding processes.

3.1.2 Submerged Arc welding Equipment
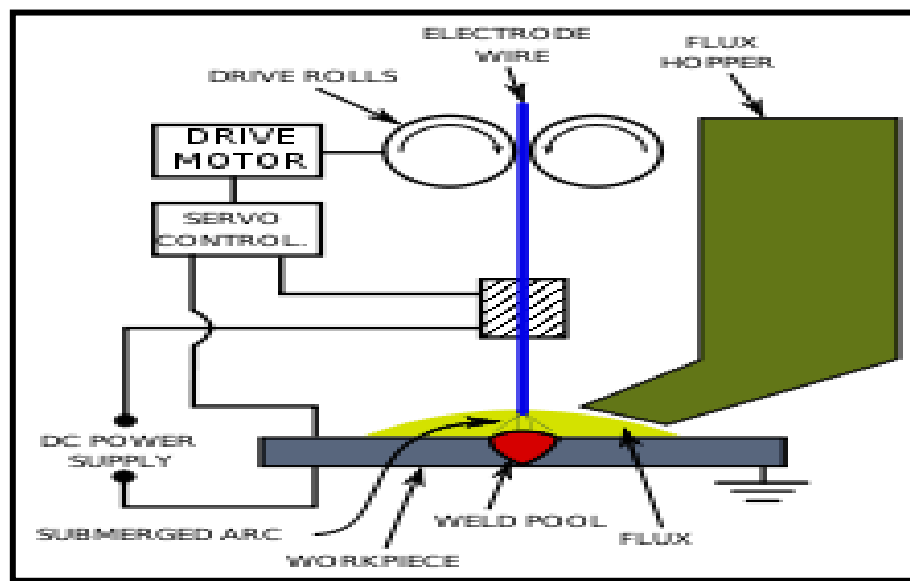
Figure 3.2: SAW machine in operation

The basic SAW equipment is shown in figure 3.2. For semi-automatic SAW system, it consists of a welding power source, a wire feeder and control system, an automatic welding head, a flux hopper and a travel mechanism which usually consists of a travelling carriage and rails. In some machines, clamps may be provided on to clamp

the work pieces in perfect alignment with each other. In modern machines a system is provided for the recovery of the unused flux from the base plate and to transport it back to the flux hopper. This reduces the post weld operations to be performed on the base plate and speeds up the process.

3.1.3 Process Variables

In SAW since the operator cannot see the bead while the welding is in progress it is very important that the parameters must be set with great accuracy. All the variables have a certain effect upon the bead geometry and rate of the deposit weld material. It is very essential to set several variables to correct range before starting SAW for achieving good quality welds. Following are the Process variables in SAW:

- Welding current

- Arc voltage

- Travel speed

- Size of electrode

- Electrode stick out

- Heat input rate

Welding Current:

It controls the melting rate of the electrode and thereby the weld deposition rate. It also controls the depth of penetration. Too high a current causes excessive weld reinforcement, which is wasteful, and burn through in case of thinner plates or in badly fitted joints, which are not properly backed. Excessive current also produces too narrow bead and undercut. Excessively low current gives an unstable arc.

Arc Voltage

The arc voltage varies in direct proportion to the arc length. With the increase in arc length the arc voltage increases and thus more heat is available to melt the metal

and the flux. However, increased arc length means more spread of the arc column; this leads to increase in weld width and volume of reinforcement while the depth of penetration decreases. The arc voltage varies with the welding current and wire diameter. Flux consumption is also increased as more flux is melted at higher voltage.

Travel Speed:

For a given combination of welding current and arc voltage, increase in welding speed results in lesser penetration, lesser weld reinforcement and lower heat input rate Excessively high travel speed, decreases fusion between the weld deposit and the parent metal, increases the tendencies for undercut ,porosity and irregular bead shape. As the speed decreases, penetration and reinforcement increases but too slow a speed results in poor penetration because the molten metal flows ahead of the arc. Excessively high welding speed decreases the wetting action.

Size of Electrode:

For a given welding current, a decrease of wire diameter results in increase in current density. This results in a weld with deeper penetration but somewhat reduced width. The submerged arc welding process usually employs wires of 2 to 5 mm diameter, thus for deeper penetration at low currents a wire diameter 2 to 3 mm is best suited.

Electrode Stick out:

It is also termed as electrode extension. It refers to the length of electrode between end of contact tube and the arc, which is subjected to resistance heating at the high current densities used in the process. Short welding wire extension results in deeper penetration due to low resistive heating (I^2R), while long extension results in shallow penetration due to high resistive heating. Higher resistive heating due to long

extension however results in increase in welding wire temperature and metal deposition rate.The longer the stick out, the greater is the deposition rate accompanied by a decrease in penetration. Hence longer stick-out is avoided when deep penetration is desired.

Heat Input Rate:

The heat input rate is directly proportional to the current and arc voltage and inversely proportional to the travel speed, as the formula is given by

HIR= VxA/ S

Where, HIR= heat input rate in j/mm

V = Arc voltage

A= welding current (amp)

S= Arc travel speed in mm/sec

For a given joint thickness, higher the heat input rate the lower is the cooling rate of the weld metal and heat affected zone of parent metal and vice versa. Heat input rate has an important bearing on the weld metal microstructure and the final microstructure of HAZ and thereby on the toughness. Heat input if suitably controlled can produce suitable microstructure for different applications, for eg. A very high heat input rate followed by a high rate of cooling results in increased hardness of the weld metal.

3.1.4 Nomenclature of weld bead:

Weld Bead Geometry - The mechanical properties of the welded joints greatly depend on weld bead geometry, which in turn, is influenced by welding parameters like arc current, arc voltage, and arc travel speed. The bead geometry is specified by weld bead width, reinforcement height, reinforcement area, penetration height, penetration area and the contact angle of weld bead etc as shown in figure 3.3.

A_p	Penetration Area	
A_r	Reinforcement area	
α	Angle of convexity	
β	Angle of entry	
A_t	$A_p + A_r$ Total weld bead area	

$$\% D = \frac{A_P}{A_t} 100 = \% \text{ dilution}$$
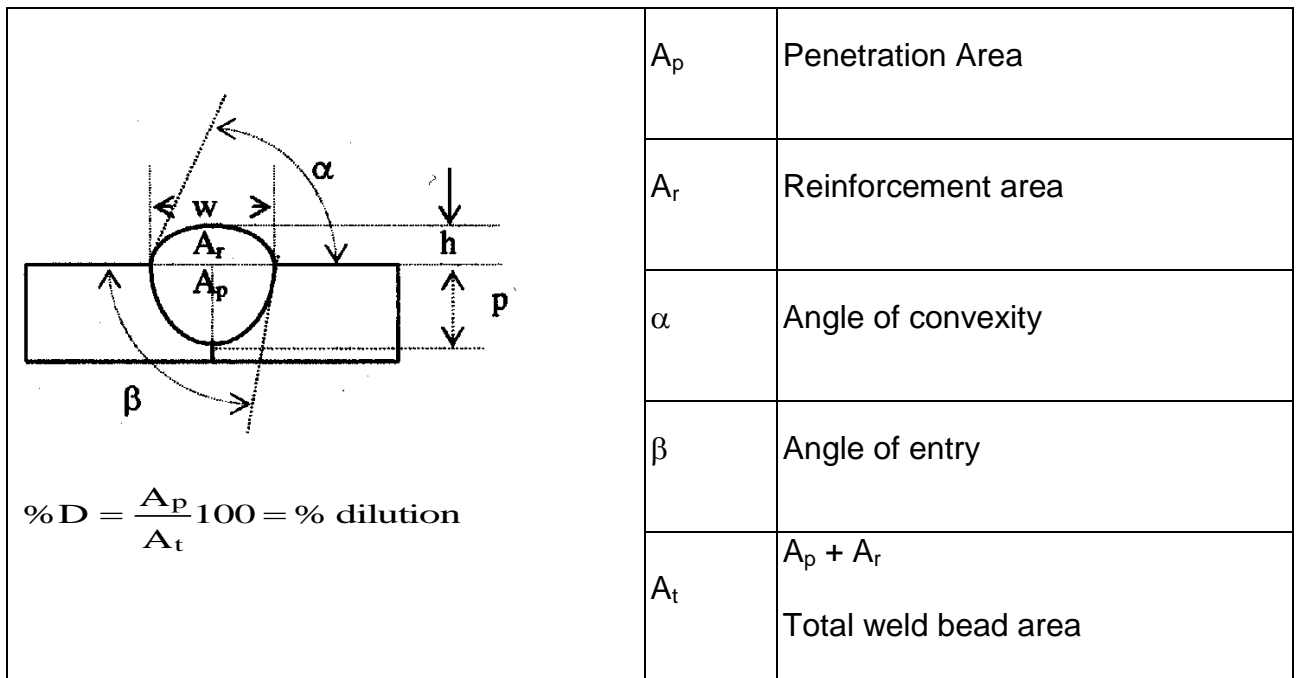
Figure 3.3: Weld Bead Nomenclature

The Weld Bead Width is the maximum width of the weld metal deposited. It increases with arc current, arc voltage; electrode weaving and decreases as arc travel speed increases.

Penetration Height or simply penetration is the distance from base plate top surface to the maximum depth of the weld nugget. Penetration determines the load carrying capacity of a welded structure.

Penetration Area is that covered by the fusion line below the base metal level. Penetration area affects the weld strength.

Reinforcement Height is the maximum distance between the base metal level and the top point of the deposited metal.

Reinforcement Area is one included between the contour line of the deposited metal above the base metal level.

3.1.5 SAW Wire

SAW is normally operated with a single wire on either AC or DC current. Common variants are:

- twin wire

- triple wire

- single wire with hot wire addition

- metal powder addition

All contribute to improved productivity through a marked increase in weld metal deposition rates and/or travel speeds. When joining steel the wire shall be of the same chemical composition as the base material or over-alloyed

3.1.6 SAW Fluxes [37]

Fluxes are chemical compound used to prevent oxidation and other unwanted chemical reactions. They help to make the welding process easier and ensure the making of a good, sound weld. Most metals in their molten condition become oxidized by the absorption of oxygen from the atmosphere .To make certain that amount of oxidation is kept a minimum, that any oxides formed are dissolved or floated off, and that welding is made as easy and free from difficulties as possible, fluxes are used. The flux is specially formulated to be compatible with a given electrode wire type so that the combination of flux and wire yields desired mechanical properties.

The welding flux must have the following features:

1. it must not evolve appreciable amount of gases under intense heat

2. It should be granular in form and should be capable of flowing freely through the flux feeding tubes of standard welding equipment

3. It should have arc initiators and arc stabilizers

4. It should have slag formers in the form of metallic oxides CaO, MgO, FeO etc. which will aid the formation of slag and thus will protect the weld zone from

atmospheric contamination or oxidation. The slag also helps in concentrating the heat and allows deeper penetration for SAW.

5. It may have alloying elements like Mn, Si for fortification of the weld.

The properties of the flux enables submerged arc welds to be made over a wide range of welding currents, voltage and speeds, each of which can be controlled independently of the other. Thus one can obtain welded joints of desired shapes, chemistry and mechanical properties by using an appropriate welding procedure.

SAW fluxes can be classified into two main groups:

- According to the method of manufacturing.

- According to the chemical nature.

<u>According to the method of manufacturing</u>

SAW can be classified according to the methods by which they are manufactured. There are mainly two methods of manufacturing the flux.

a. Fused Fluxes: The constituents such as quartz, limestone and manganese dioxide (MnO_2) with small quantities of fluorspar and aluminium oxide (Al_2O_3) are melted in an electric arc furnace where the manganese dioxide (MnO_2) is reduced to MnO. When the melt attains the state of a glossy paste it can be cooled, crushed and then grounded, and suitable grain size obtained by sieving, the grains being about 0.2-1.6 mm diameter. This type of flux is homogeneous and was the first type of flux used.

b. Agglomerated Fluxes: These are more easily manufactured than the fused type, being made at a lower temperature. They are heterogeneous because they include compounds in powder form whose grains join together by the agglomeration process and make larger grains, each grain having the correct proportion of each component. The dry powder is fed into a rotating disc with the

addition of water glass (a concentrated and viscous solution of sodium and potassium silicate) as a binding agent. The grains are then furnace- dried at about 700-800 ^{o}C and then sieved to give grain somewhat the same as for fused flux, 0.2-1.6 mm.

<u>According to the chemical nature</u>

Basicity is calculated from a flux's chemical components, independently of the wire. The chemical nature of a welding flux can be expressed as the basicity or Basicity index.
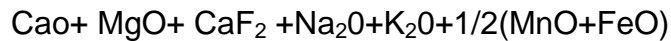
$$B \text{ (Basicity)} = \frac{Cao+ MgO+ CaF_2 + Na_20 + K_20 + 1/2(MnO+FeO)}{SiO_2 + 1/2(Al_2O_3 + TiO_2 + ZrO_2)}$$
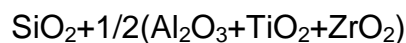
The formula of basicity or Basicity index is based upon the ratio of basic oxide to acidic oxides. The formula shows that low basicity fluxes contain more multiple oxides. A certain amount of atomically bonded oxygen is favourable for the weld microstructure. Based on chemical nature welding fluxes can thus be divided as shown in table 3.1.

Table 3.1 : Classification of flux based on chemical nature

Welding flux	Basicity	Melting point (^{o}C)	Typical Oxygen Level
Acidic	< 0.9	1100-1300	>750ppm
Neutral	=0.9-1.2	1300-1500	550-750 ppm
Basic	>1.2-2.0	>1500	300-550 ppm
High Basic	>2.0	>1500	< 300 ppm

Higher basicity gives better impact values, but reduces features such as welding speed, parameter envelope or fine rippling of the weld bead. It is therefore beneficial to choose the lowest possible flux basicity at the specified toughness.

3.1.7 Advantages of Submerged Arc Welding process:

- High deposition rates (over 45 kg/h have been reported).

- Deep weld penetration.

- Sound welds are readily made (with good process design and control).

- High speed welding of thin sheet steels up to 5 m/min is possible.

- Minimal welding fume or arc light is emitted.

- Practically no edge preparation is necessary.

- The process is suitable for both indoor and outdoor works.

- Distortion is much less.

- Welds produced are sound, uniform, ductile, corrosion resistant and have good impact value.

- Single pass welds can be made in thick plates with normal equipment.

- The arc is always covered under a blanket of flux, thus there is no chance of spatter of weld.

- 50% to 90% of the flux is recoverable.

3.1.8 Limitations of SAW process:

- Limited to ferrous (steel or stainless steels) and some nickel based alloys.

- Normally limited to the flat, horizontal positions

- Normally limited to long straight seams or rotated pipes or vessels.

- Requires relatively troublesome flux handling systems.

- Flux and slag residue can present a health & safety concern.

- Requires inter-pass and post weld slag removal.

<u>3.1.9 Applications of SAW process:</u>

SAW is ideally suited for longitudinal and circumferential butt and fillet welds. However, because of high fluidity of the weld pool, molten slag and loose flux layer, welding is generally carried out on butt joints in the flat position and fillet joints in both the flat and horizontal-vertical positions. For circumferential joints, the work piece is rotated under a fixed welding head with welding taking place in the flat position. Depending on material thickness, either single-pass, two-pass or multi-pass weld procedures can be carried out. There is virtually no restriction on the material thickness, provided a suitable joint preparation is adopted. Most commonly welded materials are C-Mn steels, low alloy steels and stainless steels, although the process is capable of welding some non-ferrous materials with judicious choice of electrode filler wire and flux combinations. Major application in industry:

- Used in manufacturing of ship and heavy structural parts.

- Nowadays it is widely used in repairing of machine parts by depositing cladding and hard facing.

- Fabrication of pipes, penstocks, pressure vessels, boiler, railroad, structure of railway coaches and locomotive.

3.2 Artificial Neural Network

<u>3.2.1 Introduction</u>

An Artificial Neural Network (ANN), usually called neural network (NN), is a mathematical model or computational model that is inspired by the structure and/or functional aspects of biological neural networks. A neural network consists of an interconnected group of artificial neurons, and it processes information using a connectionist approach to computation. In most cases an ANN is an adaptive system that changes its structure based on external or internal information that flows

through the network during the learning phase. ANN can identify and learn co-related patterns between input data sets and the corresponding target values **[29-31]**.
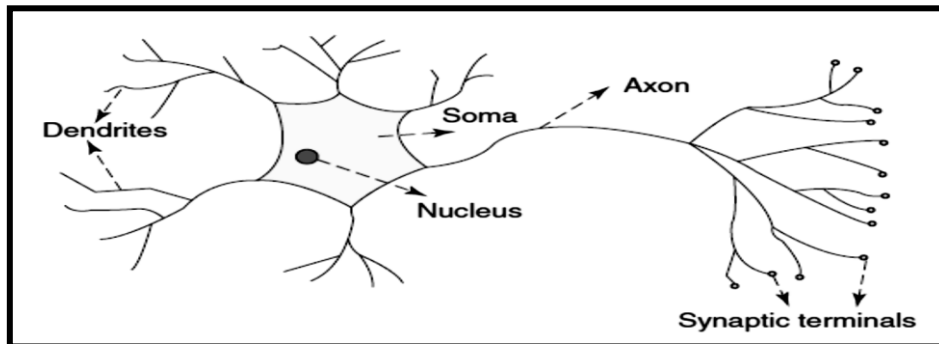
Figure 3.4 Basic structure of human neuron

ANN is basically a mathematical analogy of human brain. The advantage of the brain is its effective use of massive parallelism, the highly parallel computing structure, and the imprecise information-processing capability. The human brain is a collection of more than 10 billion interconnected neurons. A neuron, like any human cell, has a membrane that separates internal metabolic events from the environment and allows them to proceed in organized, controlled ways.

A neuron contains many short slender extensions, called Dendrites. Dendrites serve as the "input signals" for the neuron, receiving stimuli from other neurons and are connected to the cell body or soma, where the cell nucleus is located. Extending from the cell body is a single long fibre called the *axon*, which eventually branches into strands and sub strands, and is connected to other neurons through synaptic terminals or synapses. The singular axon serves as the output terminal of the neuron by which nerve impluses are sent to other cells. Neurons are not physically connected to each other. They communicate via the exchange of the neurotransmitters. Between Axon terminals of one neuron, called the presynaptic neuron and a Dendrite of another neuron, called the postsynaptic neuron, is a small gap known as a Synapse. Each neuron is a cell (Figure 3.4) that uses biochemical

reactions to receive, process, and transmit information. The transmission of signals from one neuron to another at synapses is a complex chemical process in which specific transmitter substances are released from the sending end of the junction. The effect is to raise or lower the electrical potential inside the body of the receiving cell. If the potential reaches a threshold, a pulse is sent down the axon and the cell is 'fired'.

In modern software implementations of artificial neural networks, the approach inspired by biology has been largely abandoned for a more practical approach based on statistics and signal processing. In some of these systems, neural networks or parts of neural networks (such as artificial neurons) are used as components in larger systems that combine both adaptive and non-adaptive elements. What they do have in common, however, is the principle of non-linear, distributed, parallel and local processing and adaptation. The word *network* in the term 'artificial neural network' refers to the inter–connections between the neurons in the different layers of each system .More complex systems will have more layers of neurons with some having increased layers of input neurons and output neurons. The synapses store parameters called "weights" that manipulate the data in the calculations.

3.2.2 Processing element of ANN

A processing element is generally a simple device that receives a number of input signals that may or may not generate an output signal based upon those signals. For each input (X_i) there is a relative weight(W_i) associated with it such that the effective input to the processing element is the weighted total input(I).

$$I = \sum_{i=1}^{n}(w_i \cdot x_i)$$

The output(Y) is computed as a result of a transfer function (f) of the weighted input, or Y = f (I) **[40]**. Normally, the transfer function for a given processing element is fixed at the time that the network is constructed. This transfer function, also known as an input-output function, generally falls into one of three classes: Threshold, Linear, and sigmoidal

  a. Threshold Units: In threshold type processing elements; the weighted input is compared to an arbitrary threshold (T). If the input is less than the threshold value, then the processing element does not fire and no output signal is generated.

  b. Linear Units: A network that computes real-valued functions needs processing elements whose transfer functions produce real-valued outputs. The simplest such type is the linear unit, whose output signal equals its weighted sum input, thus giving a real-valued output, albeit linear in nature.

  c. Sigmoidal Units: the problem with linear type processing elements is that their transfer functions are not differentiable sothe networks using linear type processing elements are difficult to train. To overcome this limitation smooth nonlinear transfer functions, which are continuous and differentiable everywhere, are often used. Of these, the sigmoidal type is most popular. The output of a sigmoidal unit asymptotically goes to 1 as the weighted sum of its inputs approaches positive infinity and to 0 as the weighted sum of its inputs approaches negative infinity. This function is defined as: f (x) = 1/(1 + e(-x)), where x is the net input to the unit.
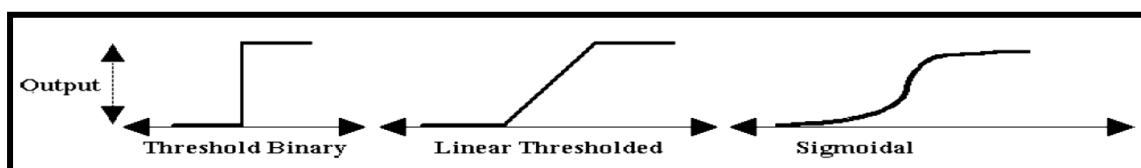
Figure 3.5: the 3 basic classes of transfer functions

Figure 3.5 summarizes the three classes of processing elements. The horizontal axis for each type represents the net input showing a higher weighted sum as you go from left to right. The vertical axis represents the activity of the output going from lower to higher as it goes away from the horizontal axis.

<u>3.2.3 Learning of ANN</u>

What has attracted the most interest in neural networks is the possibility of *learning* **[41]**. Given a specific *task* to solve, and a *class* of functions F, learning means, using a set of *observations* to find $f^* \in F$ which solves the task in some *optimal* sense. This entails defining a cost function C(f) such that, for the optimal solution f^*, $C(f^*) \leq C(f)$ $\forall f \in F$ (i.e., no solution has a cost less than the cost of the optimal solution). Learning algorithms search through the solution space to find a function that has the smallest possible cost. For applications where the solution is dependent on some data, the cost must necessarily be a *function of the observations*; otherwise we would not be modeling anything related to the data. There are three major learning paradigms **[42]** each corresponding to a particular abstract learning task.

These are supervised learning, unsupervised learning and reinforcement learning.

a.) Supervised learning: In supervised learning, we are given a set of example pairs $(x,y), x \in X, y \in Y$ and the aim is to find a function $f:X \to Y$ in the allowed class of functions that matches the examples. In other words, we wish to *infer* the mapping implied by the data; the cost function is related to the mismatch between our mapping and the data and it implicitly contains prior knowledge about the problem domain. Tasks that fall within the paradigm of supervised learning are pattern recognition (also known as classification) and regression (also known as function approximation).

b.) Unsupervised learning: Unsupervised learning refers to the problem of trying to find hidden structure in unlabeled data. Since the examples given to the learner are unlabeled, there is no error or reward signal to evaluate a potential solution. In unsupervised learning, some data x is given and the cost function to be minimized, that can be any function of the data x and the network's output, f. The cost function is dependent on the task and it can be much complicated. Its form depends on the application.

c.) Reinforcement learning: Reinforcement Learning is concerned with how an *agent* ought to take actions in an environment so as to maximize some notion of cumulative reward. In reinforcement learning, data are usually not given, but generated by an agent's interactions with the environment. At each point in time , the agent performs an action and the environment generates an observation and an instantaneous cost , according to some usually unknown dynamics. The aim is to discover a policy for selecting actions that minimizes some measure of a long-term cost; i.e., the expected cumulative cost.

3.2.4 Artificial Neural Network architecture:

Artificial Neural networks are mathematical entities that are modeled after existing biological neurons found in the brain. All the mathematical models are based on the basic block known as artificial neuron. A simple neuron is shown in fig 3. 6.This is a neuron with a single R-element input vector as shown below. Here the individual element inputs are multiplied by weights and the weighted values are fed to the summing junction. Their sum is simply Wp, the dot product of the (single row) matrix W and the vector p.
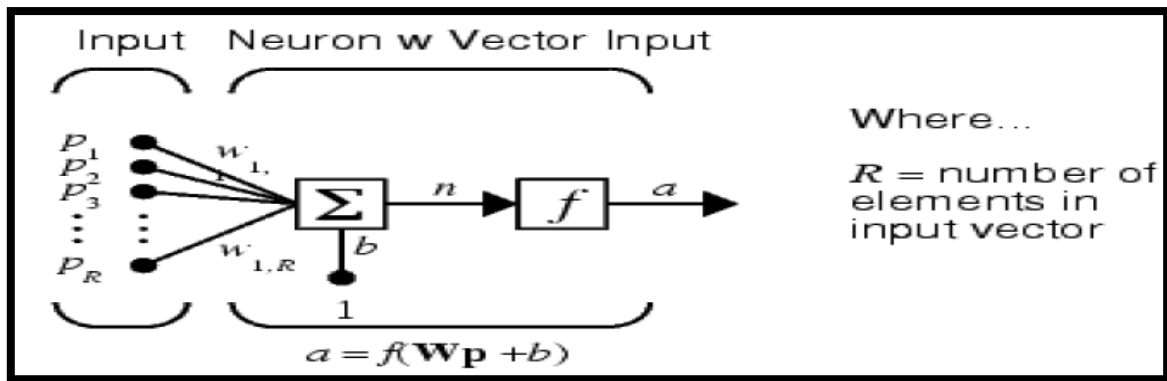
Figure 3.6: Simple Neuron

The neuron has a bias b, which is summed with the weighted inputs to form the net input n. This sum, n, is the argument of the transfer function f. Figure 3.6 can be represented in a more compact form as figure 3.7.
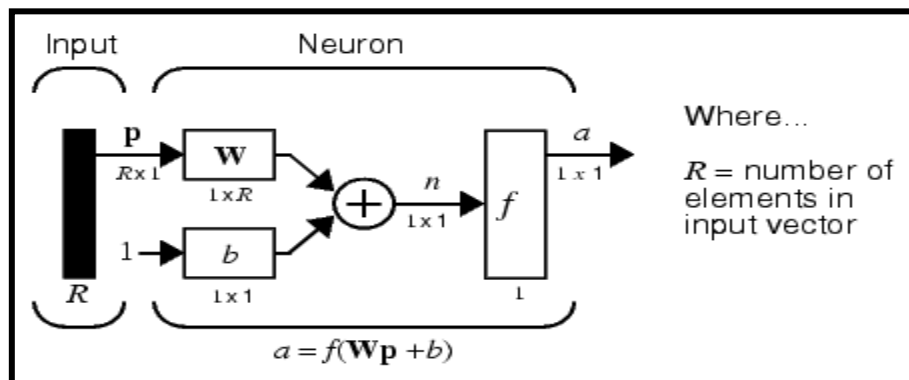
Figure 3.7 Simple neuron in vector notation

One Layer Network: A one-layer network with R input elements and S neuron is shown in Fig 3.8. In this network, each element of the input vector p is connected to each neuron input through the weight matrix W. The ith neuron has a summer that gathers its weighted inputs and bias to form its own scalar output n(i).
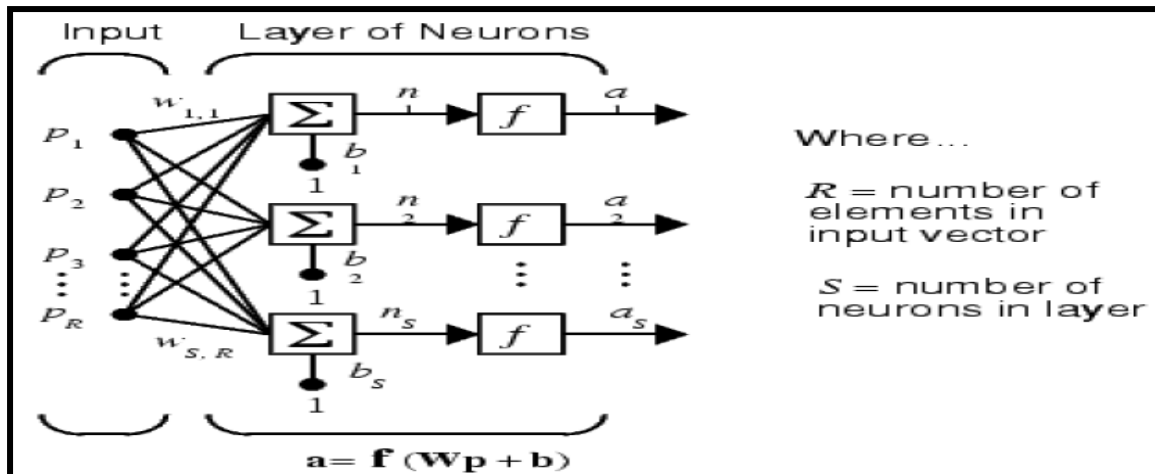
Figure 3.8: One layer Network

It is common for the number of inputs to a layer to be different from the number of neurons (i.e., R≠S) **[46]**. A layer is not constrained to have the number of its inputs equal to the number of its neurons. We can create a single (composite) layer of neurons having different transfer functions simply by putting two of the networks shown earlier (figure 3.6) in parallel. Both networks would have the same inputs, and each network would create some of the outputs. The input vector elements enter the network through the weight matrix W. it can be represented vectorially as figure 3.9.
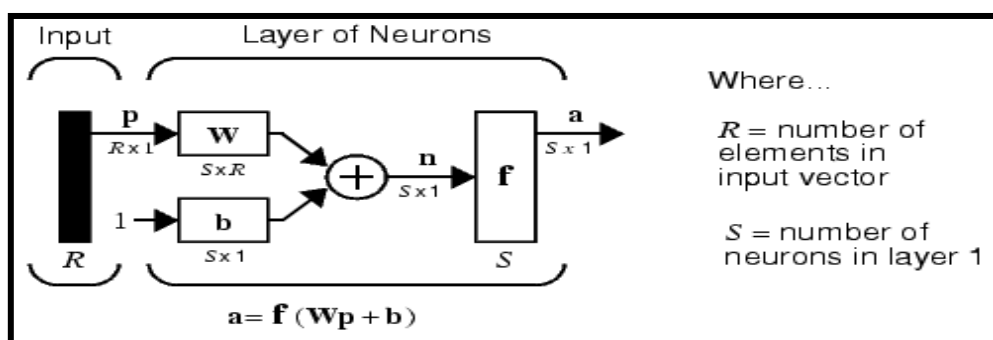
Figure 3.9 One Layer Networks in Vector Notation

Multi-layer network: A network can have several layers. Each layer has a weight matrix W, a bias vector b, and an output vector a. To distinguish between the weight

34

matrices, output vectors, etc., for each of these layers in our figures, we append the number of the layer as a superscript to the variable of interest. We can see the use of this layer notation in the three-layer network shown in Figure 3.10 below.
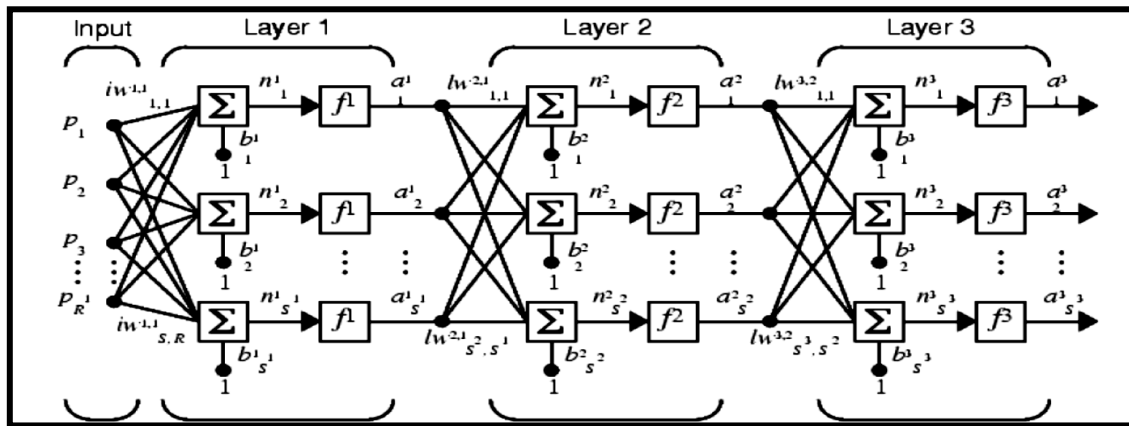
Figure 3.10: Multi-Layer network

The network shown above has R1 inputs, S1 neurons in the first layer, S2 neurons in the second layer, etc. It is common for different layers to have different numbers of neurons. A constant input 1 is fed to the biases for each neuron. Note that the outputs of each intermediate layer are the inputs to the following layer. Thus layer 2 can be analyzed as a one-layer network with S1 inputs, S2 neurons, and an S2 x S1 weight matrix W2. The input to layer 2 is a1; the output is a2. Now that we have identified all the vectors and matrices of layer 2, we can treat it as a single-layer network on its own. This approach can be taken with any layer of the network. The layers of a multilayer network play different roles. A layer that produces the network output is called an output layer. All other layers are called hidden layers. The three-layer network shown earlier has one output layer (layer 3) and two hidden layers (layer 1 and layer 2). It is shown in vector notation in Figure 3.11.
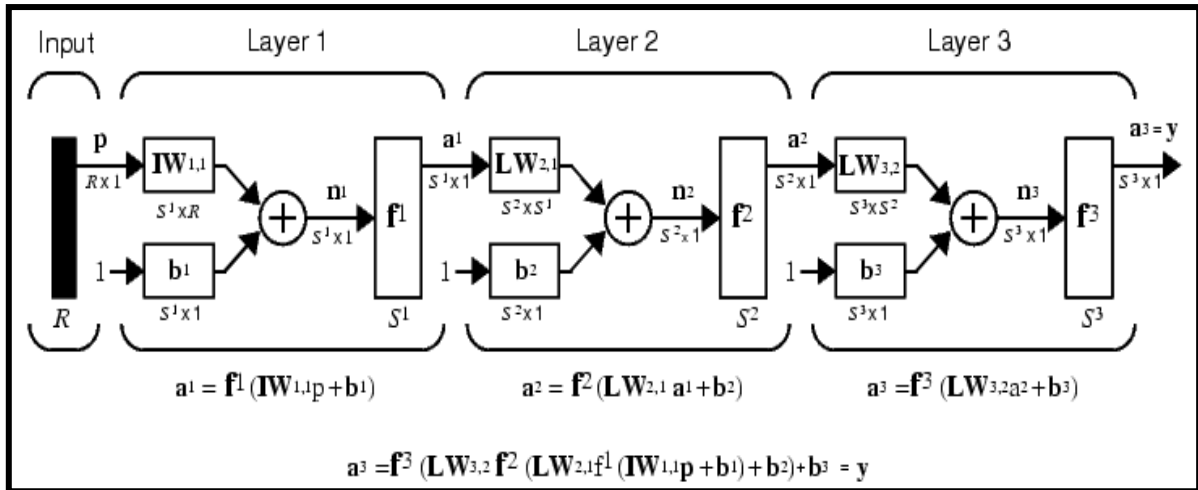
Figure 3.11: Multi-Layer Network in Vector Notation

Multiple-layer networks are quite powerful. For instance, a network of two layers, where the first layer is sigmoid and the second layer is linear, can be trained to approximate any function with acceptable degree of accuracy **[40]**. Here we assume that the output of the third layer, a3, is the network output of interest, and we have labeled this output as y. We will use this notation to specify the output of multilayer networks. The previous networks considered are Feed Forward in the sense of the flow of information through the network.

3.3 Weld metallurgy

3.3.1Introduction

Welding metallurgy may be defined as the changes that occur in metals as a result of being joined by the welding process. These changes are manifested by changes in mechanical properties. Whenever we begin a discussion about metallurgy, we try to find out the changes brought about in the microstructure of the base metal and hence the changes in the mechanical properties of the base metal, a result of the welding **[35].** In welding metallurgy, we are concerned with the time the material is at an elevated temperature and the rate at which the heat energy is applied to the base during welding as well as the rate at which the heat energy is removed during

cooling after welding. Mild steel is an alloy of Iron and Carbon having carbon content from0.5 % to 0.3 %, 0.4%-0.7% manganese, 0.1%-0.5% Silicon and some traces of other elements such as phosphorous, it may also contain lead (free cutting mild steel) or sulphur (free cutting steel called re-sulphurised mild steel).

3.3.2 Microstructure of Mild Steel

The best way to understand the microstructural changes taking place in mild steel is through the Fe-C equilibrium diagram.
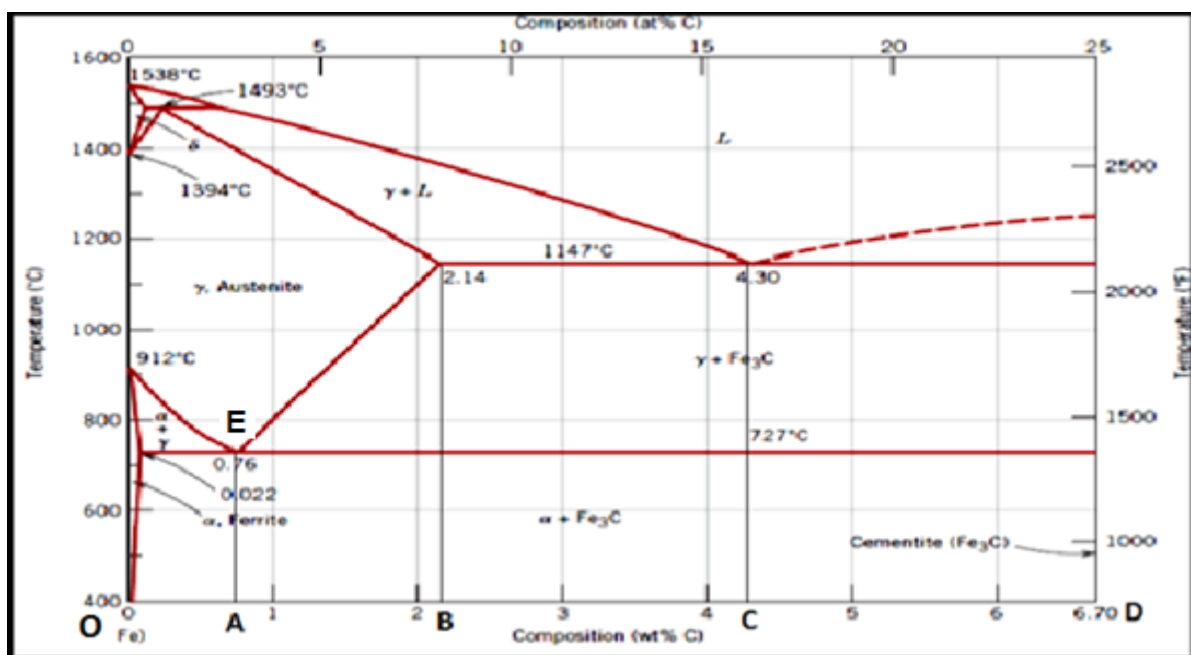
Figure 3.12 Iron-iron carbide phase diagram

The Iron exists in different allotropic forms as shown in the figure. The different allotropes of iron are:

a.) Alpha Ferrite: The solid solution of carbon in iron. At 0% C this is pure iron having BCC crystal structure. The maximum solubility of carbon in iron is 0.02% at 723°C. At 0°C temperature the solubility falls to 0.008%. The carbon atoms are located in the crystal interstices.

b.) Austenite: The solid solution of carbon in γ iron is called austenite. This has a FCC crystal structure with a high solubility for carbon compared with α

37

ferrite. The solubility reaches a maximum of 2.08% at 1148$^{\text{o}}$C. The solubility decreases to 0.8% at 723$^{\text{o}}$C. The carbon atoms are dissolved interstitially. The difference in solubility between the austenite and α Ferrite is the basis for the hardening of steels.

c.) Cementite: This is an inter-metallic compound which contains 6.67% C and 93.3% Fe. Cementite is a hard brittle compound with and orthorhombic crystal structure each unit cell has 12 Fe atoms and 4 C atoms. Cementite (Fe_3C) forms when the solubility limit of carbon in ferrite is exceeded below 727$^{\text{o}}$C (for compositions within the alpha + Fe_3C phase region). As indicated in Figure 3.12, Fe_3C will also coexist with the gamma phase between 727 and 1147$^{\text{o}}$C. Mechanically, cementite is very hard and brittle; the strength of some steels is greatly enhanced by its presence.

d.) Delta Ferrite: This is a solid solution of carbon in iron and has a BCC crystal structure. The maximum solubility or C in Fe is 0.09% at 1493$^{\text{o}}$C. This has no real practical significance in engineering.

Point E in figure 3.12 is called eutectoid point where, austenite converts into ferrite and cementite. This eutectoid reaction may be represented by

$$\gamma(0.76 \text{ wt\% C}) \underset{\text{heating}}{\overset{\text{cooling}}{\rightleftharpoons}} \alpha(0.022 \text{ wt\% C}) + Fe_3C (6.7 \text{ wt\% C})$$
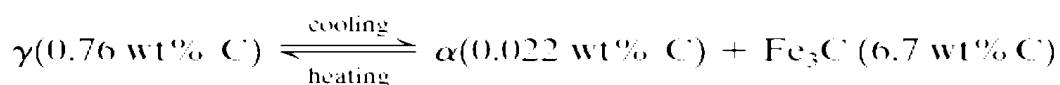
or, upon cooling, the solid austenite phase is transformed into iron and cementite.

The steel is classified according to the carbon content in it. Steel in the region

OA – Hypo Eutectoid steel

AB- Hyper Eutectoid steel

BC- Hypo Eutectic steel

CD- Hyper Eutectic steel

Mild steel with maximum Carbon content of 0.3% falls in the category of hypo eutectoid steel. The phase changes taking place in the mild steel when it cools from a higher temperature to room temperature is shown in figure 3.13.
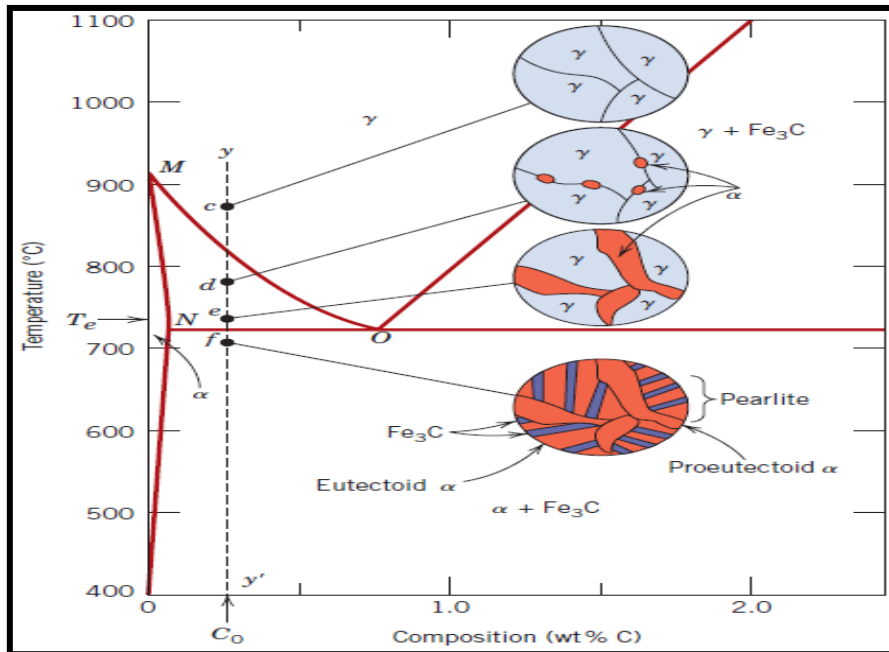
Figure 3.13 Microstructural changes taking place during cooling of mild steel from welding temperature to room temperature

At about, 875°C point *c*, the microstructure will consist entirely of grains of the gamma phase, as shown schematically in the figure. In cooling to point *d*, about 775°C, which is within the alpha +gamma phase region, both these phases will coexist as in the schematic microstructure. Most of the small alpha particles will form along the original gamma grain boundaries. Cooling from point *d* to *e*, just above the eutectoid but still in the alpha + gamma region, will produce an increased fraction of the alpha phase and a microstructure similar to that also shown: the alpha particles will have grown larger. As the temperature is lowered just below the eutectoid, to point *f*, all the gamma phase that was present at temperature T_e (and having the eutectoid composition) will transform to pearlite, according to the eutectoid reaction. There will be virtually no change in the alpha phase that existed at point *e* in crossing the eutectoid temperature—it will normally be present as a continuous matrix phase

39

surrounding the isolated pearlite colonies. The microstructure at point *f* will appear as the corresponding schematic inset of Figure 3.13. Thus the ferrite phase will be present both in the pearlite and also as the phase that formed while cooling through the alpha + gamma phase region. The ferrite that is present in the pearlite is called eutectoid ferrite*,* whereas the other, that formed above is termed proeutectoid (meaning pre- or before eutectoid) ferrite**,** as .Figure 3.16 is a photomicrograph of a 0.38 wt% C steel; large, white regions correspond to the proeutectoid ferrite. For pearlite, the spacing between the and Fe_3C layers varies from grain to grain; some of the pearlite appears dark because the many close spaced layers are unresolved at the magnification of the photomicrograph in Figure 3.14.
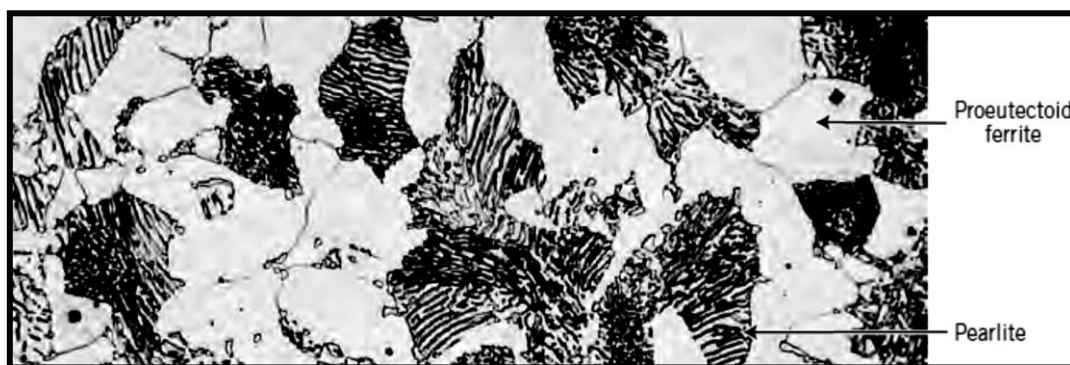
Figure 3.14: Photomicrograph of hypo eutectoid steel cooled from a high temperature to room temperature

Pearlite is mixture of alternate strips of ferrite and cementite in a single grain. The distance between the plates and their thickness is dependent on the cooling rate of the material; fast cooling creates thin plates that are close together and slow cooling creates a much coarser structure possessing less toughness. A fully pearlitic structure occurs at 0.76% Carbon. Further increases in carbon will create cementite at the grain boundaries, which reduces toughness but improves the hardness of the steel.

Martensite is produced when steel is cooled rapidly from austenite, the F.C.C structure rapidly changes to B.C.T (body centred tetragonal) leaving insufficient time for the carbon to form pearlite. This results in a distorted structure that has the appearance of fine needles. There is no partial transformation associated with martensite, it either forms or it doesn't. However, only the parts of a section that cool fast enough will form martensite; in a thick section it will only form to a certain depth, and if the shape is complex it may only form in small pockets. The hardness of martensite is solely dependent on carbon content; it is normally very high, unless the carbon content is exceptionally low.

3.3.3 Weld pool solidification [51-52]

Most knowledge of weld pool solidification is derived from the extrapolation of the knowledge of freezing of castings, ingots, and single crystals at lower thermal gradients and slower growth rates. Therefore, parameters important in determining microstructures in casting, such as growth rate (R), temperature gradient (G), undercooling (δT), and alloy composition determine the development of microstructures in welds as well. However, microstructure development in the weld zone is more complicated because of physical processes that occur due to the interaction of the heat source with the metal during welding, including re-melting, heat and fluid flow, vaporization, dissolution of gasses, solidification, subsequent solid-state transformation, stresses, and distortion. These processes and their interactions profoundly affect weld pool solidification and microstructure. During welding, where the molten pool is moved through the material, the growth rate and temperature gradient vary considerably across the weld pool. Along the fusion line the growth rate is low while the temperature gradient is steepest. As the weld centreline is approached, the growth rate increases while the temperature gradient

decreases. Consequently, the microstructure that develops varies noticeably from the edge to the centreline of the weld. In welds, weld pool solidification often occurs spontaneously by epitaxial growth on the partially melted grains. Since solidification of the weld metal proceeds spontaneously by epitaxial growth of the partially melted grains in the base metal, the weld zone grain structure is mainly determined by the base metal grain structure and the welding conditions. Crystallographic effects will influence grain growth by favouring growth along particular crystallographic directions, namely the easy growth directions. Conditions for growth are optimum when one of the easy growth directions coincides with the heat-flow direction. Thus, among the randomly oriented grains in a polycrystalline specimen, those grains that have one of their easy growth crystallographic axes closely aligned with heat-flow direction will grow at the expense of their neighbouring less favourably oriented grains. This is called competitive growth. Without additional nucleation, this will promote a columnar grain structure.
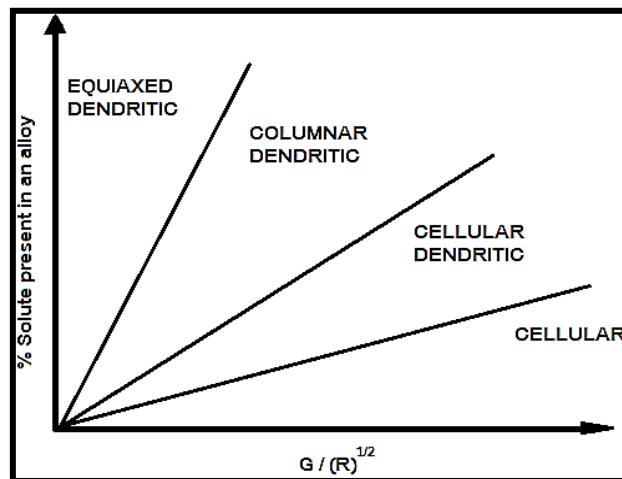
Figure 3.15: influence of grain growth rate R and temperature gradient G, on the pattern of solidification

Low values of $G/(R)^{1/2}$ indicate as increased tendency to constitutional super cooling thus favouring the dendritic mode of solidification. On the other hand steep temperature gradients in the liquid and slow growth rates favour cellular growth.

3.3.4 Zones in a weld [32-34]

If one looks closely at macrostructure of the weld zone he can clearly identify three distinct zones:
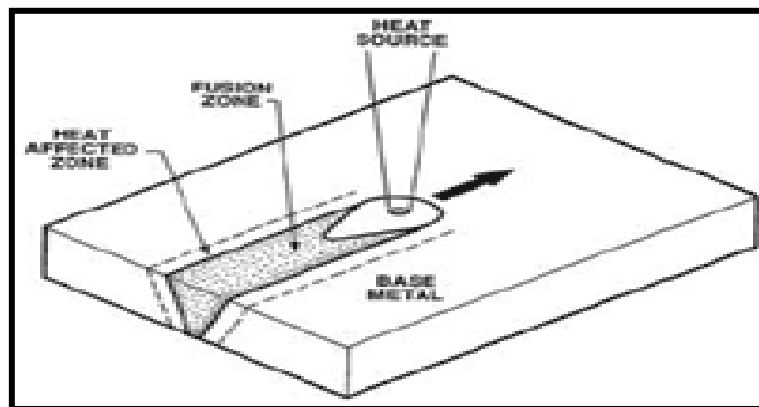
Figure 3.16: Regions in a weldment

Weld metal zone:

Weld metal zone is formed as the weld metal solidifies from the molten state. This is a mixture of parent metal, electrode, filler metal; the ratio depending upon the welding process used, the type of joint plate thickness. Weld metal zone is a cast metal of particular composition of mixture that has cooled; its microstructure reflects the cooling rate in the weld. Depending upon the chemical composition a martensitic structure in the weld indicates a very high cooling rate; fine pearlite and coarse pearlite shows comparatively slower cooling rates. From the molten weld pool the first metal solidifies epitaxially upon the solid grains of the un-melted base metal.

Depending upon the composition and solidification rates the weld solidifies in a cellular or dendritic growth mode. Both modes cause segregation of alloying elements and consequently the weld metal is less homogeneous on the micro level

43

than the base metal and therefore cannot be expected to have the same properties as wrought parent metal unless the filler metal in the as deposited condition has same properties as that of parent metal.

Heat Affected Zone:

It consists of parent metal that did not melt but was heated to high enough temperature for a sufficient period of time that grain growth occurred and mechanical as well as microstructural properties have been altered by the heat of welding. The HAZ is subjected to complex thermal cycle in which all temperatures from the melting range of the steel down to comparatively much lower temperatures are involved. HAZ usually consists of a variety of microstructures. These structures may range from very narrow regions of hard martensite to coarse pearlite. This renders HAZ the weakest area in weld. Except where there are obvious defects in the weld deposit, most welding failures originate in the HAZ. In SAW the HAZ consists of 3 sub zones

a. Grain growth region: It is immediately adjacent to the weld metal zone. In this zone the parent metal has been heated well above the upper critical temperature, this resulted in grain growth or coarsening of the structure. The maximum grain size and extent of this region increases as the cooling rate decreases.

b. Grain refined region: The refined zone indicates that in this region the parent metal has been heated to just above upper critical temperature where grain refinement is complete and finest grain structure exists. Complete recrystallization has taken place in this zone

c. Transition zone: Temperature exists between upper and lower recrystallization temperature where partial allotropic recrystallization takes place.

Unaffected parent metal: Outside the HAZ is the base metal which was not affected by the thermal cycles during welding.

3.4 Response Surface Methodology (RSM)

3.4.1 Introduction [**50]**

The *Response Surface Methodology* (*RSM*) is a collection of mathematical and statistical techniques useful for the modelling and analysis of problems in which a response of interest is influenced by several variables and the objective is to optimize this response. The most extensive application of RSM is particularly in situations where several input variables potentially influence some performance measure or quality characteristic of the product or process. This performance measure or quality characteristic is called Response. It is typically measured on continuous scale. Most of the real world application of RSM will involve more than one response. The input variables are sometimes called independent variables and they are subject to the control of the engineer or scientist, at least for the purpose of a test or an experiment.

In most *RSM* problems, the true response function *f* is unknown. In order to develop a proper approximation for *f*, the experimenter usually starts with a low-order polynomial in some small region. If the response can be defined by a linear function of independent variables, then the approximating function is a first-order model. A first-order model with 2 independent variables can be expressed as

$y = b_0 + b_1 x_1 + b_2 x_2 + e$

If there is a curvature in the response surface, then a higher degree polynomial should be used. The approximating function with 2 variables is called a second-order model:

$$y = b_0 + b_1 + b_2 + b_{11}x^2_{11} + b_{22} x^2_{22} + b_{12} x_{12} + e$$

In general all *RSM* problems use either one or the mixture of the both of these models. In order to get the most efficient result in the approximation of polynomials the proper experimental design must be used to collect data. Once the data are collected, the *Method of Least Square* is used to estimate the parameters in the polynomials. The response surface analysis is performed by using the fitted surface. The response surface designs are types of designs for fitting response surface.

3.4.2 Central Composite Design [43-45]

A Box-Wilson Central Composite Design commonly called 'a central composite design,' contains an imbedded factorial or fractional factorial design with centre points that is augmented with a group of `star points' that allow estimation of curvature. If the distance from the centre of the design space to a factorial point is ±1 unit for each factor, the distance from the centre of the design space to a star point is ±α with | α | > 1. The precise value of α depends on certain properties desired for the design and on the number of factors involved. Similarly, the number of centre point runs the design is to contain also depends on certain properties required for the design. Figure 3.17 schematically shows the generation of CCD for 2 factors.
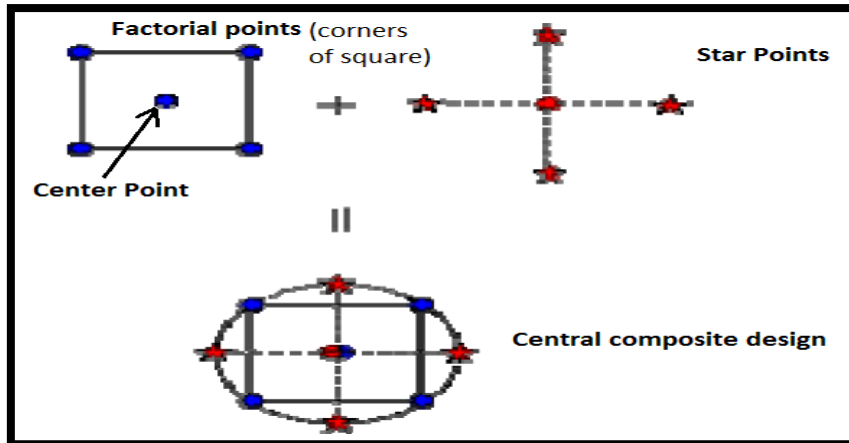
Figure 3.17 Generation of a central composite design for 2 factors

The number of star points in a central composite design is twice the number of factors in the design. There are 3 varieties of Central composite design. Table 3.2 gives a comparison between the 3 variants of the design.

Table 3.2 Comparison of the variants of Central Composite Design

Central Composite Design Type	Terminology	Design space covered for 2 factor CCD	Features
Circumscribed	CCC		These designs are fully rotatable and have circular, spherical or hyper spherical symmetry. They require 5 levels for each factor. Augmenting an existing factorial design with star points produces this design

Inscribed	CCI		Basically a CCI design is a scaled down CCC design with each factor level of the CCC design divided by α to generate the CCI design. The CCI design uses the factor settings as the star points and creates a factorial or fractional factorial design within those limits. This design also required 5 levels for each factor.
Face centred	CCF		In this design the star points are at the centre of each face of the factorial space, so = ± α 1. This variety requires 3 levels of each factor.

*As can be seen from Table 3.2, the CCC design covers the greatest design space, while the CCI covers the lowest design space. Both the CCC and CCI design are rotatable, while CCF is not rotatable.

3.5 Experimentation

The main aim of the project was to find the effect of input process variables on the bead geometry of SAW and to develop mathematical models to describe the relationship between the input and output variables. After that ANN modelling of the SAW process was done and it was compared with the RSM modelling. Metallurgical analysis was also done to co-relate the effects of input parameters on the microhardness and the micro structure of the welded specimen. To achieve the above mentioned objectives, following are the sequence of steps which were carried out:

1. Identification of important process control variables

2. Deciding the working range of the process control variables, viz. Arc Voltage (V), Current (A), Travel Speed (S) and Nozzle-to-plate-distance (N)

3. Developing the design matrix

4. Conducting the experiments as per the design matrix

5. Recording the responses viz. bead height (H), bead width (W) and bead penetration (P)

6. Developing the mathematical models

7. Checking the adequacy of the models

8. Finding the significance of co-efficient

9. Developing the final proposed models

10. Plotting of graphs and drawing conclusions

11. Development of an ANN architecture to model and to predict the bead geometry

12. Comparison of performances of RSM models and ANN models

13. Metallurgical analysis to co-relate the micro hardness and the micro structure of the welded material with the process variables

14. Discussion of the results

3.5.1 Identification of important process control variables

Based on the effect on weld bead geometry, ease of control and capability of being maintained at the desired level, four independently controllable process parameters were identified namely, the arc voltage (V); the welding current (A); the travel speed (S) and the nozzle-to-plate distance (N).the weld bead geometry parameters chosen for this study were bead height (H), bead width (W) and bead penetration (P).

3.5.2 Deciding the working range of the process control variables

Trial runs were conducted by varying one of the process parameters at a time while keeping the rest of them at constant value **[49-50]**. The working range was fixed by inspecting the bead for a smooth appearance and the absence of visible defects.

The upper and lower limits were coded as +2 and −2, respectively. The coded values for intermediate values can be calculated from the relationship:

$$X_i = \frac{2[2X - (X_{max} + X_{min})]}{(X_{max} - X_{min})}$$

Where, X_i is the required coded value of a variable X, when X is any value of the variable from X_{min} to X_{max}; X_{max} and X_{min} are the maximum and minimum levels of the variables. The selected process parameters and their upper and lower limits together with notations and units are given in Table 3.3.

Table 3.3: Process control parameters and their limits

Sl.No	PARAMETERS	Units	Notation	-2	-1	0	+1	+2
1	Current	Amperes	A	250	325	400	475	550
2	Arc Voltage	Volts	V	22	22.5	29	32.5	36
3	Travel speed	mm/sec	S	6	9	12	15	18
4	Nozzle to plate distance	Mm	N	20	23.5	27	30.5	34

3.5.3 Developing the design matrix

A fully rotatable 4 factor 5 level central composite design matrix was used for the experiment. To maintain rotatability the value of alpha is chosen as 2. A fully rotatable central composite design matrix covers greater design space than the factorial design matrix, thus resulting in greater accuracy of the established relationships [43]. Table 3.4 shows the 31 sets of coded conditions used to form the design matrix. The first 16 conditions have been formulated as per 2^4 (two levels and 4 factors) factorial design. These factorial points represents the variance optimal design for a first order or first order plus 2 factor interaction model. The next eight experimental conditions are called as Star points, i.e. keeping one factor at the lowest/highest level and the remaining factors at middle level. Addition of Star points

allow for efficient estimation of pure quadratic terms in case of existence of curvature in the system. Curvature is an indication of presence of interaction between 2 or more variables. The last seven experimental conditions are known as centre points i.e., keeping all the factors at the middle level and it is normally done to know the repeatability of the experimental procedures. Centre points provide information about the existence of curvature in the system. Thus the 31 experimental runs allowed the estimation of the linear, quadratic and the two way interactive effects of the welding variables on the bead geometry and provide results with greater accuracy while dealing with large number of factors **[22-25]**.

Table 3.4: Design matrix

Weld No.	*Trial No.*	*Input parameters*			
		V	*A*	*S*	*N*
1	5	-1	-1	-1	-1
2	7	+1	-1	-1	-1
3	3	-1	+1	-1	-1
4	9	+1	+1	-1	-1
5	1	-1	-1	+1	-1
6	6	+1	-1	+1	-1
7	4	-1	+1	+1	-1
8	6	+1	+1	+1	-1
9	10	-1	-1	-1	+1
10	13	+1	-1	-1	+1
11	23	-1	+1	-1	+1
12	18	+1	+1	-1	+1
13	15	-1	-1	+1	+1
14	26	+1	-1	+1	+1
15	29	-1	+1	+1	+1
16	27	+1	+1	+1	+1
17	24	-2	0	0	0

18	19	+2	0	0	0
19	31	0	-2	0	0
20	38	0	+2	0	0
21	22	0	0	-2	0
22	16	0	0	+2	0
23	12	0	0	0	-2
24	25	0	0	0	+2
25	30	0	0	0	0
26	11	0	0	0	0
27	14	0	0	0	0
28	17	0	0	0	0
29	20	0	0	0	0
30	8	0	0	0	0
31	21	0	0	0	0

3.5.4 Conducting the experiments as per the design matrix

The experiments were conducted at the Welding Laboratory of Delhi Technological University with the following experimental set-up:

The equipment used:

Figure 3.18: The SAW machine used for the experiments.

Machine Model - QSW800, Manufactured by- Quality Engineer (Baroda Pvt. Ltd.), A/18, Gujarat Estate, Dharamsingh Desai Marg, Chhani Road Baroda -390002

The welding wire used:

A 3.2 mm diameter copper coated mild steel wire manufactured by ESAB INDA LTD was used. Specification of filler wire used was (AWS-A5.17 EL-8).The chemical composition of filler wire was:

C   Mn   Si

0.10%   0.45%   0.02%

The base metal used:

For carrying out the research work, test specimens were prepared from 12 mm thickness AISI 1012 Mild steel plate. Dimension of each plate were 150x75x12mm. Composition of the base material as supplied by the supplier was as follows:

C   S   Mn   S   Cr   Ni

0.102% 0.179% 0.466%   0.0705%   0.036   0.022

Type of joint: Bead-on-plate joint

Flux:

The study was carried out by using available flux i.e. an agglomerated flux manufactured by ESAB INDIA LTD. The specification of the flux was:

Automelt Gr.II, Coding - AWS / SFA 5.17

F7AZ - EL8; F7PZ - EL8

The chemical composition was:

C   Mn   Sn

0.08%   1.00%   0.25%

Thirty-one sets of plates were welded as per the design matrix by selecting trials at random and welding was carried out. Figure 3.19 shows few samples in welded condition.

Figure 3.19: Welded samples

3.5.5 Recording the responses:

Two transverse specimens were cut from each welded plate. Figure 3.20 shows few of the cut samples.

Figure 3.20: Few samples in cut condition

These specimens were prepared by the usual metallurgical polishing methods and etched with 5% Nital (95% Alcohol + 5% Nitric Acid). The profile of the beads was traced with an optical profile projector. And the bead dimensions, *viz* bead height

(H), bead width (W) and bead penetration (P) were measured. The observed values of the H, W and P are given in Table 3.5

Table 3.5 Recording of responses

Weld No.	Input parameters				Responses		
	V	A	S	N	Bead height (H)	Bead width (W)	Bead Penetration (P)
1	-1	-1	-1	-1	2.38	10.55	3.94
2	+1	-1	-1	-1	2.54	12.43	5.08
3	-1	+1	-1	-1	3.07	9.76	5.12
4	+1	+1	-1	-1	2.79	13.14	6.4
5	-1	-1	+1	-1	2.03	10.27	3.05
6	+1	-1	+1	-1	1.98	9.26	3.59
7	-1	+1	+1	-1	1.89	9.37	4.79
8	+1	+1	+1	-1	1.99	9.42	5.37
9	-1	-1	-1	+1	1.81	9.17	3.33
10	+1	-1	-1	+1	1.66	11.21	3.18
11	-1	+1	-1	+1	3.23	9.48	7.31
12	+1	+1	-1	+1	2.72	12.79	5.77
13	-1	-1	+1	+1	2.09	8.08	2.6
14	+1	-1	+1	+1	2.08	9.74	2.08
15	-1	+1	+1	+1	3.66	8.48	6.06
16	+1	+1	+1	+1	3.05	10.58	4.19
17	-2	0	0	0	2.72	8.82	4.44
18	+2	0	0	0	2.13	11.4	5.3
19	0	-2	0	0	1.96	8.4	2.35
20	0	+2	0	0	3.20	9.34	5.76
21	0	0	-2	0	2.31	13.95	4.88
22	0	0	+2	0	2.1	9.33	3.24
23	0	0	0	-2	1.96	10.4	4.34
24	0	0	0	+2	2.07	9.87	3.43
25	0	0	0	0	2.29	10.55	3.6
26	0	0	0	0	2.14	11.15	3.66

27	0	0	0	0	1.79	10.73	4.37
28	0	0	0	0	2.2	11.68	4.17
29	0	0	0	0	1.93	11.4	3.94
30	0	0	0	0	1.75	11.19	4.3
31	0	0	0	0	1.94	10.72	3.68

Chapter 4

DEVELOPMENT OF MATHEMATICAL MODELS

Mathematical models can be proposed as the basis for a control system for the SAW process to predict particular weld bead geometry and to establish the interrelationship between weld process parameters to weld bead geometry. These mathematical models can be fed into computer to predict the weld bead geometry for a particular combination of input parameters. The experimental data were used to develop nonlinear models, and analysis of the models was carried out through ANOVA and surface plots. Design expert 8.5.0 was used for this purpose.

4.1 Developments of mathematical models:

The response function representing any of the weld-bead dimensions can be expressed as:

Y. = f (V, A, S, N)

Where,

Y= Weld bead response; V= Arc voltage; A= Current; S= Welding speed;

N= Nozzle-to-plate distance.

The relationship selected being a second-degree response surface expressed as follows:

$Y=b_0+b_1V+b_2A+b_3S+b_4N+b_{12}VA+b_{13}VS+b_{14}VN+b_{23}AS+b_{24}AN+b_{34}SN+b_{11}V^2+b_{22}A^2+b_{33}S^2+b_{44}N^2$

Where b_0, is constant and b_1, b_2, b_3, b_4, b_{11}, b_{22}, b_{33}, b_{44}, b_{12}, b_{13}, b_{14}, b_{23}, b_{24}, b_{34} are co-efficient of the model.

4.2 Evaluation of the Co Efficient of the Model:

The values of the co efficient of the response surface were calculated using regression analysis. The calculations were carried out using Design Expert 8.5.0 and values listed in Table 4.1.

Table 4.1 estimated value of the co-efficients of the model

Sl. No.	Coefficient	Reinforcement Height (h)	Width (w)	Penetration (p)
1	b_0	2.01	11.06	3.96
2	b_1	-0.11	0.77	0.049
3	b_2	0.35	0.17	1.04
4	b_3	-0.077	-0.94	-0.49
5	b_4	0.077	-0.24	-0.19
6	b_{12}	-0.078	0.27	-0.16
7	b_{13}	0.013	-0.49	-0.12
8	b_{14}	-0.076	0.30	-0.48
9	b_{23}	-0.063	-0.082	1.25E-003
10	b_{24}	0.26	0.25	0.38
11	b_{34}	0.27	0.11	-0.057
12	b_{11}	0.13	-0.23	0.27
13	b_{22}	0.17	-0.54	0.069
14	b_{33}	0.071	0.15	0.071
15	b_{44}	0.024	-0.22	0.027

The bead geometry parameters were expressed as a non –linear function of the input process parameters as follow:

Bead height = $2.01-0.11(V)+0.35(A)-0.077(S)+0.077(N)-0.078(VA)+0.013(VS)-0.076(VN)-0.063(AS)+0.26(AN)+0.27(SN)+0.13(V^2)+0.17(A^2)+0.071(S^2)+0.024(N^2)$

Bead width = $11.06+0.77(V)+0.17(A)-0.94(S)-0.24(N)+0.27(VA)-0.49(VS)+0.30(VN)-0.082(AS)+0.25(AN)+0.11(SN)-0.23(V^2)-0.54(A^2)+0.15(S^2)-0.22(N^2)$

Bead penetration= 3.96+0.049(V)+1.04(A)-0.49(S)-0.19(N)-0.16(VA)-0.12(VS)-0.48(VN)+1.250E-003(AS)+0.38(AN)-0.057(SN)+0.27(V^2)+0.069(A^2)+0.071S^2+0.027(N^2)

4.3 Checking adequacy of the model

The analysis of variance (ANOVA) technique was used to check the adequacy of the developed models. As per this technique:

(a) The F-ratio of the developed model is calculated and is compared with the standard tabulated value of F-ratio for a specific level of confidence

(b) If calculated value of F-ratio does not exceed the tabulated value, then with the corresponding confidence probability the model may be considered adequate. For our analysis, we have taken a confidence interval of 95%.

4.3.1 Response: Bead Height

Table 4.2 ANOVA for bead height:

Source	Sum of squares	Df	Mean square	F value	p-value Prob> F
Model	7.15	14	0.51	14.07	<0.0001 (significant)
b_1- arc voltage	0.27	1	0.27	7.34	0.0155
b_2-current	2.88	1	2.88	79.20	<0.0001
b_3-travel speed	0.14	1	0.14	3.93	0.0650
b_4-NPD	0.14	1	0.14	3.93	0.0650
b_{12}	0.098	1	0.098	2.69	0.1206
b_{13}	2.765E-003	1	2.765E-003	0.076	0.7865
b_{14}	0.092	1	0.092	2.52	0.1321
b_{23}	0.064	1	0.064	1.76	0.2039
b_{24}	1.11	1	1.11	30.49	<0.0001
b_{34}	1.18	1	1.18	32.56	<0.0001
b_{11}	0.46	1	0.46	12.57	0.0027

b$_{22}$	0.78	1	0.78	21.47	0.0003
b$_{33}$	0.15	1	0.15	4.01	0.0624
b$_{44}$	0.016	1	0.016	0.045	0.5124
Residual	0.58	16	0.036		
Lack of fit	0.32	10	0.032	0.75	0.6735(not significant)
Pure error	0.26	6	0.043		
Cor total	7074	30			

The model F value of 14.07 implies that the model is significant. There is only a 0.01% chance that a "Model F- value" this large could occur due to noise. Values of "Prob>F" less than 0.0500 indicates that model terms are significant. In this case b1, b2, b24, b34, b11, b22 are significant model terms. Values greater than 0.1000 indicate the model terms are not significant. The "Lack of Fit F-value" of 0.75 implies that the Lack of fit F-value is not significant relative to the pure error. There is 67.35 % chance that a "Lack of fit F-value" this large could occur due to noise. Non-significant Lack of fit is good- we want the model to fit.

The " pred R-Squared" is 0.7142 which is in reasonable agreement with the " Adj R-squared" which is 0.8591. "Adeq Precision" measures the signal to noise ratio. A ratio greater than 4 is desirable. The Adeq Precision obtained for our model is 14.862, which indicates an adequate signal. This model can be used to explore the design space.

4.3.2Response : Bead Width

Table 4.3 ANOVA for bead width

Source	Sum of squares	Df	Mean square	F value	p-value Prob> F
Model	56.92	14	4.07	18.88	<0.0001
b$_1$- arc voltage	14.37	1	14.37	66.71	<0.0001

b_2-current	0.73	1	0.73	3.40	0.0839
b_3-travel speed	21.23	1	21.23	98.55	<0.0001
b_4-NPD	1.37	1	1.37	6.35	0.0227
b_{12}	1.14	1	1.14	5.29	0.0352
b_{13}	3.81	1	3.81	17.70	0.0007
b_{14}	1.45	1	1.45	6.71	0.0197
b_{23}	0.11	1	0.11	0.50	0.4905
b_{24}	0.98	11	0.98	4.53	0.0492
b_{34}	0.20	1	0.20	0.93	0.3493
b_{11}	1.51	1	1.51	7.03	0.0174
b_{22}	8.34	1	8.34	38.73	<0.0001
b_{33}	0.66	1	0.66	3.08	0.0982
b_{44}	1.43	1	1.43	6.65	0.0202
Residual	3.45	16	0.22		
Lack of Fit	2.44	10	0.24	1.45	0.3370(not significant)
Pure error	1.01	6	0.17		
Cor total	60.37	30			

The model F-value of 18.88 implies the model is significant. There is only a 0.01% chance that a "Model F-value" this large could occur due to noise.

Values of "Prob > F" less than 0.0500 indicates model terms are significant. In this case b1, b3, b4, b12, b13, b14, b24, b11, b22,b44 are significant model terms. Values greater than 0.1000 indicates the model terms are not significant.

The "lack of Fit F-value" of 1.45 implies the lack of fit is not significant relative to the pure error. There is a 33.07% chance that a "Lack of fit F-value" this large could occur due to noise. Non-significant lack of fit is good- we want the model to fit.

The "pred R-squared" is 0.7448 which is in reasonable agreement with the "Adj R-squared" of 0.8930. "adeq Precison" measures the signal to noise ratio. A ratio

greater than 4 is desirable. . The Adeq Precision obtained for our model is 15.669 which indicates an adequate signal. This model can be used to navigate the design space.

4.3.3 Response : Bead Penetration

Table 4.4 ANOVA for Bead penetration

Source	Sum of squares	Df	Mean square	F value	p-value Prob> F
Model	41.55	14	2.97	17.73	<0.0001 (significant)
b_1- arc voltage	0.058	1	0.058	0.35	0.5642
b_2-current	26.00	1	26.00	155.34	<0.0001
b_3-travel speed	5.68	1	5.68	33.96	<0.0001
b_4-NPD	0.90	1	0.90	5.36	0.0342
b_{12}	0.41	1	0.41	2.45	0.1373
b_{13}	0.25	1	0.25	1.49	0.2393
b_{14}	3.63	1	3.63	21.68	0.0003
b_{23}	2.500E-005	1	2.500E-005	1.494E-004	0.9904
b_{24}	2.34	11	2.34	13.99	0.0018
b_{34}	0.053	1	0.053	0.32	0.5818
b_{11}	2.13	1	2.13	12.75	0.0026
b_{22}	0.14	1	0.14	0.82	0.3780
b_{33}	0.14	1	0.14	0.85	0.3696
b_{44}	0.021	1	0.021	0.12	0.7300
Residual	2.68	16	0.17		
Lack of Fit	2.05	10	0.21	1.97	0.2108(not significant)
Pure error	0.63	6	0.10		
Cor total	44.22	30			

The model F-value of 17.73 implies the model is significant. There is only a 0.01% chance that a "Model F-value" this large could occur due to noise. Values of "Prob >F" less than 0.0500 indicate the model terms are significant. In this case b2, b3, b4, b14, b24, b11 are significant model terms. Values greater than 0.100 indicate the model terms are not significant. The "lack of fit F-value" of 1.97 implies that the lack of fit is not significant relative to the pure error. There is a 21.08% chance that a "Lack of fit F-value" this large could occur due to noise. Non-significant lack of fit is good- we want the model to fit.

The "pred R squared" is 0.7135 is in reasonable agreement with the "Ädj R-squared" of 0.8865. "adeq Precision" measures the signal to noise ratio. A ratio greater than 4 is desirable. The Adeq Precision obtained for our model is 16.829 indicates an adequate signal. This model can be used to navigate the design space.

Table 4.5: Calculation of variance for testing the adequacy of models:

Bead geometry parameters	1st order terms		2nd order terms		Lack of fit		Error terms			Adequate or not
	S.S	D.f	S.S	D.f	S.S	D.F	S.S	D.f	F ratio	
Height	3.776	4	5.012917	10	1.7160	10	0.25857	6	3.9820	YES
Width	32.69328	4	19.6338	10	2.4365	10	1.0096	6	1.4480	YES
Penetration	32.63937	4	9.116259	10	2.0517	10	0.6262	6	1.9658	YES

Table 4.5 shows the results of the calculation of variance for testing the adequacy of the models **[38]**. The different terms used in table are as follows: The term 'S.S' stands for the sum of squares. The term 'df' indicates degree of freedom. F-ratio (10, 6, 0.05) = 4.06

4.3.4 Development of the final proposed models:

The models developed to predict the weld bead geometry relationship are as follows:

Bead height = 2.01-0.11(V) +0.35(A) +0.26(AN) +0.27(SN) +0.13(V^2) +0.17(A^2)

Bead width = 11.06+0.77(V) -0.94(S)-0.24(N) +0.27(VA)-0.49(VS) +0.30(VN) +0.25(AN) -0.23(V^2)-0.54(A^2) -0.22(N^2)

Bead penetration= 3.96+1.04(A)-0.49(S)-0.19(N)-0.48(VN) +0.38(AN) +0.27(V^2)

4.3.5 Testing the models

The developed models were tested for the accuracy of their predictive ability. 5 test cases were selected at random from the design matrix and the experimental bead geometry parameters were compared to the parameters obtained from the mathematical models. The results are summarised in Table 4.6 below:

Table 4.6 : Testing of mathematical model

Weld no.	V (volts)	A (Ampere)	S (mm/s)	N (mm)		H(mm)	W(mm)	P(mm)
5	25.5	325	15	23.5	Actual	2.03	10.27	3.05
					Predicted	2.09	9.91	2.73
					% error	2.9	3.5	10.49
8	32.5	475	15	23.5	Actual	1.99	9.42	5.37
					Predicted	2.02	9.37	5.01
					% error	-1.5	0.53	6.70
16	32.5	475	15	30.5	Actual	3.05	10.58	4.19
					Predicted	3.08	9.99	4.43
					% error	-0.98	5.57	-5.72
23	29	400	12	20	Actual	1.96	10.4	4.34
					Predicted	2.01	10.66	4.28
					% error	-2.55	-2.5	1.38
31	29	400	12	27	Actual	1.94	10.72	3.68
					Predicted	2.01	11.06	3.9
					% error	-3.6	-3.17	-5.97

we see from table that the performance of the mathematical model is good and it can be used for predicting the weld bead parameters in SAW.

Chapter 5

RESULTS AND DISCUSSIONS

The mathematical models developed above can be employed to predict the geometry of weld bead and shape relationships for the range of parameters used in the investigation by substituting their respective values in coded form. Based on these models, the main and the interaction effects of the process parameters on the bead geometry were computed and plotted as depicted in Figs. The results show the general trends between cause and effect.

5.1 Direct effect of process variables on the bead parameters:

5.1.1 Direct effect of **V** on bead parameters
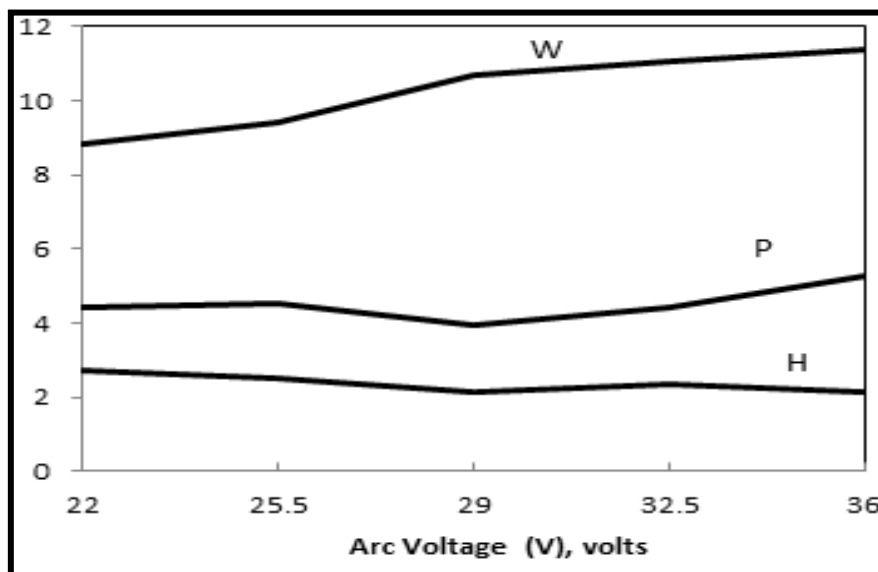
Figure 5.1: Effect of V on bead parameters

From **Figure 5.1** it is clear that bead width steadily increases as the arc voltage reaches higher levels. This may be attributed to the facts that increase in arc voltage results in increase in arc length and spreading of arc cone at its base, which results

in more melting of work piece surface instead of melting the work piece. This ultimately results in wider bead. The increased arc voltage resulted in increased bead width with corresponding reduction in reinforcement height. An excessive increase in voltage may result in nearly a flat weld bead. Penetration decreases gradually from the lower limit of arc voltage (-2) to its center level (0), then increases for higher a level of arc voltage.
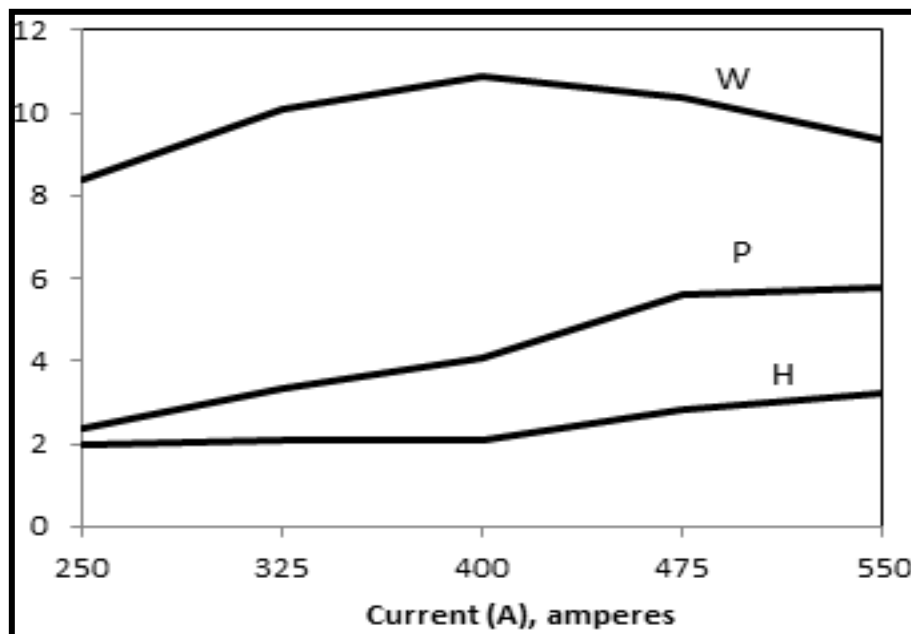
5.1.2 Direct effect of **A** on bead parameters

Figure 5.2: Effect of A on bead parameters

It is apparent from **Figure 5.2** that penetration increases gradually but reinforcement height remains almost constant for rise in current from its lowest level (250A) to centre point level (400A). For higher levels of current the rate of increase in penetration is steeper than the increase in reinforcement height. This is due to the fact that upon increasing the current the power per unit length of the weld bead and current density both increases, causing larger volume of base material to melt. As current increases the temperature and hence the heat content of the droplets

increases which results in more heat being transferred to the base metal. Increase in current also results in increased momentum of the droplets which on striking the weld pool causes deeper penetration. As a result deeper penetration is observed. Also from figure 3 it can be concluded that from 25A to 400A, the major portion of the line power goes in increasing the bead width while smaller portions are used in increasing the bead height and penetration. At higher levels of current (400A to 550A) , the major portion of the line power is used up in increasing the bead penetration and reinforcement height, while the bead width shows a minor reduction from its peak value of 10.86 at 400A to 9.86 at 550A. It is safe to conclude that increase in current, with other variables remaining constant, results in increased depth of penetration, weld width and increased weld bead shape and size at any cross section.

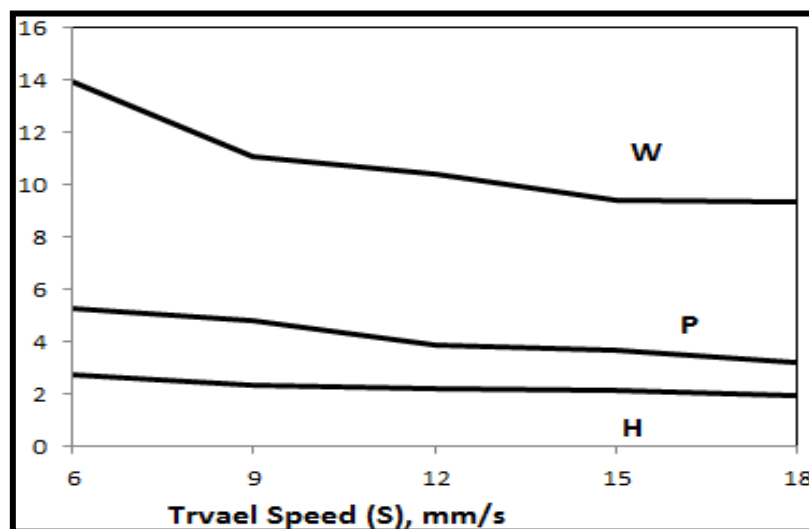5.1.3 Direct effect of **S** on bead parameters:

Figure 5.3: Direct effect of S on bead parameters

From **Figure 5.3** it is clear that travel speed has negative effect on all the bead parameters. This is because of the fact that when the welding torch travels at a

greater speed over the base metal the line power per unit length of weld bead is reduced and also the welding torch covers more distance per unit time. The combined effect of lesser line power and faster electrode travel speed results in decreased metal deposition rate per unit length of the bead. Thus the penetration and the reinforcement height decreases, though the extent of decrease in reinforcement height (from 2.74 mm at 6mm/s to 1.92 mm at 18mm/s)is less appreciable than the decrease in bead penetration (from 5.3 at 6mm/s to 3.24 at 18mm/s). Bead width decreases steadily as the travel speed is increased. This is due to the fact that with increase in speed the thermal energy transmitted to the base plate form the arc or line power per unit of the weld bead decreases and less filler material is deposited per unit length of the weld bead resulting in thinner and narrower weld bead. It is safe to conclude at lower travel speeds, the weld bead is larger in mass and vice versa. With increase in travel speed the bead becomes flatter.

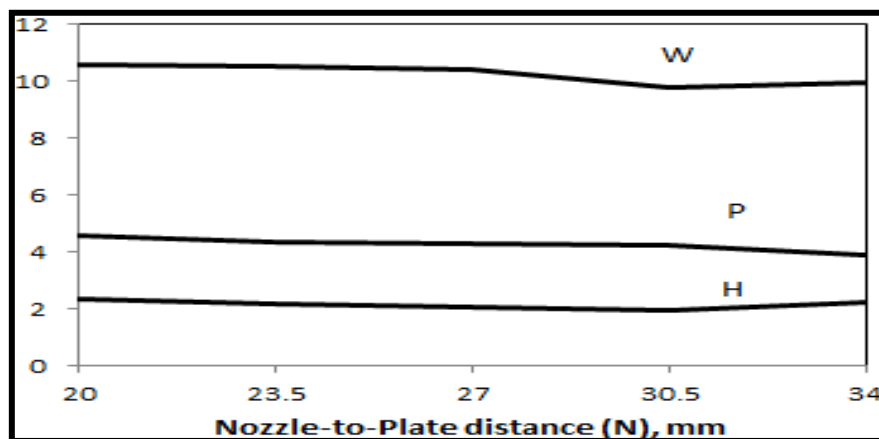5.1.4 Direct effect of **N** on bead parameters

Figure 5.4: Effect of N on bead parameters

As can be seen from **Figure 5.4,** the NPD increases the reinforcement height decreases. With the increase in NPD the welding current and heat input decreases. Because of the reduced heat input the value of reinforcement height and penetration decreases in general with the increase in NPD. The value of bead width remains practically unaffected by increase in NPD from 20 mm to 27 mm. at the highest level of NPD the bead width shows increase in its value, this could be attributed to the fact that when the NPD is too high , due to the increased arc length the arc cone spreads at its base. Also, the metal fusion rate increases slightly at higher values of N because of the joules heating effect.

5.2 Interaction effects of process variables on the bead parameters:

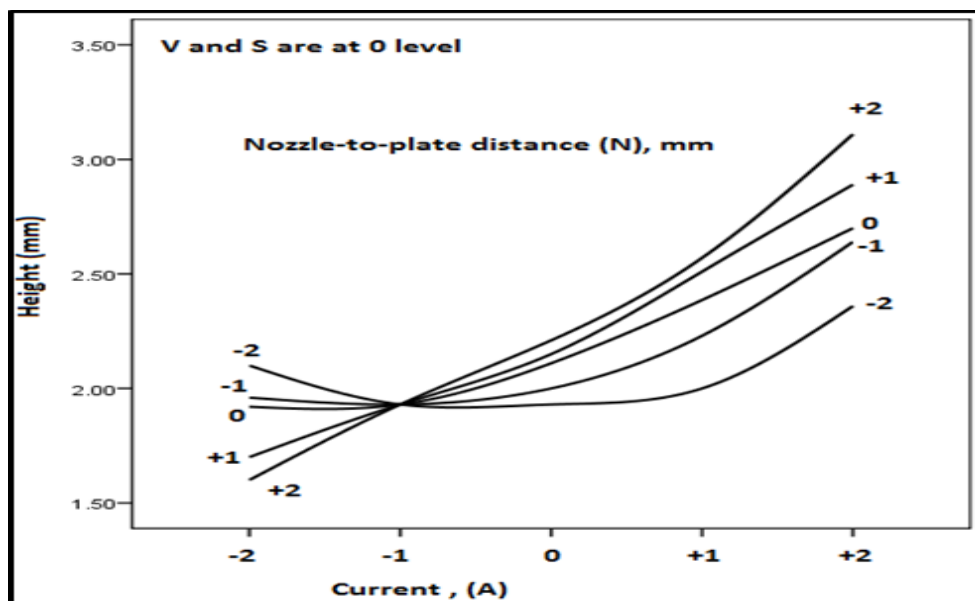5.2.1 Interaction effect of **A** and **N** on **H**

Figure 5.5: Interaction effect of A and N on H

From **Figure 5.5** it can be observed that the bead height increases with increase in N for all values of current A. Also it can be seen that the increase in the value of the reinforcement height is most pronounced in the case of +2 level of N i.e. from 1.6

69

mm at 250 A to 3.11mm at 550A. This is due to the fact that upon increasing the current the power per unit length of the weld bead and current density both increases, causing larger volume of base material to melt, thus increasing the reinforcement height. This trend is also supported by the positive value of co-efficient of A in the direct effect of reinforcement height. With increase in N the momentum of the molten metal droplet from the wire is reduced, so their tendency to penetrate into the base metal is subsequently reduced as well. This explains the maximum increase in the value of reinforcement height for the +2 level of N. the trend is also supported by the surface plot as shown in figure 5.6.
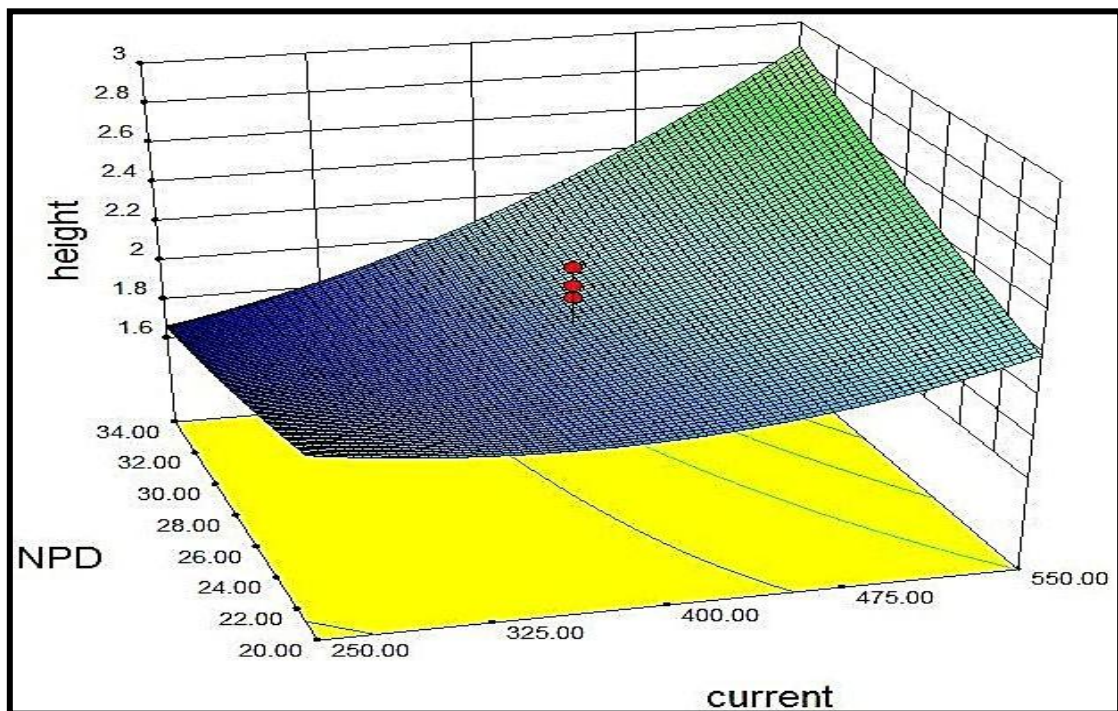
Figure 5.6: Surface and contour plots showing interaction effect of A and N on H

5.2.2 Interaction effect of **S** and **N** on **H**:

It can be seen that the reinforcement height decreases with increase in travel speed for all values of N from -2 to 0 levels. This is because of the fact that when the welding torch travels at a greater speed over the base metal the line power per unit

length of weld bead is reduced and also the welding torch covers more distance per unit time.
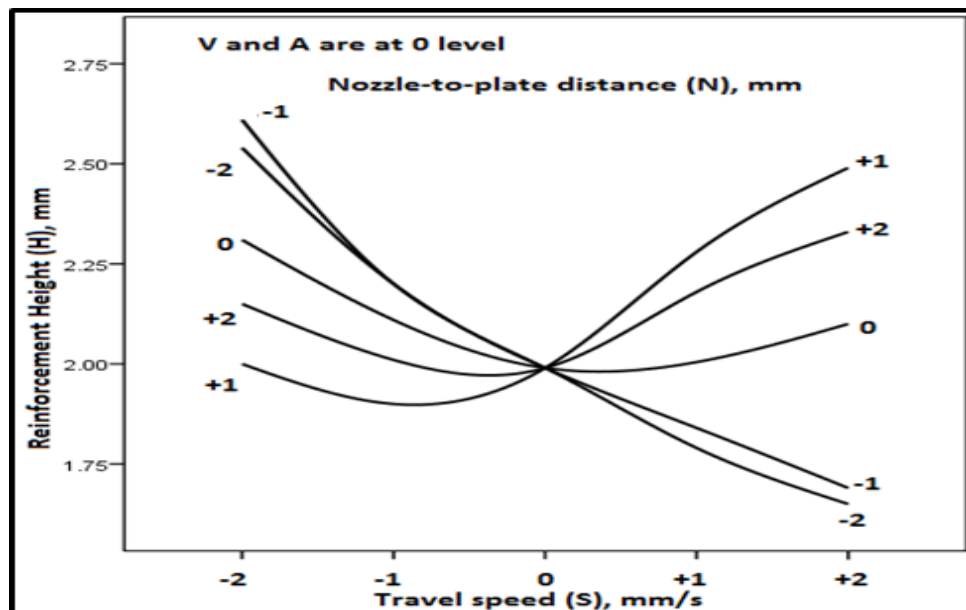

Figure 5.7: Interaction effect of S and N on H

The combined effect of lesser line power and faster electrode travel speed results in decreased metal deposition rate per unit length of the bead. But for higher levels of N (i.e. from 0 to +2) an increase in reinforcement height is observed with increase in travel speed. As already explained with increase in N the tendency of molten metal to penetrate into the base metal is reduced and this results in increased reinforcement height. From **Figure 5.7** we can observe that reinforcement height increase for higher values of N. Figure 5.8 shows the contour and surface plots.
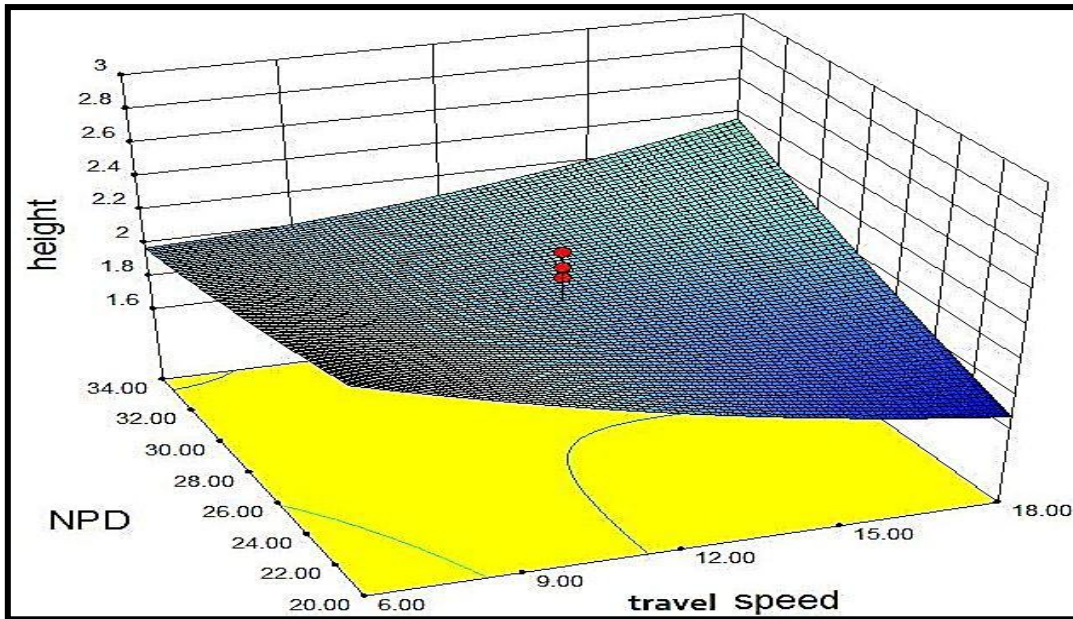
Figure 5.8: Surface and contour plots showing interaction effect of S and N on H

5.2.3 Interaction effect of **V** and **A** on **W**:

The value of bead width increases continuously from -2 to 0 levels of arc voltage for all values of current. After the 0 level, the value of bead width decreases with further increase of current for -1 level of current i.e. 325 A, but the decrease in arc voltage is very insignificant from 10.69 mm at 29 Volts to 10.42 mm at 36 volts.
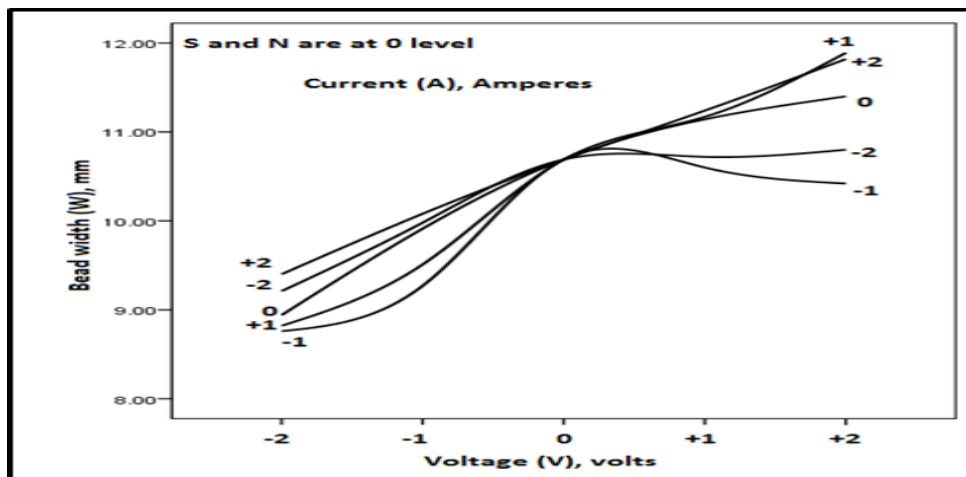

Figure 5.9: interaction effect of V and A on W

While for higher values of current the bead width continue to increase with increase of arc voltage. This may be attributed to the facts that increase in voltage results in increase in arc length and spreading of arc cone at its base, which results in more melting of work piece surface instead of melting the work piece. Also with increase in current the melting rate of wire increases and due to spreading of arc cone at its base, ultimately a wider bead results from the combined effect of increasing the arc voltage and current. The effects are easily seen from **Figure 5.9**. Figure 5.10 further demonstrates these effects, where in the surface tilts upwards at higher values of current and arc voltage.
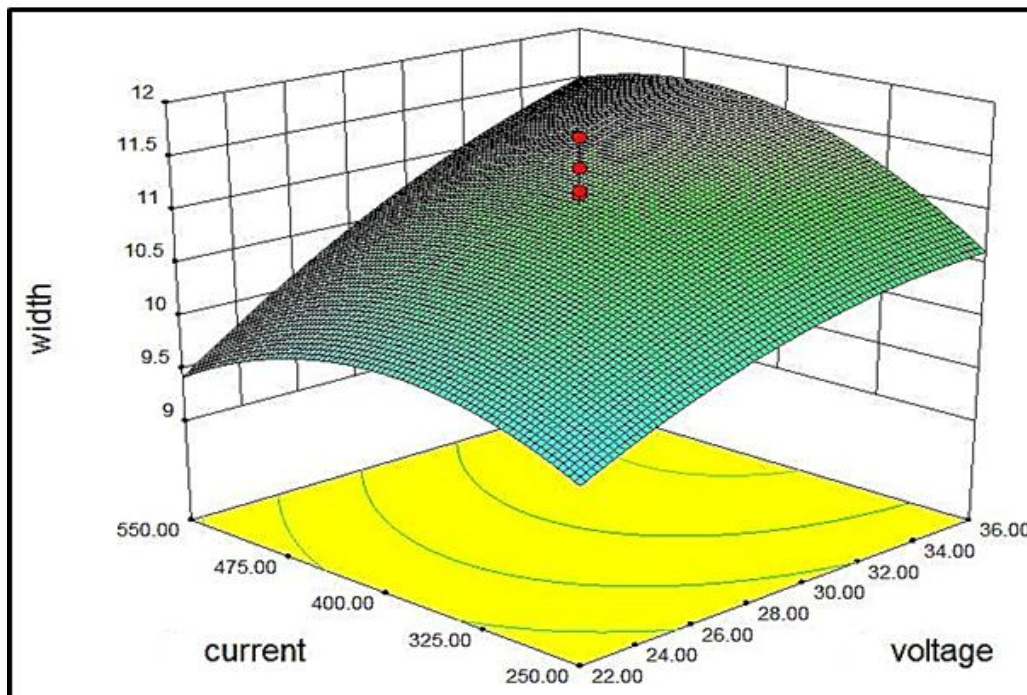

Figure 5.10: Surface and contour plots showing interaction effect of V and A on W

5.2.4 Interaction effect of **V** and **S** on **W**:

Form **Figure 5.11** we can observe that with increase in arc voltage the bead width increase for all levels of arc voltage when the travel speed is low i.e. 6mm/s and 9 mm/s, while the opposite trend is observed for higher speeds. Travel speed and arc

voltage both have conflicting effects on the bead width. We already discussed that bead width decreases steadily as the travel speed is increased. This is due to the fact that with increase in speed the thermal energy transmitted to the base plate form the arc or line power per unit of the weld bead decreases.
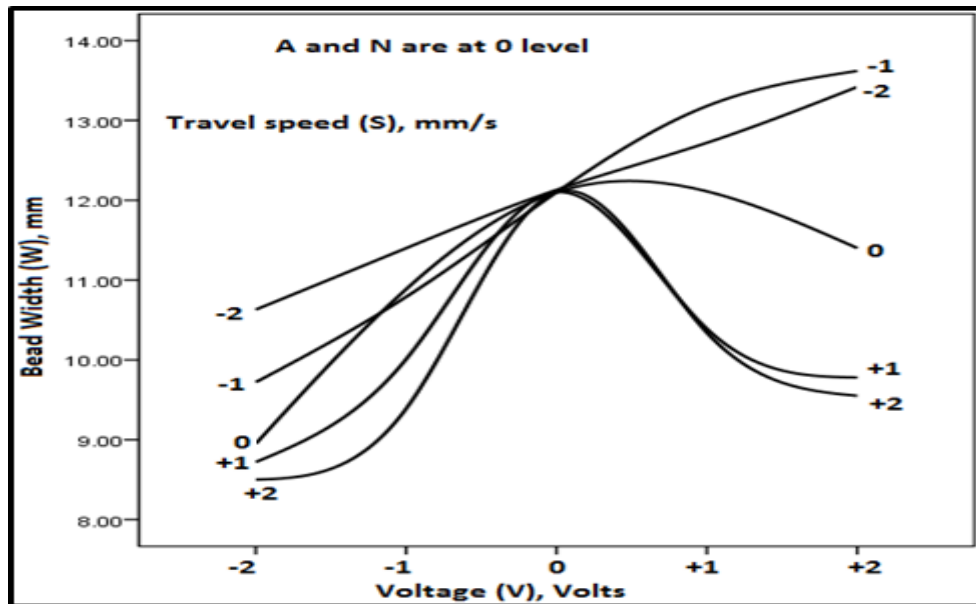

Figure 5.11: Interaction effect of V and S on W

Thus less filler material is deposited per unit length of the weld bead resulting in thinner and narrower weld bead. While upon increasing arc voltage the bead width increases steadily due to widening of arc cone at its base. For lower values of speed the effect of spreading of arc cone at its base dominates negative effect of travel speed on the bead width, thus the bead width continues increasing throughout all the levels of voltage. But when the speed is increased beyond its 0th level i.e. for 12mm/s, 15mm/s and 18mm/s, the negative effect of increased travel speed on the bead width dominates over the effect of increasing arc voltage, thus the bead width decreases beyond 29V for the higher values of travel speed. Figure 5.12 shows the surface and contour plots for the interaction effects. We can observe the bead width

is maximum for highest value of arc voltage and lowest value of travel speed, as explained in the interaction plots above.
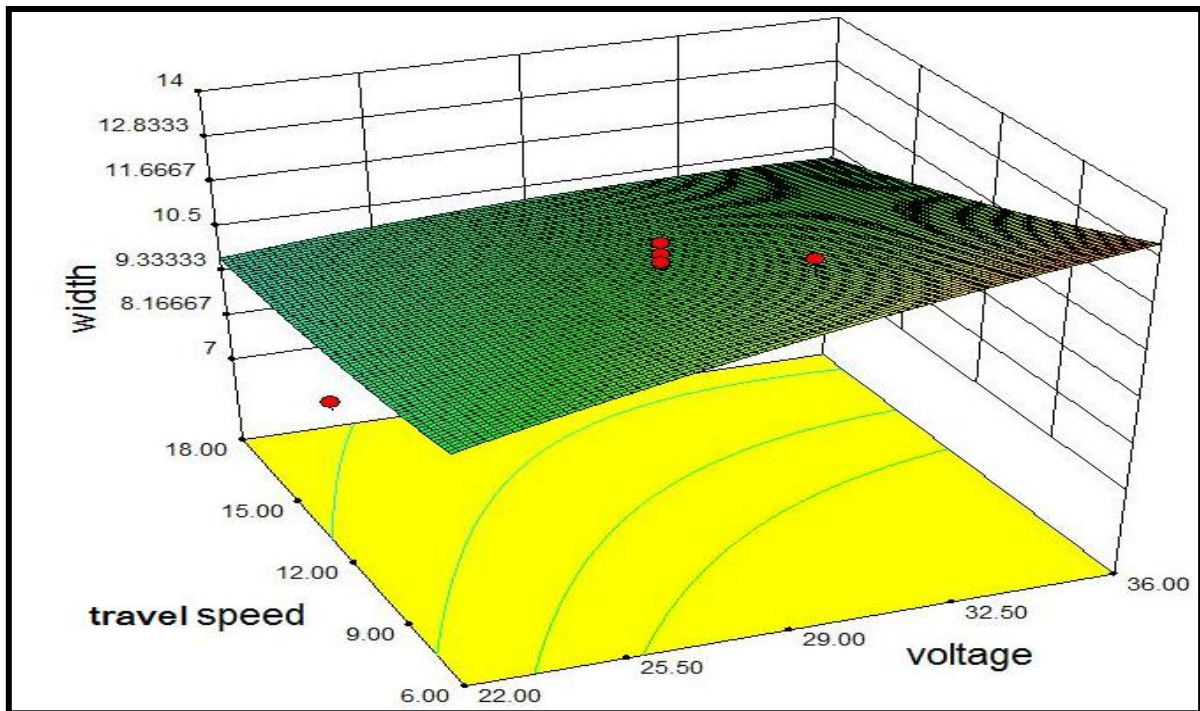

Figure 5.12 : Surface and contour plots showing interaction effect of V and S on W

5.2.5 Interaction effect of **V** and **N** on **W**:

It can be seen from **Figure 5.13**,that the bead width increases with increase in arc voltage for all levels of N. for lower levels of N the value of bead width reaches a maximum at 0th level of arc voltage (29V), followed by a decrease in the subsequent levels. The decrease in bead width with increase in arc voltage could be attributed to the lower nozzle-to-plate distance, which prevents the spreading of arc cone at its base. While a steady increase in bead width is observed for higher values of N, throughout all the levels of arc voltage. Highest value of bead width 11.76 mm, is observed for the highest level of arc voltage and nozzle-to-plate distance i.e. 36 V and 34 mm. this could be attributed to the fact that when the NPD is too high , due to

the increased arc length the arc cone spreads at its base. Also, the metal fusion rate increases slightly at higher values of N because of the joules heating effect.
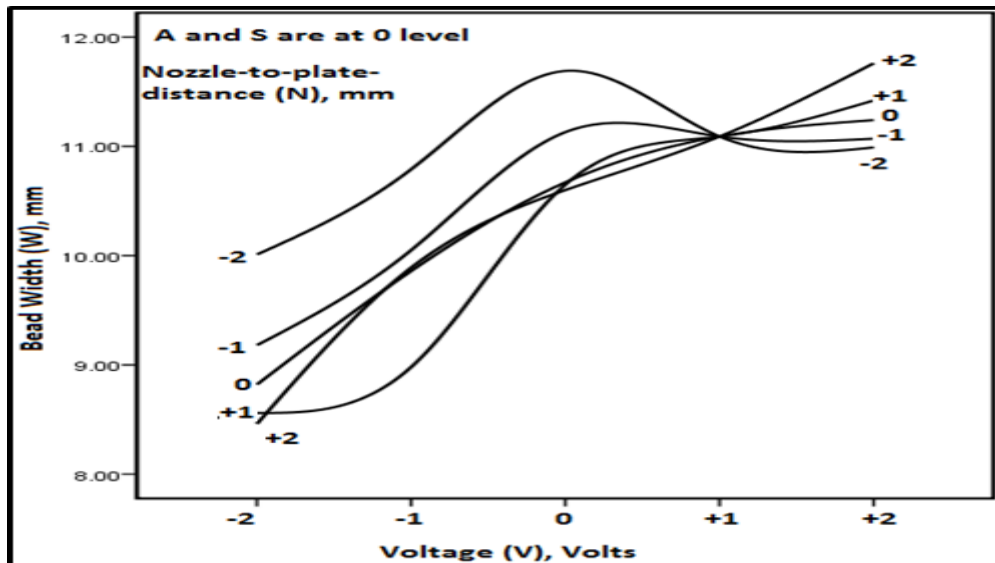

Figure 5.13 : Interaction effect of V and N on the W

5.2.6 Interaction effect of **A** and **N** on **W**:

Bead width increases to maximum value and then decreases nearly back to the same value with increase in current for all levels of N. increase in current basically results in higher melting rate of wire. From **Figure 5.14** we can see that at lower levels of current i.e. up to 400 A the increased melting rate of wire demonstrates itself in the form of increased bead width, while at higher levels of current i.e. from 400A to 550A, the increased melting rate of wire results in deeper penetration rather than wider bead. For a particular level of current the rate of melting of the wire is constant, but with increase in nozzle-to-plate distance the penetration also increases. This is the reason that the value of bead width is higher at lower values of N for all levels of current and vice versa.
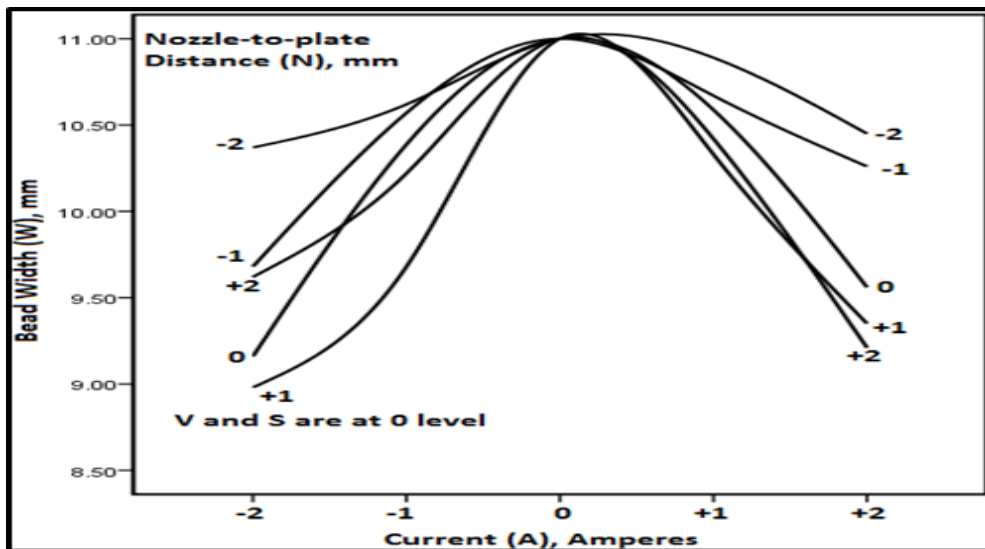
Figure 5.14: Interaction effect of A and N on W

Figure 5.15 shows the surface and contour plots. Just as the interaction plots, the surface plot for the bead width also attains a maximum at roughly the mid-level then decreases.
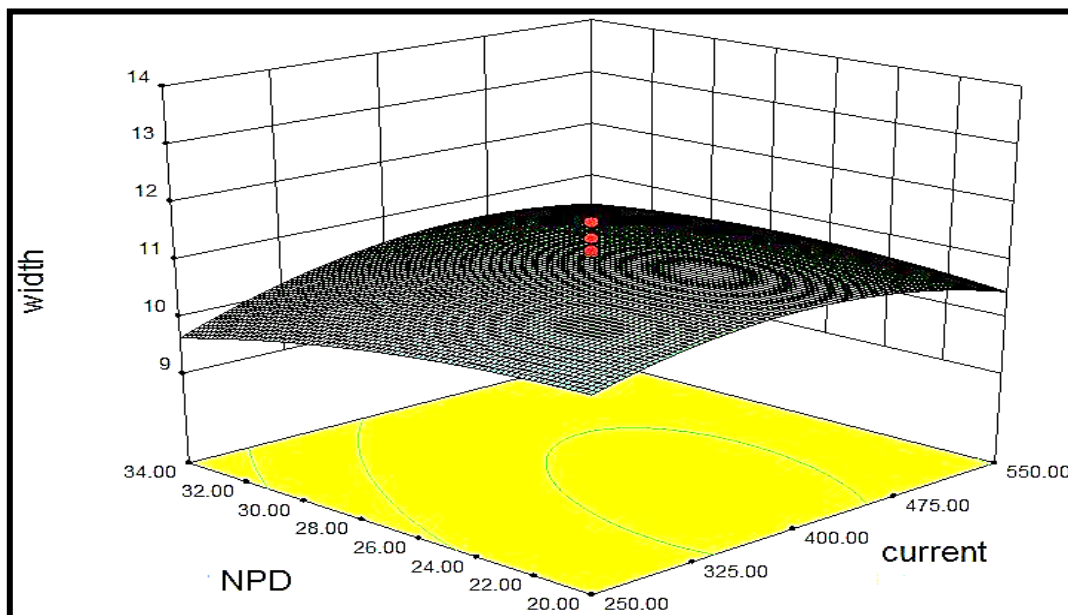

Figure 5.15: Surface and contour plots showing interaction effect of A and N on W

5.2.7 Interaction effect of **V** and **N** on **P**:

As can be seen from **Figure 5.16**, for lower levels of N i.e. from -2 to 0 levels (20 mm to 27 mm), the bead penetration starts from a lower value and increases steadily with increase in the levels of arc voltage. But at higher levels of NPD, the value of bead penetration starts from a high value and decreases with the increase in arc voltage. With increase in arc voltage the arc gets spread out at its base, this results in lesser penetration for high levels of N. At higher levels of N the spreading out of arc decreases the momentum of the molten metal droplets, this resulting in lesser penetration. When the N is at low level the effect of spreading out of arc cone at its base is dominated by the increased melting rate of the wire, thus the bead penetration value shows steady increase with increase in arc voltage. Figure 5.17 shows the related surface and the contour plots.
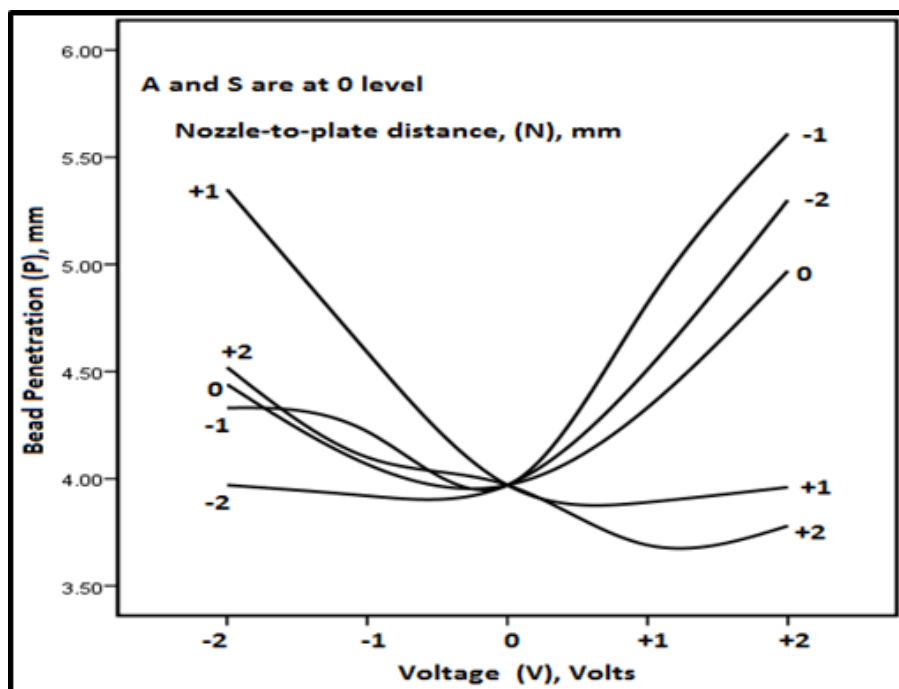

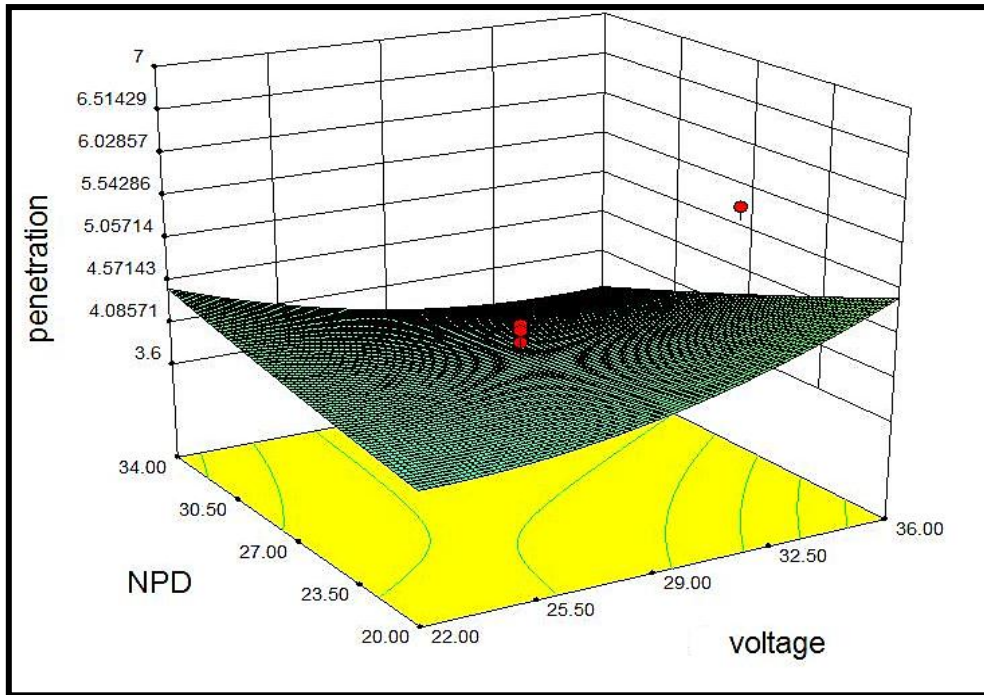**Figure 5.16: Interaction effect of V and N on P**

Figure 5.17 : Surface and contour plots showing interaction effect of V and N on P

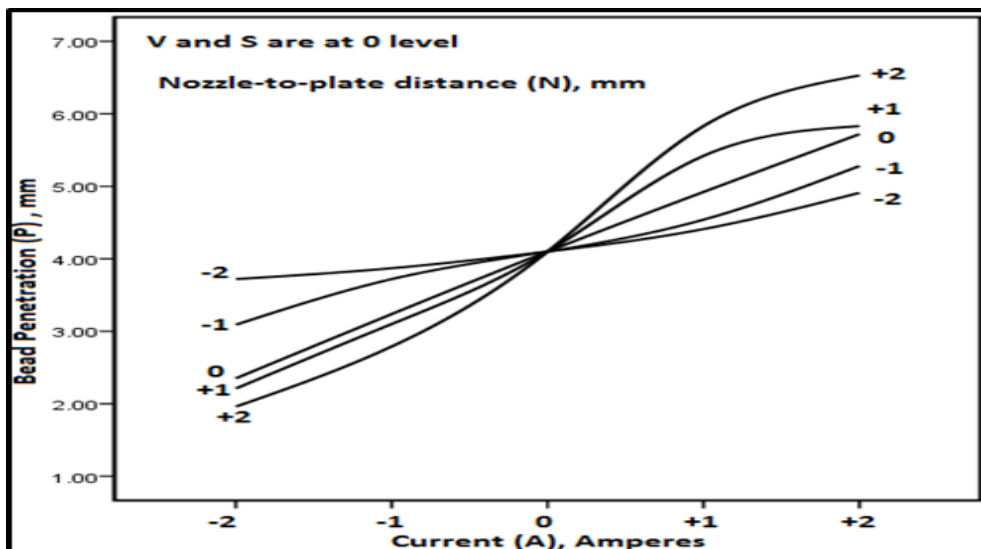5.2.8 Interaction effect of **A** and **N** on **P**:

Figure 5.18: Interaction effect of A and N on P

Bead penetration increases steadily for all values of N throughout all the levels of current as can be seen from **Figure 5.18**. As discussed earlier; increasing the current results in an increase of both the power per unit length of the weld bead and

current density, hence causing larger volume of base material to melt. As current increases the temperature and hence the heat content of the droplets increases, which results in more heat being transferred to the base metal. Increase in current also results in increased momentum of the droplets which on striking the weld pool causes deeper penetration. As a result deeper penetration is observed. The effect of increase in momentum is augmented with the increase in N, which explains the higher value of bead penetration at higher levels of current and nozzle-to-plate distance.
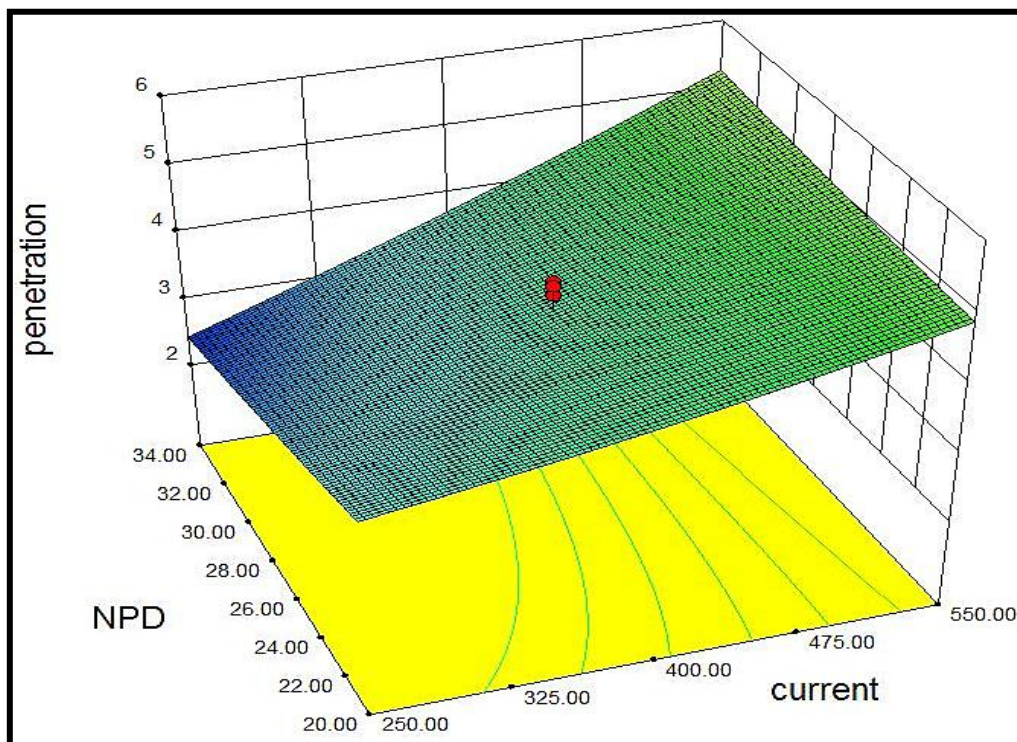

Figure 5.19: Surface and contour plots showing interaction effect of A and N on P:
From the surface and contour plots figure 5.19, we can see that the value of bead penetration increases continuously as we move towards higher levels of Current and NPD.

CHAPTER 6

MODELLING USING ARTIFICIAL NEURAL NETWORK

6.1 Basic approach to Mathematical modelling using Artificial Neural Network in arc welding scenario

A neural network is an adaptable system that can learn relationships through repeated presentation of data and is capable of generalizing to new, previously unseen data **[40]**.
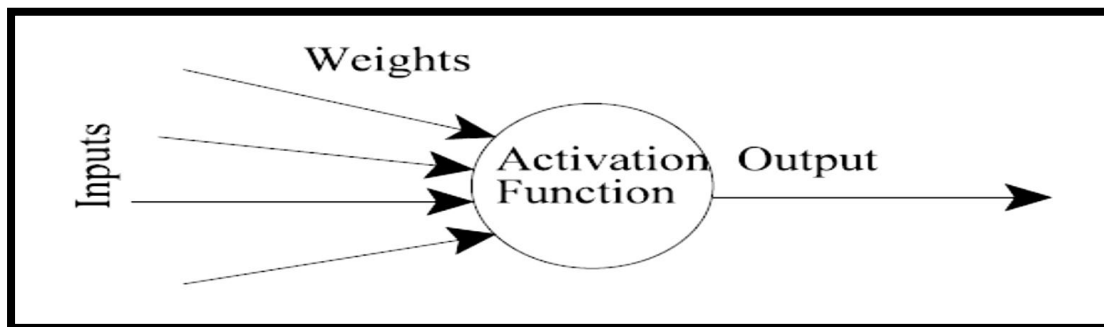

Figure 6.1: Basic scheme of an Artificial Neural Network

If a network is to be of any use, there must be inputs (which carry the values of variables of interest in the outside world) and outputs (which form predictions, or control signals) **[39]**. There may also be hidden neurones, which play an internal role in the network. The input, hidden and output neurones need to be connected together. The artificial neurone, as shown in Figure 6.1, receives a number of inputs (either from original data, or from the output of other neurones in the neural network) and processes the input to generate the output for that particular neurone. The steps

are schematically shown in Figure 6.2. For our application, this function is a sigmoid function, which is the same for all neurones.
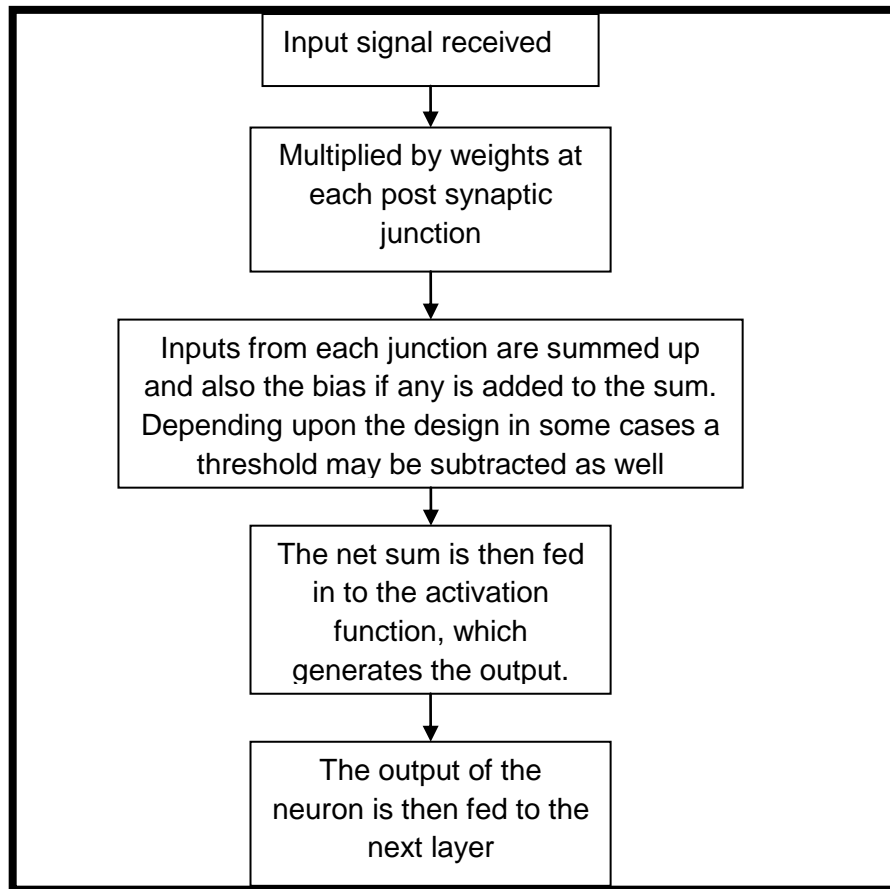
```
┌─────────────────────────────────────────────────────────────┐
│              ┌─────────────────────────┐                     │
│              │   Input signal received │                     │
│              └────────────┬────────────┘                     │
│                           ▼                                   │
│              ┌─────────────────────────┐                     │
│              │  Multiplied by weights at│                     │
│              │    each post synaptic    │                     │
│              │        junction          │                     │
│              └────────────┬────────────┘                     │
│                           ▼                                   │
│         ┌──────────────────────────────────────┐             │
│         │ Inputs from each junction are summed up│            │
│         │ and also the bias if any is added to the sum.│       │
│         │ Depending upon the design in some cases a │          │
│         │   threshold may be subtracted as well     │          │
│         └────────────────┬─────────────────────┘             │
│                          ▼                                    │
│              ┌─────────────────────────┐                     │
│              │    The net sum is then fed│                    │
│              │     in to the activation  │                    │
│              │      function, which      │                    │
│              │   generates the output.   │                    │
│              └────────────┬────────────┘                     │
│                           ▼                                   │
│              ┌─────────────────────────┐                     │
│              │     The output of the    │                     │
│              │  neuron is then fed to the│                    │
│              │        next layer         │                     │
│              └─────────────────────────┘                     │
└─────────────────────────────────────────────────────────────┘
```

Figure 6.2: Sequence of steps in the processing of signal by neurone

The back propagation algorithm is used in layered feed-forward ANNs. This means that the artificial neurons are organized in layers, and their signals are fed "forward", and then the errors are propagated backwards. The back propagation algorithm uses supervised learning, which means that we provide the algorithm with examples of the inputs and outputs we want the network to compute, and then the error (difference between actual and expected results) is calculated **[26-28]**. The idea of the back propagation algorithm is to reduce this error, until the ANN *learns* the training data. The training begins with random weights, and the goal is to adjust them so that the

error will be minimal. The sequence of steps of for the training of a simple 2 layer network using Back Propagation Training Algorithm is shown in Figure 6.3.
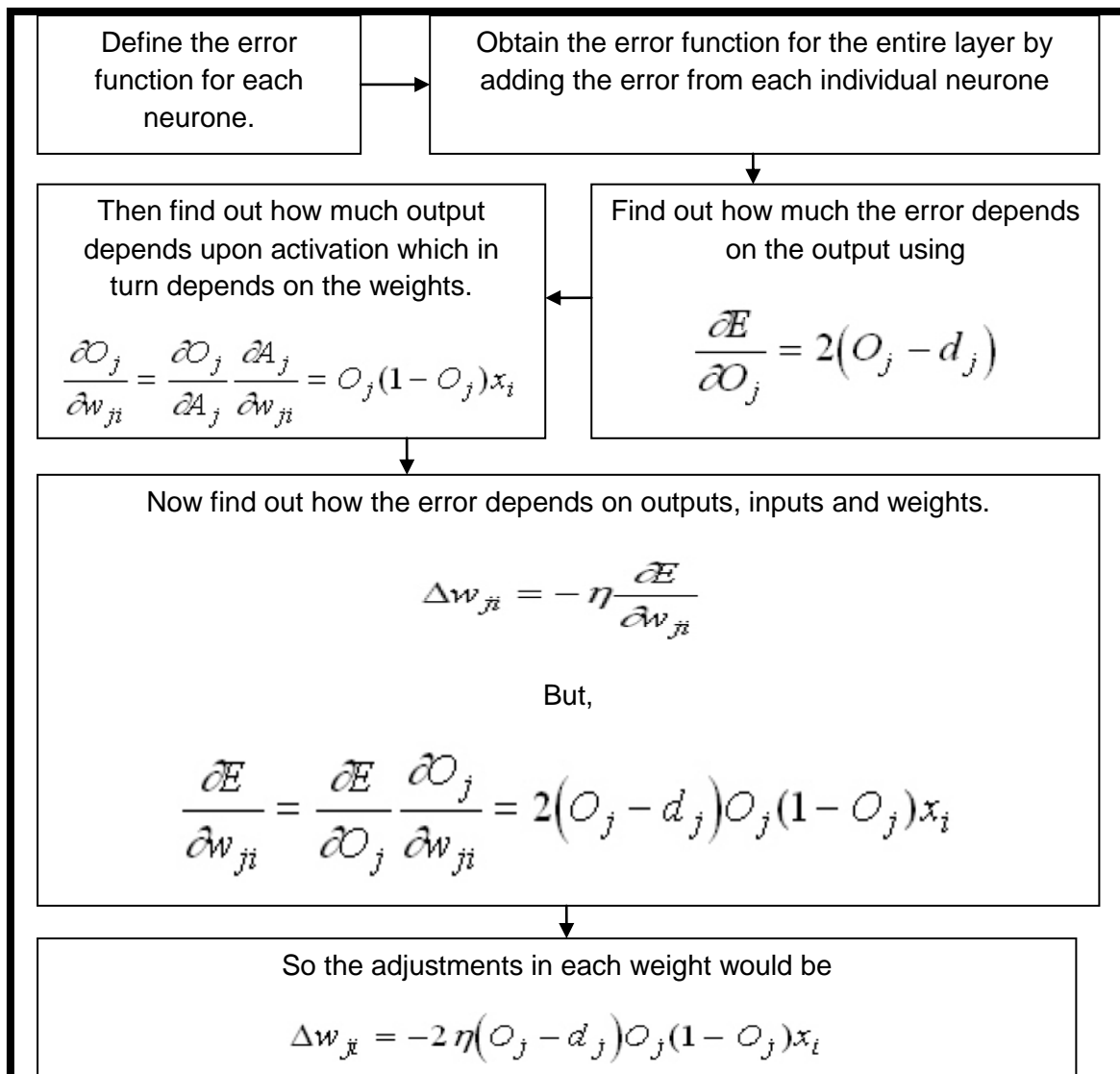

Figure 6.3: Approach for training of a 2 layer network using Back Propagation Training Algorithm

E is the error function, i and j are the number of layers and number of neurons in each layer respectively, O is the network output, D is the desired output, w is the weights, A is the activation function for the 'j'th neurone. For training the network with one more layer we need to make some considerations. If we want to adjust the weights of a previous layer, we need first to calculate how the error depends not on

the weight, but in the input from the previous layer. Thus by generalizing the above approach we can model any number of layers in the network **[47]**.

The algorithm progresses iteratively through a number of epochs. At each epoch the training cases are each submitted to the network and the output and the error is calculated. This error is used together with the error surface gradient to adjust the weights and then the process is repeated till the outputs are within a desired level of accuracy **[48]**.
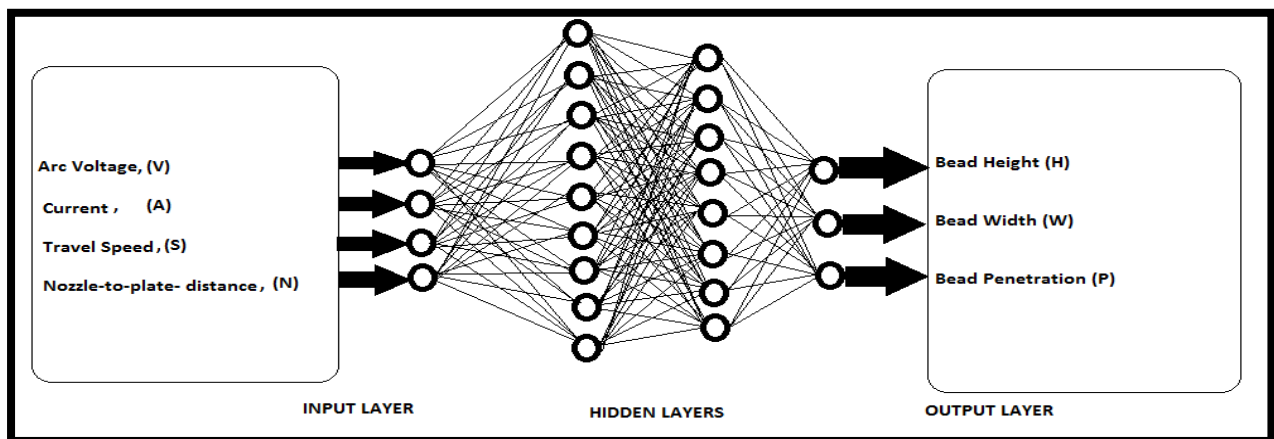
Figure 6.4: Back propagation Neural Network used for prediction of bead geometry features

A typical Back propagation network is shown in Figure 6.4. This network is used in the present research for the modeling of the process. To model the process 4 input parameters viz, Arc Voltage, Current, Welding Speed and Nozzle-to-plate-distance were considered and their effect on 3 bead geometry parameters namely Bead height, Bead width and Bead Penetration was studied, so for our modelling the input and the output layer of the network had 4 and 3 neurons respectively. The input layer is not a neural layer in the true sense of the word; it is just used to introduce the input variables in the network. The performance of a neural is dependent on the number of hidden layers and the number of hidden neurones in the hidden layers. Therefore

sufficiently large number of trials must be carried out before deciding the optimum number of hidden layers and the number of neurones in the hidden layers. The goal was kept as 0.01.

6.2 Computational work

Computational work for the training of the networks was carried out in MATLAB R2010a software **[47]**. Few of the examples are given below.

6.2.1 Computational Experimental Work 1

Network Name: Ex-3

No. of Hidden Layers: 3

Network Type: Feed Forward Back Propagation

Training Function: Gradient descent with momentum back propagation

No. of Neurons in First Hidden Layer: 20

No. of Neurons in Second Hidden Layer: 20

Adaptation Learning Function: Gradient descent with momentum weight and bias learning function

No. of Neurons in Input Layer: 4

Performance Function: MSE

Transfer Function: Log sigmoid transfer function

Epochs: 10000

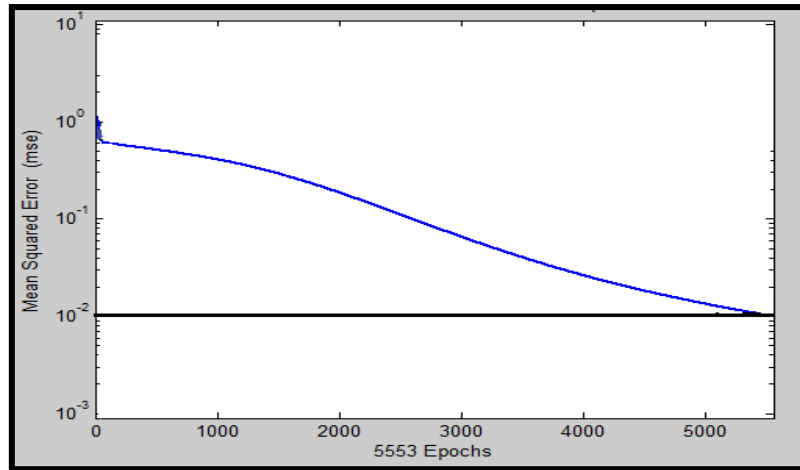Goal: 0.01

Learning Rate: 0.01

Epochs made: 5844
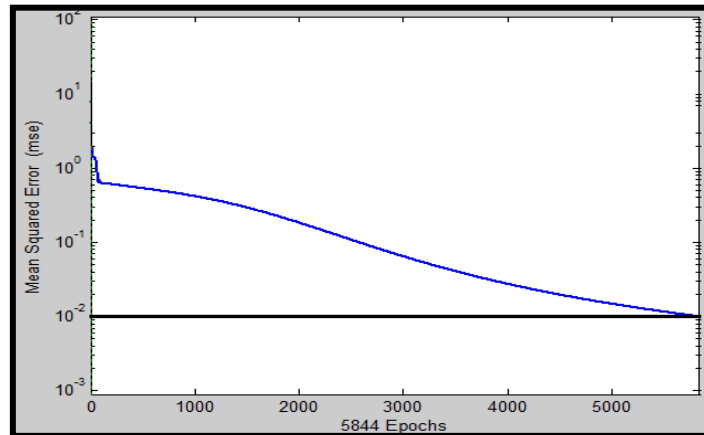
Figure 6.5 Epochs vs MSE for 4-20-20-3

This architecture was trained with neural network parameters i.e. Feed forward Back Propagation, we selected mean square error concept, goal was set at 0.01 and learning rate was set at 0.01. The result has been shown in the Fig 6.5.In this case it was able to converge after 5844 Epochs. After converging we will get the predicted value by the network.

6.2.2 Computational Experimental Work 2

Network Name: Ex-11

No. of Neurons in First Hidden Layer: 15

No. of Neurons in Second Hidden Layer: 20

All other parameters are identical as previous example.

Epochs made: 5553

Figure 6.6 Epochs vs MSE for 4-15-20-3

This architecture was trained with neural network parameters i.e. Feed forward Back Propagation, we selected mean square error concept, goal was set at 0.01 and learning rate was set at 0.01. The result has been shown in the Fig 6.6 , as this is a plot of No. of Epoch versus Mean square error. In this case it was able to converge after 5553 Epochs. After converging we will get the predicted value by the network. A large number of trials were performed; details of few of them are given in Table 6.1.

Table 6.1: Performance of different ANN architectures

Sl.no	Network structure	Training function	Learning rate	Momentum coefficient	Epochs made before attaining the desired goal
1	4-30-20-3	traingdm	0.01	0.9	4166
2	4-20-30-3	traingdm	0.01	0.9	3758
3	4-20-20-3	traingdm	0.01	0.9	5844
4	4-20-15-3	traingdm	0.01	0.9	4682
5	4-20-10-3	traingdm	0.01	0.9	6181

6	4-25-30-3	traingdm	0.01	0.9	3622
7	4-25-25-3	traingdm	0.01	0.9	9067
8	4-25-10-3	traingdm	0.01	0.9	6361
9	4-25-20-3	traingdm	0.01	0.9	4313
10	4-25-15-3	traingdm	0.01	0.9	3998
11	4-15-20-3	traingdm	0.01	0.9	5553
12	4-15-25-3	traingdm	0.01	0.9	3266
13	**4-15-10-3**	**traingdm**	**0.01**	**0.9**	**2755**
14	4-14-22-3	traingdm	0.01	0.9	3636
15	4-14-12-3	traingdm	0.01	0.9	5144
16	4-12-20-3	traingdm	0.01	0.9	5028
17	4-10-20-3	traingdm	0.01	0.9	5956
18	4-10-15-3	traingdm	0.01	0.9	3105
19	4-10-25-3	traingdm	0.01	0.9	2889
20	4-10-30-3	traingdm	0.01	0.9	4402

For this study the structure of the neural network was 4-15-10-3 (4 in the input layer, 15 in the first hidden layer, 10 in the second hidden layer and 3 in the output layer). The network was trained for 2755 iterations before the performance goal was met. After the training the network was simulated to obtain the outputs at the input experimental conditions and the ANN output was compared to with that of the experimental values and the outputs from the RSM models. The results of the comparison are shown and discussed in the next section.

6.3 Results and Discussion

6.3.1 Comparison of experimental, ANN and RSM models for the Bead Width

Table 6.2: Comparison of experimental, ANN and RSM model results for the bead height

Sl.no	Experimental value	ANN output	%error in ANN prediction	RSM output	%error in RSM prediction
1	2.38	2.13	10.5	2.6	-9.24
2	2.54	2.746	-8.1	2.38	6.2
3	3.07	3.2765	-6.7	2.78	9.4
4	2.79	2.7554	1.2	2.56	8.2
5	2.03	1.8002	11.3	2.09	2.9
6	1.98	1.6655	16.1	1.84	7.07
7	1.89	1.712	9.4	2.24	-18.5
8	1.99	1.8703	6.04	2.02	-1.5
9	1.81	1.8984	-4.8	1.54	14.9
10	1.66	1.721	-3.6	1.32	14.4
11	3.23	2.7904	13.6	2.76	14.5
12	2.72	2.8996	6.6	2.54	6.61
13	2.09	1.7535	16.1	2.08	0. 47
14	2.08	1.8966	9.1	1.86	10.5
15	3.66	3.4567	5.5	3.3	9.8

16	3.05	2.6852	11.9	3.08	-0.98
17	2.72	2.6567	3.3	2.75	-1.10
18	2.13	2.4394	14.08	2.31	-8.45
19	1.96	1.6775	14.4	1.99	-1.53
20	3.20	2.9929	6.4	3.39	-5.93
21	2.31	2.1148	8.6	2.01	12.98
22	2.1	1.9021	9.4	2.01	4.28
23	1.96	1.7758	9.6	2.01	-2.55
24	2.07	2.2133	6.7	2.01	2.89
25	2.29	2.0541	10.3	2.01	12.2
26	2.14	2.0541	4.01	2.01	6.07
27	1.79	2.0541	-14.7	2.01	-12.29
28	2.2	2.0541	6.6	2.01	8.63
29	1.93	2.1798	-12.94	2.01	-4.14
30	1.75	2.0541	17.3	2.01	-14.85
31	1.94	2.0541	5.88	2.01	-3.6

Absolute mean percentage error for ANN prediction= 9.18

Absolute mean percentage error for RSM prediction= 7.87
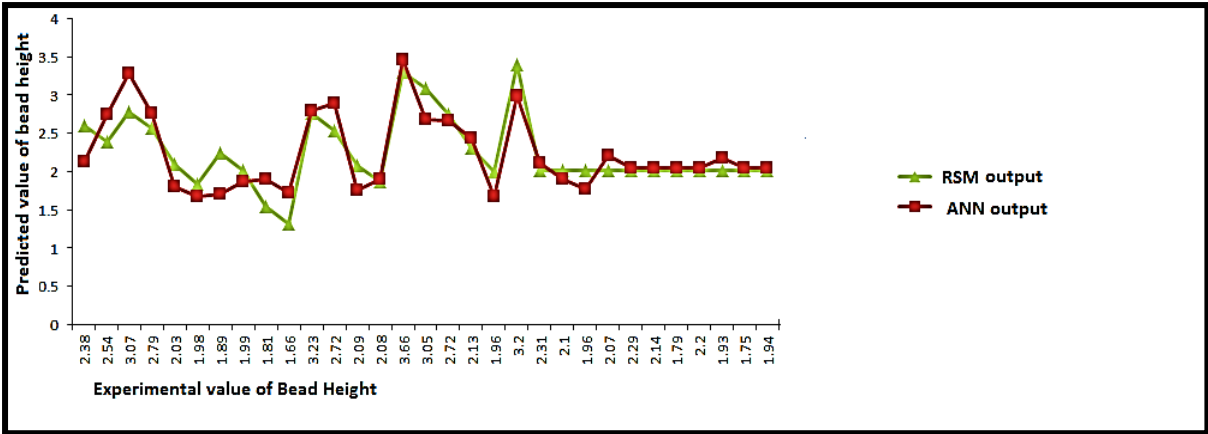
Figure6.7: Comparison of experimental, ANN and RSM results for the bead height

The absolute mean percentage error of ANN prediction is a little greater than the absolute mean percentage error of regression model predictions, which shows that the RSM model is more accurate than the ANN model for the bead height predictions. From Figure 6.7 it can be concluded that the outputs from the ANN model and the RSM models are comparable which is inferred from the overlap between the plots of ANN output and RSM output versus the actual output for the bead height
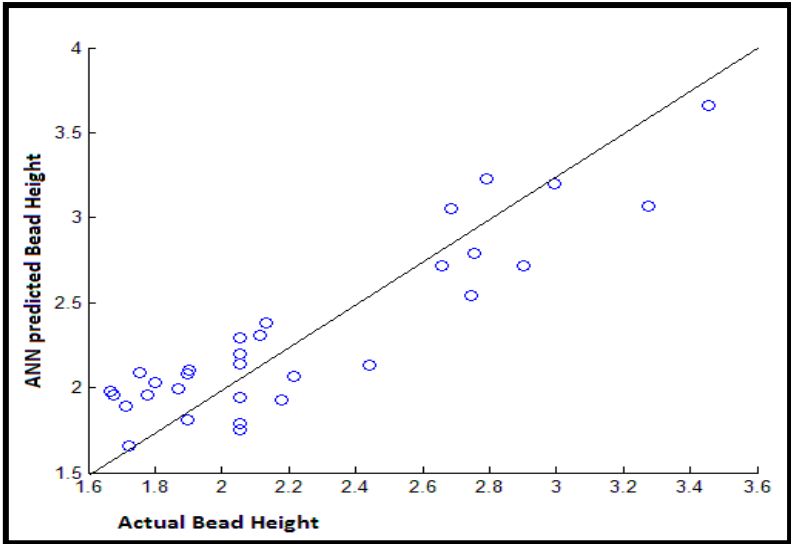
Figure 6.8: Comparison of ANN prediction of bead height with actual bead height
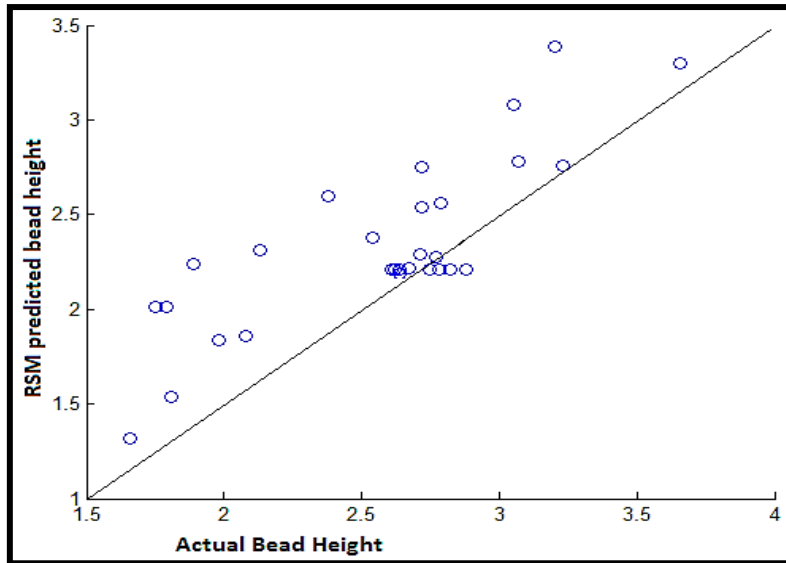
Figure 6.9: Comparison of RSM prediction of bead height with actual bead height

The greater accuracy of the RSM model over the ANN model is further highlighted from the scatter plots wherein more number of outputs are located on or near the line y=x for RSM model predicted bead height (figure 6.9) as compared to ANN predicted bead height (figure 6.8). Also it is to be noted that the percentage error in ANN prediction never exceeded 17.3 and that in RSM model never exceeded 18.5 (absolute), so these two models can be successfully used for prediction of bead height.

6.3.2 Comparison of experimental, ANN and RSM models for the bead width

**Table 6.3: Comparison of experimental, ANN and RSM model results for the bead width**

Sl.no	Experimental value	ANN output	%error in ANN prediction	RSM model output	%error in RSM model prediction
1	10.55	11.442	-8.436	10.81	-2.46

2	12.43	12.47	-0.32	12.19	1.93
3	9.76	11.09	-13.66	9.77	-0.102
4	13.14	12.42	5.41	12.23	6.9
5	10.27	9.76	4.96	9.91	3.505
6	9.26	8.72	5.83	9.33	-0.75
7	9.37	8.46	9.71	8.87	5.33
8	9.42	9.204	2.29	9.37	0.53
9	9.17	10.606	-15.66	9.23	-0.65
10	11.21	12.28	-9.5	11.81	-5.35
11	9.48	10.57	-11.59	9.19	3.05
12	12.79	11.27	11.88	12.85	-0.46
13	8.08	8.54	-5.69	8.33	-3.09
14	9.74	8.88	8.82	8.95	8.11
15	8.48	9.00	-6.13	8.29	2.24
16	10.58	10.32	2.45	9.99	5.57
17	8.82	10.007	-14.34	8.6	2.49
18	11.4	11.94	-4.73	11.68	-2.45
19	8.4	9.23	-9.88	8.9	-5.95
20	9.34	10.14	-8.56	8.9	4.71
21	13.95	12.808	8.18	12.94	7.24
22	9.33	8.1342	12.86	9.18	1.607
23	10.4	9.27	10.86	10.66	-2.5

24	9.87	9.76	1.11	9.7	1.722
25	10.55	11.07	-4.98	11.06	-4.83
26	11.15	11.07	0.71	11.06	0.807
27	10.73	11.07	-3.35	11.06	-3.07
28	11.68	11.07	5.13	11.06	5.308
29	11.4	11.07	2.89	11.06	2.98
30	11.19	11.94	-6.70	11.06	1.16
31	10.72	11.07	-3.26	11.06	-3.17

Absolute mean percentage error for ANN prediction= 7.09

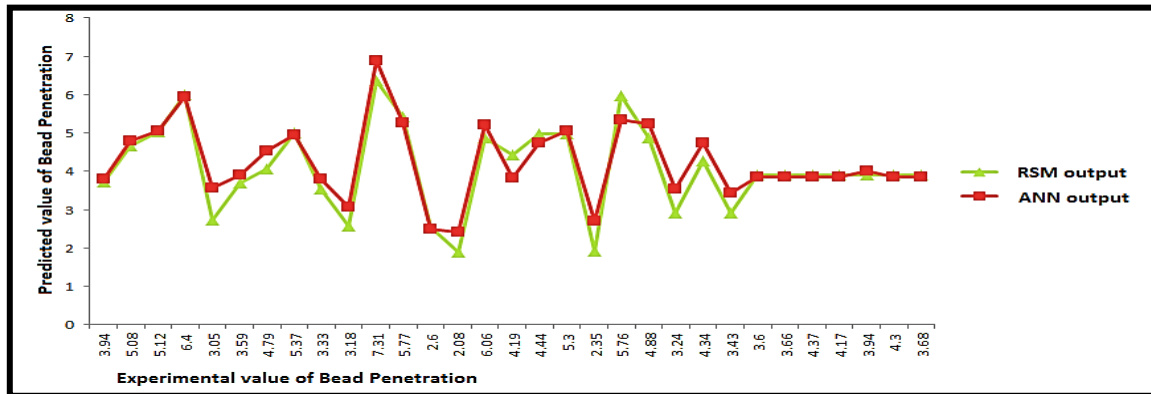Absolute mean percentage error for RSM model prediction= 3.22
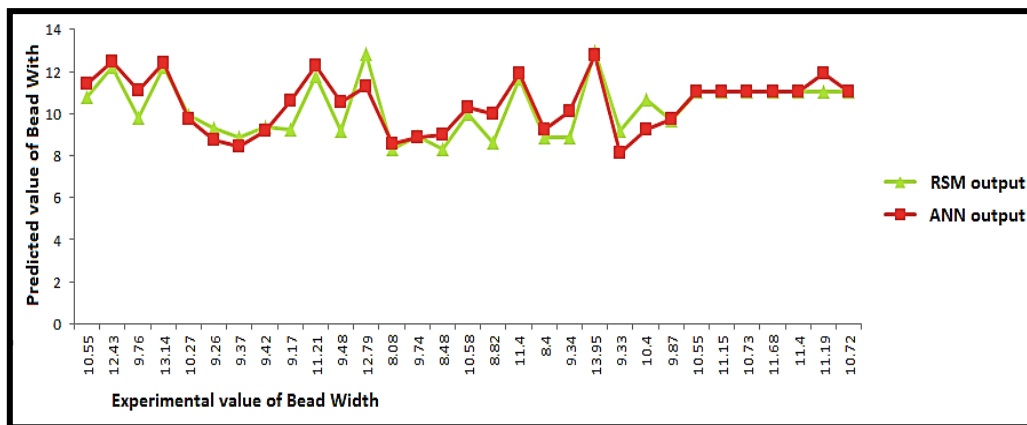
Figure6.10: Comparison of experimental, ANN and RSM model results for the
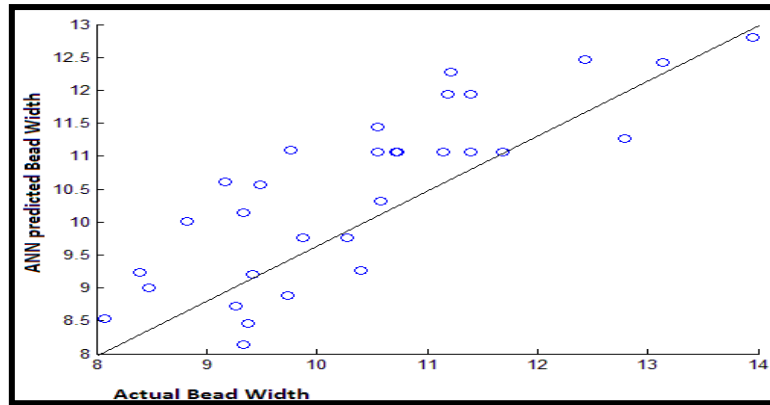
bead width

Figure 6.11: Comparison of ANN prediction of bead width with actual bead width

The absolute mean percentage error of ANN prediction, 7.09 is far more than the absolute mean percentage error of RSM model predictions 3.22, which shows that the RSM model is more accurate than the ANN model for the bead height predictions. From Figure 6.10 it can be concluded that the outputs from the ANN model and the RSM models are comparable which is inferred from the overlap between the plots of ANN output and RSM model output versus the actual output for the bead height.
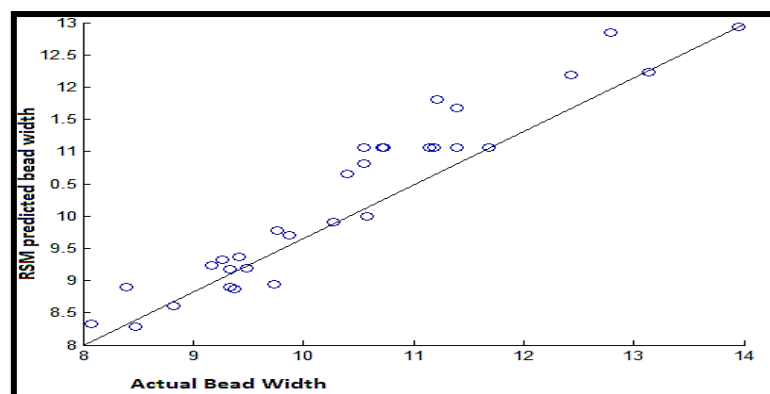
Figure 6.12: Comparison of RSM model prediction of bead width with actual bead width

The greater accuracy of the RSM model over the ANN model is further highlighted from the scatter plots wherein more number of outputs are located on or near the line y=x for RSM model predicted bead height (figure 6.12) as compared to ANN

predicted bead height (figure 6.11). Also it is to be noted that the percentage error in ANN prediction never exceeded 15.66 and that in RSM model never exceeded 8.11 (absolute), so these two models can be successfully used for prediction of bead height.

6.3.3 Comparison of experimental, ANN and RSM models for bead penetration

Table 6.4: Comparison of experimental, ANN and RSM model results for bead penetration

SI.no	Experimental value	ANN output	%error in ANN prediction	RSM model output	%error in RSM model prediction
1	3.94	3.81	3.29	3.71	5.83
2	5.08	4.78	5.905	4.67	8.07
3	5.12	5.04	1.562	5.03	1.75
4	6.4	5.93	7.34	5.99	6.406
5	3.05	3.55	-16.39	2.73	10.49
6	3.59	3.89	-8.3	3.69	-2.78
7	4.79	4.53	5.42	4.05	15.44
8	5.37	4.96	7.06	5.01	6.70
9	3.33	3.81	-14.41	3.53	-6.006
10	3.18	3.07	3.45	2.57	19.18
11	7.31	6.88	5.88	6.37	12.85
12	5.77	5.26	8.83	5.41	6.23
13	2.6	2.48	4.615	2.55	1.92

14	2.08	2.41	-15.8	1.89	9.13
15	6.06	5.209	14.04	4.88	19.47
16	4.19	3.82	8.83	4.43	-5.72
17	4.44	4.741	-6.81	4.98	-12.16
18	5.3	5.05	4.71	4.98	6.03
19	2.35	2.71	-15.31	1.92	18.29
20	5.76	5.35	7.11	5.98	-3.81
21	4.88	5.24	-7.37	4.88	0
22	3.24	3.54	-9.25	2.92	9.87
23	4.34	4.73	-8.98	4.28	1.38
24	3.43	3.43	0	2.92	14.86
25	3.6	3.84	-6.66	3.9	-8.33
26	3.66	3.84	-4.91	3.9	-8.33
27	4.37	3.84	12.12	3.9	10.75
28	4.17	3.84	7.91	3.9	6.47
29	3.94	4.002	-1.57	3.9	1.01
30	4.3	3.84	2.48	3.9	9.302
31	3.68	3.84	-4.34	3.9	-5.97

Absolute mean percentage error for ANN prediction= 7.44

Absolute mean percentage error for RSM model prediction= 8.21

For the prediction of bead penetration the absolute mean percentage error for ANN prediction 7.44 is lesser than that for RSM model prediction which is 8.21. Thus the

ANN model is more accurate than the RSM model in this case. As observed from figure 6.13, the prediction from the ANN model is comparable to the predictions made by the RSM model. This is supported from the scatter plots.

Figure 6.13: Comparison of experimental, ANN and RSM model results for the bead penetration
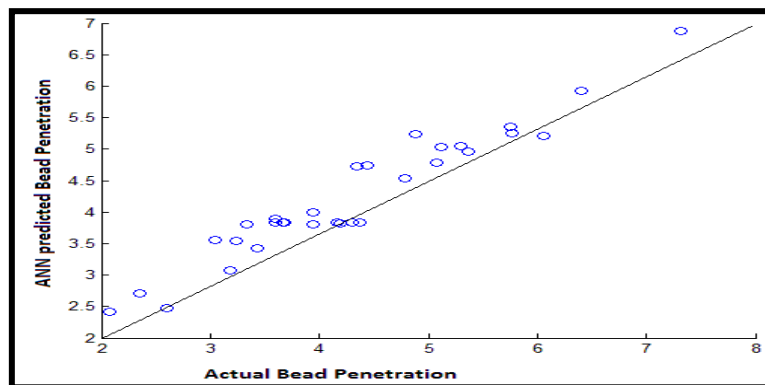
Figure 6.14: Comparison of ANN prediction of bead penetration with actual bead penetration
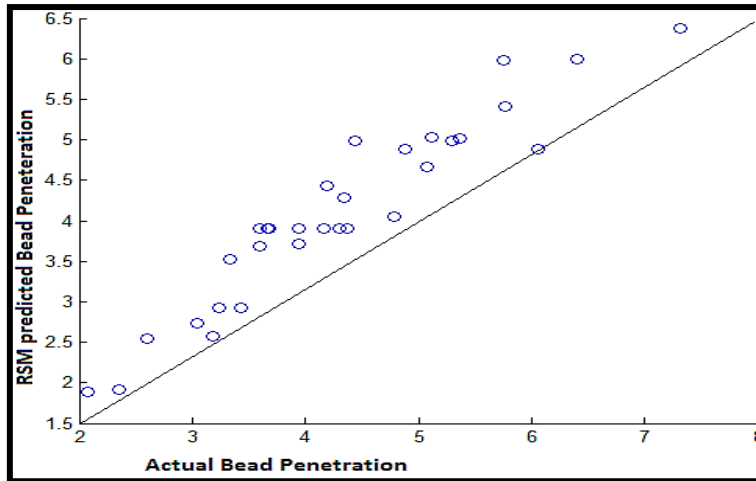
Figure 6.15: Comparison of RSM model prediction of bead penetration with

For the ANN prediction greater number of outputs lie on or near the line y=x (figure 6.14) as compared with RSM model prediction (figure 6.15). Also it is to be noted that the percentage error in ANN prediction never exceeded 16.39 (absolute) and that in RSM model never exceeded 19.47 (absolute), so these two models can be successfully used for prediction of bead height.

Chapter 7

METALLURGICAL ANALYSIS

7.1 Introduction

To carry out the metallurgical studies, specimens were cut in the transverse direction from the welded plates. After that, the specimens were polished with progressively finer grades of emery paper. After that wet polishing of the specimen was done; followed by etching with Nital's solution (2% Nitric Acid + 98% Alcohol). Microstructural studies were carried out on the weld zone, Heat Affected Zone and the Base metal, after preparing the specimens. Studies were carried out for the sample with maximum heat input and the sample with minimum heat input. The variation of micro hardness along the weld bead in horizontal direction was also determined.

7.2 Microstructural Studies

Microstructure is defined as the structure of a prepared surface or thin foil of material as revealed by a microscope above 25× magnification. The microstructure of a material can strongly influence physical properties such as strength, toughness, ductility, hardness, corrosion resistance, high/low temperature behaviour, wear resistance, and so on, which in turn govern the application of these materials in industrial practice. The microstructural features of a given material may vary greatly when observed at different length scales. For this reason, it is crucial to consider the length scale of the observations when describing the microstructure of a

material. To study the microstructure Olympus GX 41 microscope was used in conjunction with META-Lite software.
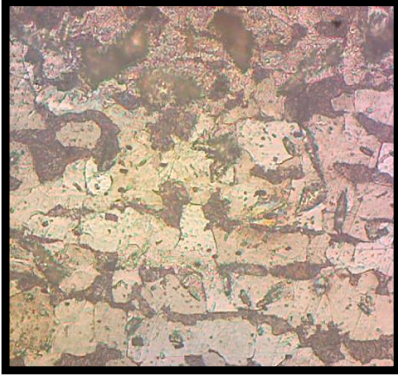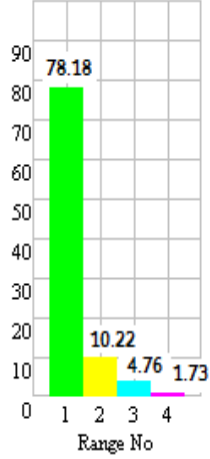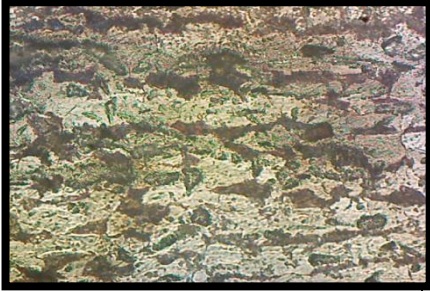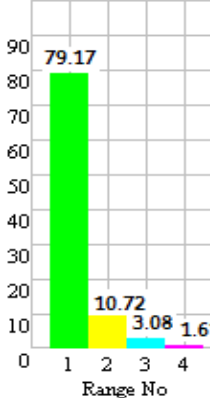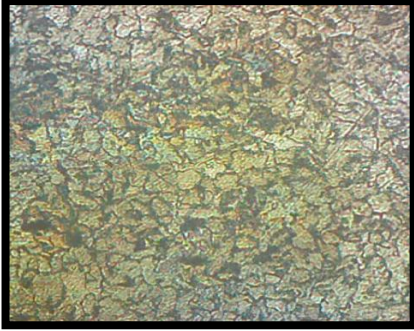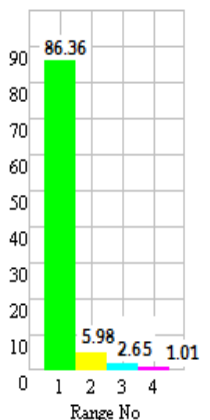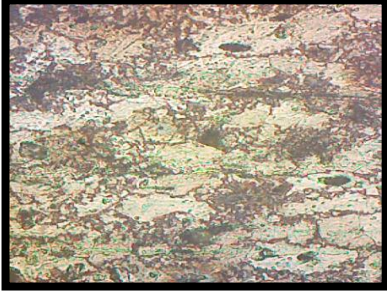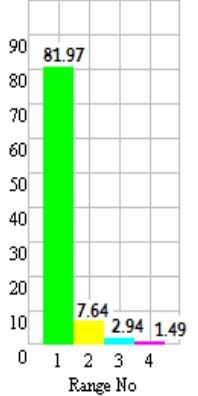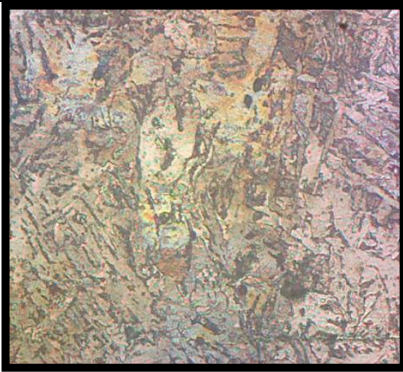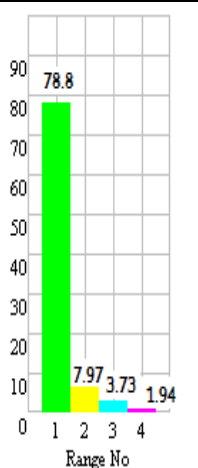

Figure 7.1Olympus GX 41microscope

7.2.1 Microstructural Analysis for the Maximum Heat Input

From the design matrix we see that the Current and Arc Voltage is maximum and the travel speed is minimum for trial number 4 and 12. Thus these trials represent the maximum Heat input. In the microstructural analysis the different phases present in the microstructure along with their respective percentages were found. In addition the percentage of particles in 4 different range of sizes, were also determined. For this purpose 4 size ranges were defined: Range 1: 1-20 microns; Range 2: 20-39 microns; Range 3: 39-59 microns; Range 4: 59-79 microns. Higher percentage of particles in the lower ranges indicates the microstructure is mainly composed of smaller sized particles and vice versa.

Table 7.1 Comparison of microstructure of different zones for maximum heat input

Sl. no	Region	Microstructure and phase percentages	Size distribution	Comments
1	Base Metal	 Pearlite: 56.97% Ferrite : 43.03%		This is the zone which was not sufficiently heated to cause a change in its microstructure.
2	HAZ1	 Pearlite: 72.58% Ferrite: 27.42%		The pearlite content is higher than base metal. Also larger % of grains are in the lower range, thus the microstructure is finer than the base metal.
3	HAZ2	 Pearlite : 82.66% Ferrite: 17.34%		Grain refinement is complete and finest grain structure exists. The pearlite content is also higher.

| 4. | HAZ3 | Pearlite: 77.23% Ferrite: 22.77% | | This is the grain growth region. Pearlite content is lesser than previous and the % of particles in higher range increases marginally. In this zone the parent metal is heated well above upper critical temperature which resulted in grain growth. |
| 5. | Weld zone | Pearlite: 68.23% Ferrite : 35.77 % | | Epitaxial solidification takes place. The range of grain size and phase composition is almost same as that of base metal. |

*HAZ1, HAZ2, HAZ3 are the heat affected zones; observed sequentially while moving from the base metal towards the centre of the weld bead (weld zone)
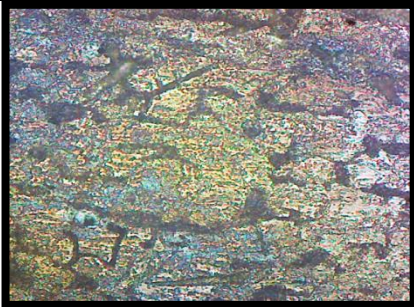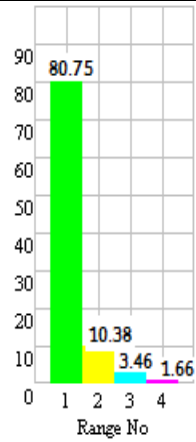
Depending upon the composition and solidification rates the weld solidifies in a cellular or dendritic growth mode. Both modes cause segregation of alloying elements and consequently the weld metal is less homogeneous on the micro level than the base metal and therefore cannot be expected to have the same properties as wrought parent metal unless the filler metal in the as deposited condition has same properties as that of parent metal.
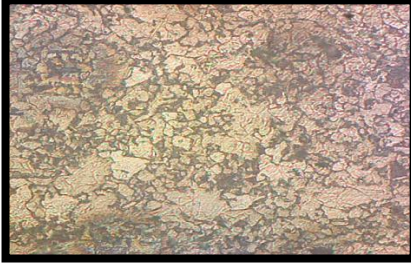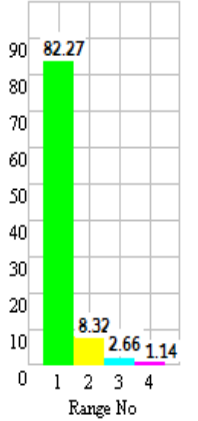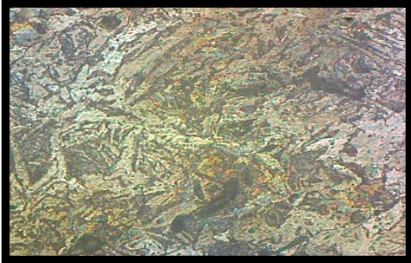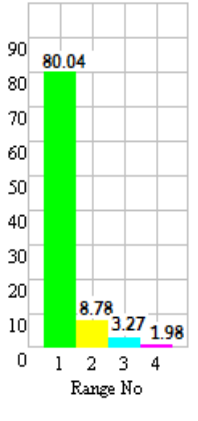
In SAW the welding is carried out under the cover of a granulated flux. So the rate of cooling of the weld is slower as compared to shielded metal arc welding. So the microstructure resulting from higher rates of cooling viz. Martensite, upper Bainite, Lower Bainite etc. are not observed. In the present study the thickness of the plates was 12.5 mm, so the heat carried away by conduction was also very less. In welding of plates with higher thickness microstructure characteristic of faster rate of cooling may be observed.

7.2.2 Microstructural analysis for minimum heat input

From the design matrix we see that the Current and Arc Voltage is minimum and the travel speed is maximum for trial number 5 and 13. Thus these trials represent the minimum Heat input. In the microstructural analysis the different phases present in the microstructure along with their respective percentages were found. In addition the percentage of particles in 4 different ranges of sizes, were also determined.

Table 7.2 Comparison of microstructure of different zones for minimum heat input

Sl. no	Region	Microstructure and phase percentages	Size distribution	Comments
1	Base Metal	Pearlite: 59.64% Ferrite: 40.36		It is unaffected by the thermal cycle of the weld. The microstructure is predominantly pearlitic.

104

2	HAZ	 Pearlite: 78.46% Ferrite: 21.54%		The pearlite content is highest and the number of grains in the lowest range is also the maximum.
3	Weld zone	 Pearlite : 62.87% Ferrite: 37.13%		The phase composition and the size distribution is almost same as that of the base metal.

From table 7.2 we can observe that the variation in the pearlitic content in the considered regions for the minimum heat input is not as pronounced as that for maximum heat input. Also the range of size distribution is very near to each other for the base metal, weld zone and HAZ. In fact it is almost identical for the base metal and the weld zone. Also we can observe that the pearlitic content in the weld zone is higher in minimum heat input as compared with the maximum heat input, this could be attributed to the fact that; for the minimum heat input the cooling rate is higher which inhibits the formation of pro-eutectoid ferrite and larger portion of Austenite gets converted to Pearlite upon crossing the eutectoid line **[51-52]**.

7.3 Variation of micro hardness

Variation of micro hardness was observed in the horizontal direction, starting from the centre of the weld as the, through the HAZ, finally up to the base metal. To measure the micro hardness, Omnitech MVH Auto Micro Hardness tester (Figure 7.2) with 100 gram load and dwell time of 20 seconds.

Figure 7.2 : Omnitech MVH Auto Micro Hardness tester

The values reported are for Knoop's Micro hardness. A pyramidal diamond point is pressed into the polished surface of the test material with a known force, for a specified dwell time, and the resulting indentation is measured using a microscope. The geometry of this indenter is an extended pyramid with the length to width ratio being 7:1 and respective face angles are 172 degrees for the long edge and 130 degrees for the short edge. The depth of the indentation can be approximated as 1/30 of the long dimension. The Knoop hardness number (KHN) can be calculated from the applied load divided by the impression area of the indention as follows:

$KHN = P / C_p . L^2$

Where, L = length of indentation along its long axis

C_p = correction factor related to the shape of the indenter, ideally 0.070279

P = load in grams

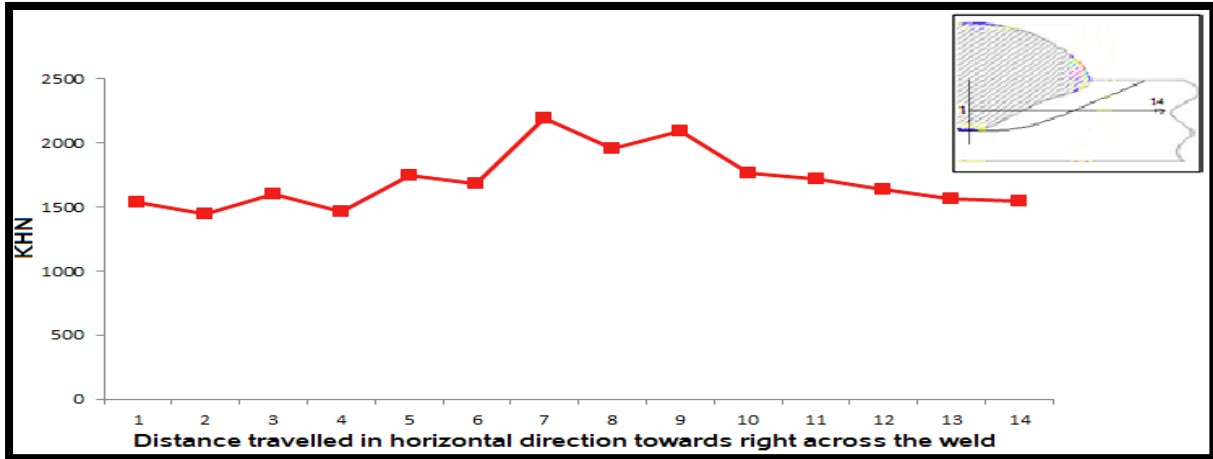7.3.1 Variation of micro hardness for maximum heat input:

Figure 7.3: Variation of micro hardness in the horizontal direction across the weld for maximum heat input

The hardness measurements were carried out from the centre of the weld bead in a horizontal direction, moving towards right. The hardness measurements were carried out at a depth of 2 mm form the base metal surface. From Figure 7.3, we see that the KHN value for the weld zone and the base metal are comparable while maximum hardness is observed in the HAZ. This observation can be attributed to pearlite content and the size range of the micro structure. From table 7.1 we know that the pearlite content and the range of size distribution for the base metal and the weld zone are almost same. While the pearlite content for the HAZ is higher and greater numbers of grains are in the lower range, indicating finer microstructure; as compared to weld zone and base metal.

Pearlite content has a positive effect on the micro hardness [21]. And increased heat input increases the ferrite content in the microstructure for SAW [20]. The increased

pearlite content combined with finer microstructure results in greater micro hardness in the HAZ. Also it can be observed that the micro hardness is greatest in the grain refined region, having the highest Pearlite content and where the grains are finest.

7.3.2 Variation of micro hardness for minimum heat input:
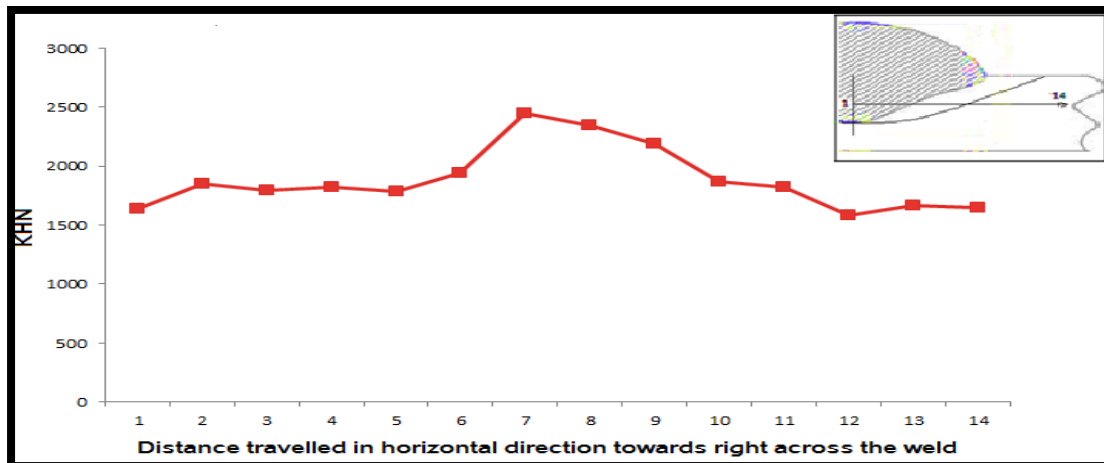
Figure7.4: Variation of micro hardness in the horizontal direction across the weld for minimum heat input

The micro hardness variation for minimum heat input follows a trend similar to that of maximum heat input. One noticeable difference is that, the values of micro hardness for minimum heat input is greater than that for maximum heat input. This can be attributed to finer grain structure owing to greater percentage of grains in lower grain size range and higher pearlite content, as seen from table 7.2. Also it can be observed that there is lesser fluctuation of micro hardness values for minimum heat input. As discussed in previous section, the micro hardness is mainly affected by fineness of micro structure and pearlite content. Since, these two factors do not change by too large a extent for minimum heat input, the micro hardness values also do not undergo much fluctuation.

Chapter 8

CONCLUSIONS AND FUTURE SCOPE

8.1 Conclusions

From the research work following conclusions were drawn:

1. A five level CCD technique can be employed to study the effect of weld parameters on bead geometry in SAW.

2. The mathematical models developed can be used for successful prediction of bead geometry features within the pre decided range of the parameters.

3. Of all the process variables considered the welding current has appreciable positive effect on all the bead geometry parameters while welding speed has negative effect on the bead parameters. For eg, the bead penetration increased by about 3.4 mm when current is increased from -2 to +2, but the bead penetration decreases by about 3 mm when the travel speed is increased from -2 to +2.

4. Increase in Nozzle-to-plate distance increases the momentum of incoming metal droplets which increases the penetration but reduces the bead width and increase in arc voltage results in spreading out of arc cone at its base and leads to increase in bead width but lesser penetration and bead height. This contrasting effect of arc voltage and nozzle-to-plate distance is evident from the interaction plots where the value of the weld parameter reaches a maximum and then drops down to lower value.

5. Most of the interaction effects of the process variables on the bead parameters show generally convincing trends between cause and effect.

6. ANN model using Back propagation Algorithm was developed for predicting the bead geometry features namely bead height, bead width and bead penetration in Submerged Arc Welding.

7. For this study the structure of the neural network was 4-15-10-3 (4 in the input layer, 15 in the first hidden layer, 10 in the second hidden layer and 3 in the output layer). The network was trained for 2755 iterations before the performance goal was met

8. Both the mathematical models and the ANN models show fair degree of accuracy in predicting the bead geometry features. The largest percentage error observed was 19.47.

9. It was found that for predicting the bead height and bead width the RSM models were more accurate than the ANN model. While for the prediction of bead penetration the ANN model was more accurate than the RSM model.

10. RSM is suitable for application where the numbers of factors are less and the interactions are mostly linear, while ANN is capable of handling larger problems and non-linear interactions between them.

11. The outputs obtained from the RSM models and the ANN models were comparable and as such any of them can be used for successful modelling of the SAW process.

12. The microstructure mainly consists of Ferrite and Pearlite. The microstructure resulting from higher rates of cooling viz. Martensite, upper Bainite, Lower Bainite etc. are not observed, this could be attributed to the covering of weld region by a granulated flux which reduces the heat carried away from the weld zone.

13. The grain size decreases while moving from base metal to HAZ. Minimum grain size is observed within the HAZ in the grain refined region. Upon moving towards the weld zone, the grain size again increases. The pearlite content follows a similar trend.

14. No cementite or flake graphite is found in the microstructure, this could be due to the fact that the Carbon content in the base metal was very low.

15. The Knoop's micro hardness was observed at 100 gram load. The micro hardness increases from the base metal to the HAZ. It reaches a maximum in HAZ where, the grain size is finest and pearlite content is maximum. Upon moving further towards weld zone the micro hardness exhibits a fall in its value.

16. One noticeable difference is that, the values of micro hardness for minimum heat input is greater than that for maximum heat input. This can be attributed to finer grain structure owing to greater percentage of grains in lower grain size range and higher pearlite content.

17. There is lesser fluctuation of micro hardness values for minimum heat input. Since the fineness of micro structure and pearlite content do not change by too large an extent for minimum heat input, the micro hardness values also do not undergo much fluctuation.

8.2 Future Scope

Every study has a scope for further improvement. Following are the areas which can still be explored in the context of the present research:

1. The study had included Voltage, Current, Travel Speed and Nozzle-to-plate-distance as the input parameters. Factors like chemical composition of flux,

multiple wire welding, different sizes of wire etc. can be incorporated to find out their effects on the bead geometry features and metallurgy.

2. Shape relationships like Weld Penetration Shape Factor and Weld Reinforcement Form Factor can also be considered along with the bead geometry features as outputs in the study.

3. Modelling of the SAW process using Neuro Genetic Algorithm, Neuro Differential Algorithm etc can be done and their results can be compared with existing models.

4. Apart from the micro hardness and metallurgy, studies can be undertaken to analyse the effect of process parameters on the mechanical properties of the joint, like Toughness, Ultimate Tensile Strength etc.

REFERENCES:

[1] Chandel R.S, Seow H.P, Cheong F.L, 1997 "Effect of increasing deposition rate on the bead geometry of submerged arc welds" , Journal of Materials Processing Technology; **72**: 124 – 128.

[2] Karadeniz E , Ozsarac U, Yildiz C, 2007, "The effect of process parameters on penetration in gas metal arc welding processes" Materials and Design; **28**: 649–656

[3] Gunaraj V, Murugan N, 1999, "Application of response surface methodology for predicting weld bead quality in submerged arc welding of pipes". Journal of Material Processing Technology; **88**:266–275.

[4] Gunaraj V, Murugan N, 1999, "Prediction and comparison of the area of the heat-affected zone for the bead-on-plates and bead-on-joint in submerged arc welding of pipes" Journal of Material Processing and Technology; **95**: 246–261.

[5] Yang L.J, Bibby M.J, Chandel R.S, 1999, "Linear regression equations for modelling the submerged-arc welding process" Journal of Material Processing and Technology; **39**:33–42

[6] Srivastav B.K, TEWARI S.P, PRAKASH J, 2010, "A review on effect of arc welding parameters on mechanical behaviour of ferrous metals/alloys" International Journal of Engineering Science and Technology; **2(5)**: 1425-1432

[7] Benyounis KY, Bettamer AH, Olabi AG, Hashmi MSJ, 2004 "Prediction the impact strength of spiral-welded pipe joints in Submerged arc welding of low carbon steel" In: Proceedings of IMC21, 1–3 September. Limerick; 2004. p. 200–210

[8] Muruganan N, Gunaraj V, 2005, "Prediction and control of weld bead geometry and shape relationships in submerged arc welding of pipes" Journal of Materials Processing Technology; **168** : 478–487

[9] Koleva E. 2005, "Electron beam weld parameters and thermal efficiency improvement" Vacuum J ; **77** : 413–421

[10] Benyounis KY, Olabi AG, Hashmi MSJ., 2005, "Effect of laser welding parameters on the heat input and weld-bead profile." Journal of Material Processing Technology; **164**: 978–985

[11] Heidarzadeh A , Khodaverdizadeh H, Mahmoudi A, Nazari E , 2012, "Tensile behavior of friction stir welded AA 6061-T4 aluminum alloy joints", Materials and Design; **37**: 166-173

[12] Andersen K, Cook G.E, Karsai G, Ramaswamy K, 1990, "Artificial neural networks applied to arc welding process modeling and control" IEEE Transactions Industrial Applications.; **26**: pp. 824–830

[13] Cook G.E**,** Barnett R.J **,** Andersen K, Straw A.M, 1993"Weld Modelling and Control Using Artificial Neural Networks," IEEE, 2181-2189.

[14] Nagesh D.S, Datta G.L, 2002 "Prediction of weld bead geometry and penetration in shielded metal-arc welding using artificial neural networks" Journal of Material Processing Technology, ; **123** : pp. 303–312

[15] Pal S, Pal S.K , Samantaray A.K, 2008, "Artificial neural network modeling of weld joint strength prediction of a pulsed metal inert gas welding process using arc signals" Journal of Material Processing Technology; **202**: 464-474

[16] Cevik A, Kutuk M.A , Erklig A , Guzelbey I.H , 2008 "Neural network modeling of arc spot welding", Journal of Materials Processing Technology; **202**: 137– 144.

[17] Eroglu M , Aksoy M , Orhan N,1999, "Effect of coarse initial grain size on microstructure and mechanical properties of weld metal and HAZ of a low carbon steel" Material Science and Engineering; **A269**: 59-66

[18] Kiran D.V, Basu B, De A, 2012, "Influence of process variables on weld bead quality intwo wire tandem submerged arc welding of HSLA steel" Journal of Material Processing Technology, doi:10.1016/j.jmatprotec.2012.05.008

[19] Gunaraj V, Murugan N, 1999, "Prediction and comparison of the area of the heat-affected zone for the bead-on-plate and bead-on-joint in submerged arc welding of pipes" , Journal of Material Processing Technology; **95** : 246-261

[20] Kolhe K.P, Datta C.K , 2008, "Prediction of microstructure and mechanical properties of multipass SAW" Journal of Material Processing Technology; 1**97**: 241-249

[21] Adnan Çalik, 2009, "Effect of cooling rate on hardness and microstructure of AISI 1020, AISI 1040 and AISI 1060 Steels" International Journal of Physical Sciences; **4 (9)**: pp. 514-518

[22] Benyounis K.Y, Olabi A.G., 2008, "Optimization of different welding processes using statistical and numerical approaches – A reference guide" Advances in Engineering Software: **39** ; 483–496

[23] Juang SC, Tarng YS, 2002, "Process parameters selection for optimizing the weld pool geometry in the tungsten inert gas welding of stainless steel." Journal of Material Processing Technology;**122**: 33–37.

[24] Wang KK, Rasmussen G. 1972. "Optimization of inertia welding process by response surface methodology." Journal of Engineering Industry; **94(4)**:999–1006.

[25] Koichi O, Hiroshi Y, Seiichi K, Kazuhiko S., 1993 "Optimization of friction welding condition for S4 5C carbon steel using a statistical technique". Journal of Japanese Welding Society; **24(2)**: 47–53.

[26] Lightfoot MP, Bruce GJ, McPherson NA, Woods K., 2005 "The application of artificial neural networks to weld-induced deformation in ship plate." Weld Journal, AWS and WRC: 23-s–6-s.

[27] Sterjovski Z, Nolan D, Carpenter KR, Dune DP, Norrish J., 2005 "Artificial neural network for modelling the mechanical properties of steels in various applications." Journal of Material Processing Technology; **170(3)**:336–544.

[28] Okuyucu H, Kurt A, Arcaklioglu E. 2007 "Artificial neural network application to the friction stir welding of aluminium plates." Journal of Material Design; **29:**78–84

[29] Wei Y, Bhadeshia HKD, Sourmail T., 2005 "Mechanical property prediction of commercially pure titanium welds with artificial neural network". Journal of Material Science Technology ;**21(3)**: 403–407.

[30] Canyurt OE., 2005 "Estimation of welded joint strength using genetic algorithm approach. International Journal Mechanical Science; **47**:1249–61.

[31] Di, L., Srikanthan, T., Chandel, R.S., Katsunori, I., 2001."Neural-network based self-organized fuzzy logic control for arc welding". Engineering Application of Artificial Intelligence; **14**: 115–124.

[32] Indacochea J.E , 1992, "Cr-Mo Steel Welding Metallurgy", Key Engineering Materials; **69-70** : 47-94

[33] Ma L. W., Wu X. and Xia K., 2008, "Microstructure and property of a medium Carbon steel processed by equal channel angular pressing" , Materials forum ;**32**

[34] Linert, T.J., Tellwag Jr., W.L., Grimmett, B.B., Waree, R.W., 2003. Friction stir welding studies on mild steel" Weld Journal; **80**: 1-s–9-s.

[35] McGrath, J.T., et al., 1988. "Microstructural mechanical property relationships in thick section narrow groove welds". Welding Journal. ;**67:** 196-s–201-s.

[36] Richard, L., Richard, W., 1994. Economical repair of turbo machinery shaft by SAW." Welding Journal ; **73**:, 39–44.

 [37] Wang, W., Liu, S., 2002. "Alloying and microstructural management in developing SMAW electrodes for HSLA-100 steel". Welding Journal;**82**: 132-s-145-s

[38] Aslan N, 2008 "Application of response surface methodology and central composite rotatable design for modelling and optimization of a multigravity separator for chromite concentration." Power Technology;**185** : 80-86.

[39] Kanti K.M, Rao P. S, 2008 "Prediction of bead geometry in pulsed GMA welding using back propagation neural network", Journal of materials processing technology; 200 : 300–305.

[40] http://arxiv.org/ftp/cs/papers/0308/0308031.pdf

[41] http://en.wikipedia.org/wiki/Unsupervised_learning

[42] http://en.wikipedia.org/wiki/Artificial_neural_network

[43] http://www.statsoft.com/textbook/experimental_design/#centrala # Introduction to Central Composite Deisgn

[44] http://en.wikipedia.org/wiki/Central_composite_design

[45] http://www.doe.soton.ac.uk/elearning/section2.18.jsp

[46] http://www.doc.ic.ac.uk/nd/surprise_96/journal/vol4/cs11/report.html Introduction to neural networks

[47] www.mathworks.com/moler/intro.pdf # Introduction to MATLAB

[48] www.mathworks.com/help/**pdf**_doc/nnet/nnet_ug.**pdf** # Introduction to Neural Network using MATLAB

[49] Davies A.C., Welding Science and technology, Vol-1,Ninth Edition Cambridge university press.

[50] Montgomery D.C, 2006, " Design and analysis of Experiments" ,Wiley-INDIA edition, New Delhi

[51] Sindo, K., 2002. "Metallurgy of Welding", second ed. Wiley-Interscience.

[52] Parmar R.S., 2010, "Welding Process and Technology", Second edition, Khanna Publication.